DESIGN OF TUNABLE IMPEDANCE MATCHING CIRCUIT FOR A GSM ANTENNA

A THESIS SUBMITTED TO
THE GRADUATE SCHOOL OF NATURAL AND APPLIED SCIENCES
OF
MIDDLE EAST TECHNICAL UNIVERSITY

BY

MEHMET ALİ ÖZTÜRK

IN PARTIAL FULFILLMENT OF THE REQUIREMENTS
FOR
THE DEGREE OF MASTER OF SCIENCE
IN
ELECTRICAL AND ELECTRONICS ENGINEERING

JULY 2015

Approval of the thesis:

DESIGN OF TUNABLE IMPEDANCE MATCHING CIRCUIT FOR A GSM ANTENNA

submitted by **MEHMET ALİ ÖZTÜRK** in partial fulfillment of the requirements for the degree of **Master of Science in Electrical and Electronics Engineering Department, Middle East Technical University** by,

Prof. Dr. Gülbin Dural
Dean, Graduate School of **Natural and Applied Sciences** _____

Prof. Dr. Gönül Turhan Sayan
Head of Department, **Electrical and Electronics Engineering** _____

Prof. Dr. Özlem Aydın Çivi
Supervisor, **Electrical and Electronics Engineering Department, METU** _____

Dr. Fatih Koçer
Co-supervisor, **Electrical and Electronics Engineering Dept., METU** _____

Examining Committee Members:

Prof. Dr. Özlem Aydın Çivi
Electrical and Electronics Engineering Department, METU _____

Prof. Dr. Sencer Koç
Electrical and Electronics Engineering Department, METU _____

Dr. Fatih Koçer
Electrical and Electronics Engineering Department, METU _____

Prof. Dr. Şimşek Demir
Electrical and Electronics Engineering Department, METU _____

Dr. Kağan Topallı
Bilkent UNAM, Bilkent University _____

Date: _____

I hereby declare that all information in this document has been obtained and presented in accordance with academic rules and ethical conduct. I also declare that, as required by these rules and conduct, I have fully cited and referenced all material and results that are not original to this work.

Name, Last Name: MEHMET ALİ ÖZTÜRK

Signature :

ABSTRACT

DESIGN OF TUNABLE IMPEDANCE MATCHING CIRCUIT FOR A GSM ANTENNA

ÖZTÜRK, MEHMET ALİ

M.S., Department of Electrical and Electronics Engineering

Supervisor : Prof. Dr. Özlem Aydın Çivi

Co-Supervisor : Dr. Fatih Koçer

July 2015, 117 pages

In this thesis, automatic impedance matching circuits are designed by using several tuning approaches. A typical automatic impedance matching system compensates for the impedance variations of the antenna due to the human hand and head using an electronically tunable impedance matching circuitry. Maximum output power, the linearity and efficiency of PA can be improved using automatic impedance matching circuit units. There are various tunable impedance matching circuits proposed in the literature to enhance RF front end operating conditions. These circuits are implemented by using inductors and varactors in various circuit topologies which can be utilized at the input of the low noise amplifier (LNA) in the receive chain and the output of the power amplifier (PA) in the transmit chain. Impedance coverage regions are investigated by sweeping all tunable components for various tuners. Our proposed automatic impedance networks are designed by utilizing a variation of available networks in the literature plus some novelties on the configuration and improvements on control voltage levels. A prototype of impedance tuner consisting of a 90 degree phase shifter and a variable transformer connected in cascade is implemented on an FR4 board. The automatic impedance tuning unit composed of directional couplers, attenuators, AD8302 is fabricated on an FR4 board to test the performance of the impedance tuner for various load impedances in the frequency bandwidth of 880-920 MHz. The automatic impedance tuner measurements show that significant VSWR improvement can be achieved for different load impedances. These measurements

also show that the VSWR value is maintained below two for most of the mismatched loads in the frequency band of 880-920 MHz. In order to study the overall efficiency of the tunable matching circuit, relative transducer gain expression is also employed to measure how much improvement or loss is introduced by the tunable matching circuit. The developed impedance tuner is compact and needs control voltage levels up to 3.3 V, so that it is a good candidate for cell phone applications.

Keywords: tunable impedance matching, automatic tuning, varactors

ÖZ

GSM ANTENİ İÇİN AYARLANABİLİR EMPEDANS UYUMLAMA DEVRESİ TASARIMI

ÖZTÜRK, MEHMET ALİ
Yüksek Lisans, Elektrik ve Elektronik Mühendisliği Bölümü
Tez Yöneticisi : Prof. Dr. Özlem Aydın Çivi
Ortak Tez Yöneticisi : Dr. Fatih Koçer

Temmuz 2015 , 117 sayfa

Bu tezde, birkaç ayarlama yaklaşımı kullanılarak otomatik empedans eşleme devreleri tasarlanmıştır. Tipik bir otomatik empedans eşleme sistemi elektronik olarak ayarlanabilen bir empedans eşleme devresi kullanılarak kullanıcının başı ve eliyle oluşan empedans değişimlerini giderir. Güç yükseltecin çıkış gücü, doğrusallığı ve verimliliği otomatik empedans eşleme devre birimleri kullanılarak iyileştirilebilir. RF ön uç çalışma koşullarını iyileştirmek için literatürde önerilen çeşitli ayarlanabilir empedans eşleme devreleri mevcuttur. Bu çalışmada otomatik empedans eşleme devreleri birkaç ayarlama yaklaşımı kullanılarak tasarlanmıştır. Verici dizisindeki güç yükseltecin çıkışında ve alıcı dizisindeki düşük gürültülü güç yükseltecin girişinde kullanılan bu devreler endüktörler ve varaktörler kullanılarak farklı topolojilerde tasarlanabilir. Empedans kapsama bölgeleri farklı devrelerde ayarlanabilir empedans değerleri taranarak araştırılmıştır. Kontrol voltaj seviyeleri iyileştirilerek ve literatürde hazır bulunan devrelere bir kaç yenilik eklenerek otomatik empedans devresi tasarlanmıştır. Ardışık bağlanmış ayarlanabilir faz kaydırıcı ve değişken dönüştürücü kullanılarak FR4 kartı üzerine bir empedans uyumlama devresi gerçekleştirilmiştir. 880-920 MHz frekans bandında farklı yük empedanslarında uyumlayıcıların performansının test edilmesi için, yönlü bağdaştırıcılar, zayıflatıcılar ve AD8302' den oluşan otomatik empedans uyumlama birimi FR4 kartı üzerine üretilmiştir. Farklı sabit yük empedansları için empedans tuner ölçümleri önemli ölçüde VSWR iyileştirmesi başarılabildiğini

göstermiştir. Bu ölçümlerde aynı zamanda ilgilenilen frekans bandı içerisinde çoğu eşlenmemiş yükler için VSWR değerinin ikinin altında tutulduğu görülmüştür. Ayarlanabilir eşleme devresinin tüm verimliliğini incelemek için ayarlanabilen empedans devresi ile ne kadar iyileşme veya kayıp getirildiğini ölçmek için relatif dönüştürücü kazancı ifadesi kullanılmıştır. Geliştirilen empedans ayarlama devresi küçük ve 3.3 Volt'a kadar kontrol voltajına ihtiyaç duyduğundan cep telefonu uygulamaları için iyi bir adaydır.

Anahtar Kelimeler: Ayarlanabilir empedans devresi, otomatik ayarlama , ayarlanabilir kapasitans

To My Family

ACKNOWLEDGMENTS

I am using this opportunity to express my gratitude to everyone who supported me throughout the course of this thesis. Firstly, I would like to thank Prof. Dr. Özlem Aydın Çivi for her invaluable guidance and support. I am fortunate to have an advisor like her who gave me the freedom to explore my own approach, without her guidance and support, this work would not have been accomplished at all.

I would also like to thank Dr. Fatih Koçer for his insightful comments, constructive criticisms and invaluable support at the different stages of my thesis. It would have been really impossible for me to accomplish this task without him.

I am grateful for Anketek Ltd. Şti. and Anketek Electronics members Dr. Tayfun Özdemir who gave technical support to me and Prof. Dr. Ali Özgür Yılmaz who provided necessary conditions for my thesis at the stage of test and fabrication of circuits. Without their support, I would not have achieved these tasks.

Many thanks would go to my colleague Amin Ronaghzadeh in Anketek Electronics for his suggestions and constructive criticism. I would like to thank to him for his inexhaustible patience. His ideas enabled me to look from different perspectives about my thesis. I will never forget his help and friendship.

I would like to acknowledge especially Şüheda Öztürk for her corrections in editing. Lastly, I would like to express my heart-felt gratitude to my family whose love, support and encouragement have always helped me to find the right path. None of this would have been possible without love and patience of my family.

TABLE OF CONTENTS

LIST OF TABLES

TABLES

LIST OF FIGURES

FIGURES

CHAPTER 1

INTRODUCTION

Impedance matching is a necessary process in RF circuit design which can be defined as matching of an arbitrary load impedance to the output impedance of another network or a given transmission line impedance. Impedance matching circuits are utilized to match the input impedance of one network to the output impedance of another one to provide maximum power transfer between devices. This improves RF link quality in wireless communication systems when it is connected between an antenna and the RF front end.

In cell phones, antennas are generally exposed to the surrounding environment variations due to the presence of a user body in the vicinity of the antenna. These variations lead to a change of the antenna feed impedance; a situation which results in performance degradation in the overall communication system. Since fixed impedance matching circuits can not compensate for the antenna input impedance variations of cell phone, tunable impedance matching circuits must be utilized to tune these variations. In order to use tunable impedance matching circuit effectively in such applications, they need to be controlled dynamically by automatic impedance detection and control circuits. Figure 1.1 depicts the general block diagram of the automatic impedance tuning unit which generally consists of an impedance detector, an impedance sensor, a controller and an impedance tuner block.

Since automatic impedance tuner system dynamically monitors the variations of the antenna feed impedance and reconfigures its tunable impedance matching circuit for correction of the mismatches coming from the user interaction between the antenna and the body, it improves communication quality by reducing power reflections from

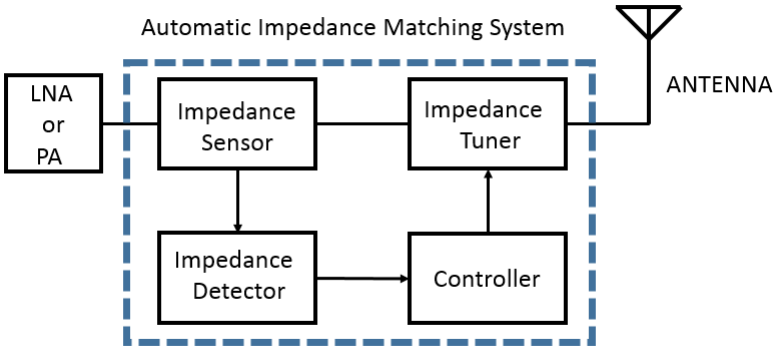

Figure 1.1: Basic block diagram of automatic impedance tuner

antenna and increases life-span of the battery. However, such improvements may bring up some limitations and drawbacks for the RF front end system. For example, tunable matching networks generally introduce more loss when compared to fixed impedance matching circuits. This may affect the overall RF system performance. Moreover, there is a compromise between impedance coverage region and the insertion loss introduced by the impedance tuner. Thus, an automatic impedance tuning system must be designed carefully by considering all the trade-offs mentioned above. In this work an automatic impedance matching circuit is designed taking all these considerations into account.

1.1 Overview of Tunable Impedance Matching Circuits in the Literature

Over the years, various kinds of tunable impedance matching circuits have been developed to cover the entire or specific areas of the Smith Chart. These circuits can be designed by using stub matching techniques, lumped element based circuits or transmission lines loaded with different varactors and switches. In this section a brief literature survey of some reported tuning circuits based on different techniques are briefly introduced.

The double stub tuning approach using Micro Electro Mechanical System (MEMS) devices is commonly studied in the literature for matching a wide variety of the load impedances for different frequency bands.

An example of this approach is presented in [1], which utilizes electrostatically ac-

tivated MEMS switches. In this application, each shunt connected stub is terminated with a variable capacitance to obtain reconfigurable impedance tuner. Input impedance of each stub can be altered by changing the capacitance value at the end of the stubs which provides tuning for different load impedances. Four sets of capacitors are connected in parallel at the end of the stubs. Each set is composed of the series combination of MEMS switches and fixed capacitors implemented by the open circuited transmission lines. Wide impedance coverage region on the Smith Chart can be achieved by increasing the number of these sets. However, matching all the load impedances is not possible by using this configuration. The distance between the stubs can determine the impedance tuning region which affects frequency sensitivity of the circuit. Unmatched impedance region can be reduced by readjusting the distance between the stubs to $0.1\,\lambda$. On and off positions of the MEMS switches on capacitor banks at the end of the stubs determine the input impedance of the stub and impedance tuning range of this tuner. Impedance tuner can match the real and imaginary part of the load impedance varying between $1.5\,\Omega < \text{Real}(Z_L) < 109\,\Omega$ and -107 $\Omega < \text{Imag}(Z_L) < 48\,\Omega$, respectively. The impedance tuning can be maintained by using several sets of these series combinations of MEMS switches and fixed capacitors.

Reconfigurable triple impedance tuner is proposed in [2]. In theory, triple stub topology gives the best Smith Chart coverage with respect to the single or double stub topologies [3]. This tuner is composed of MEMS switches and fixed metal–air-metal capacitors which are optimized to obtain a wide impedance coverage region and bandwidth as much as possible with the minimum number of switched capacitors. It can match low load impedance values between 10-20 Ω at frequencies of 6 and 20 GHz.

Design and implementation of double stub impedance tuner at 1.4 GHz based on SiC varactors is presented in [4]. This tuner is composed of a transmission line and two stubs including RF choke inductors, SiC varactors and DC coupling capacitors. The electrical length of the transmission line inserted between two parallel connected stub determines the impedance tuning region that can be achieved by this configuration. Varactors are controlled by two separate DC voltages. RF choke inductors and DC coupling capacitors provide isolation between RF and DC voltages. Reconfigurability is achieved by applying independent DC voltages to SiC varactors. In order to prevent diode from operating in the forward conduction mode for large signal applications,

minimum applied voltages to varactors are set to 5 V.

A novel spiral topology for a reconfigurable stub tuner with RF MEMS switches is proposed in [5]. Reconfigurable impedance tuning unit consists of Coplanar Waveguide (CPW) subsections, three fixed length transmission lines and eleven RF MEMS switches. Three CPW subsections connected to each other in series are separated by RF MEMS switches. These CPW subsections constitute single stub configuration whose both ends are connected to a fixed transmission line which ends via RF MEMS switches. However, only one end of the third stub is connected to the fixed transmission line in this application. Series connection of three fixed transmission line configuration with stubs including MEMS switches constitute the reconfigurable impedance tuner. This circuit allows transformation from single to double and triple stub tuning by using RF MEMS switches, which provides a wide range of tunable load impedance values. The electrical length of the stubs can be adjusted by setting the switches to single, double or triple stub configuration. This circuit has 11 identical RF MEMS switches between CPW subsections and is optimized for bandwidth between 1 to 3 GHz to obtain wide impedance coverage. The number of switches that are used in the tuner determines tunable impedance range of the loads to be matched. By increasing the number of the switches and CPW subsections, one can obtain wider impedance coverage region, which leads to more complicated control system, low reliability and the increase of the manufacturing cost. Moreover, wide impedance tuning operation results in an increase of the impedance tuner losses which reduces the performance of overall impedance tuner. The impedance coverage results show that this tuner can be used to cover specific parts of the Smith Chart at 1 GHz and 2 GHz.

Double stub tuner is proposed to match an electrically small spiral antenna operating in 800-1500 MHz [6]. Since the antenna electrical size is very small (in the order of 1/12 to 1/8 wavelength) and input impedance varies rapidly in operating bandwidth, impedance tuner must provide wide impedance tuning range without introducing large losses. Double stub tuner is designed by using a fixed stub and banks of capacitors connected to each end of the double stubs. The susceptance at each stub can be altered by changing the states of the MEMS switches to tune the input impedance of electrically small antenna. Two stubs having lengths of d_1 and d_2 are connected to each end of the fixed stub. The lengths of three stubs are optimized by

using Genetic algorithm to obtain the best impedance tuning from 800 MHz to 1500 MHz for impedance matching within the range of $2\,\Omega <$ Real(Z_L) $< 500\,\Omega$ and -500 Ω < Imag(Z_L) $< 0\,\Omega$.

Digitally controlled tunable impedance matching network composed of repetitive two element L section is proposed in [7]. These repetitive two element networks are optimized to obtain broadband impedance tuning (300 - 800 MHz) using lumped reactive elements. The proposed network topology consists of reactive lumped elements, capacitors, inductors and PIN diodes. PIN diodes are attached in series to an inductor or a capacitance in the shunt section. Therefore, two element L network has two different impedance states with respect to the PIN diode bias voltage. The number of two element networks determines the number of different impedance states. The diodes are biased by using 5 V control voltage. Genetic optimization algorithm is employed to determine the reactance values of cascade connected two element network. In this application, the use of the transducer power gain (TPG) is considered for measuring the overall system performance. It accounts for both dissipative losses in the circuit and source/load mismatches. Measurements show that impedance coverage region can be increased by the number of two element L networks. However, when return loss is greater than 10 dB and transducer power gain is below 1.5 dB, the coverage region reduces significantly in high frequency regions especially after 800 MHz.

Another example is reported by Chun and Hong [8]. They designed a special type of transmission line whose characteristic impedance can be varied by changing capacitance on a modified CPW structure. In this method, a third layer is inserted between ground plane and signal line. By connecting two varactors between the third metal and ground plane, real part impedance transformation is proposed with single control voltage. Considering the fact that impedance transformers in the literature requires two control voltages to transform real part of impedance, single control voltage feature makes this impedance tuner very attractive for adaptive impedance matching systems.

The generic low-pass pi matching topology is proposed in [9]. Since electronically tunable inductors are not easy to manufacture, shunt varactor is inserted between two J inverters in a pi matching topology to obtain a variable inductor. J inverters can

be implemented by using discrete components or quarter wavelength transmission lines. Due to the fact that semiconductor type varactors are not suitable for high power applications, they proposed to replace varactors with a set of series connected fixed capacitors and PIN diodes. In order to control this type of tuner, a group of digital signals are needed to switch the set of pin diodes. The values and number of the capacitors in the set of series configuration mainly affect the dynamic range and resolution of the tuned impedances.

Tunable impedance matching network consisting of the cascade connection of variable transformer and phase shifter designed based on all pass networks is proposed by [10]. Phase shifter is employed to change the phase of the reflection coefficient in order to set the normalized input impedance to 1. Then, variable transformer adjusts the phase of normalized impedance to 0 without changing its magnitude. Variable transformer and phase shifter are implemented by using fixed inductors and BST varactors. Full impedance coverage region on the Smith Chart can be achieved by using this impedance tuner configuration.

This section primarily focuses on the brief study of impedance tuners proposed in the literature. Tunable impedance matching circuits designed based on lumped elements and semiconductor varactors offer advantages in terms of low cost and compact circuit design for cell phone applications. Besides, semiconductor based varactors can be easily tuned in cell phone battery supply range (0-3.3 V). They can also provide moderate varactor tuning ratio in this range. Moreover, lumped components and semiconductor type varactors are commercially available from various manufacturers at low costs. Thus, in this thesis, impedance tuner circuits are designed and implemented using lumped components and semiconductor type varactors. Some of the automatic impedance tuning units proposed in the literature is discussed in detail in the following section.

1.2 Previous Work on Automatic Impedance Matching Circuits (AIMCs)

This section is devoted to a brief literature survey of some reported automatic impedance matching circuits implemented based on various approximations. Various types of

automatic impedance matching circuit employing different impedance detection and control algorithms can be found in the literature. Although each automatic tuner performs tuning based on different approaches, they are basically composed of an impedance detection and sensing circuit, an impedance control block, and one form of a tunable impedance circuit as detailed in the previous section.

An adaptive impedance tuning circuit consisting of a bidirectional coupler, a detector, an analog to digital, a digital to analog converter, a control unit, and an impedance tuner is proposed in [11]. In this system, incident and reflected power is determined by using bidirectional coupler to measure how much mismatch is present between the antenna and the power amplifier. Output of the coupled ports are fed to the detector for comparison of the incident and the reflected power levels. Impedance tuner control unit uses a control algorithm for adaptive tuning which takes the digitized output signal from the detector for producing control voltages to the impedance tuner. Two different analog control voltages varying between 0 and 6 V are produced at the output of DAC based on the digital output signals of the impedance tuner control unit. Double stub configuration with two varactor diodes is chosen for impedance tuning unit and varactors are connected to the end of each stub with bias networks. Stub length can be adjusted electronically by changing reverse bias voltage level which results in a variation of the capacitance value. Since the characteristic impedances of all the transmission lines are set to $50\,\Omega$, impedance tuning for a certain range of impedances can not be achieved. However, the electrical length of the transmission line between stubs can be reduced to increase impedance tuning range. Double stub tuner is simulated with two measurement based varactor models by sweeping applied bias voltages from 0 to 6 V. Impedance coverage region providing maximum power transfer to the load is determined by taking complex conjugate of the load side reflection coefficient, S_{22}. Adaptive impedance tuner assumes that load impedance value is $50\,\Omega$ at the initial state of the tuning process. The lookup table is filled with varactor bias voltages which control the impedance tuner for different known load impedances. The control voltages are changed for the load impedance to check whether VSWR improvement is achieved or not. When the impedance tuner control unit detects the improvement, it accepts the impedance corresponding to the changing control voltage as the new load impedance, and continues to apply different voltages to obtain better VSWR with re-

spect to previous state until the minimum value of VSWR is found. This impedance tuner is capable of tuning mismatches up to VSWR = 81 at 1.95 GHz with very small insertion loss.

Automatic impedance matching circuit compensating for the input impedance variations of a normal mode helical antenna due to human operator at 160 MHz frequency is proposed in [12]. Antenna input impedance variation with respect to the distance between the user's abdomen and the helical antenna is investigated by employing method of moments technique. EM interaction calculations show that the reactive part of the antenna input impedance increases depending on the degree of proximity between the user and the helical antenna. Figure 1.2 depicts the antenna input impedance results calculated for different distances between the helical antenna and the user's abdomen.

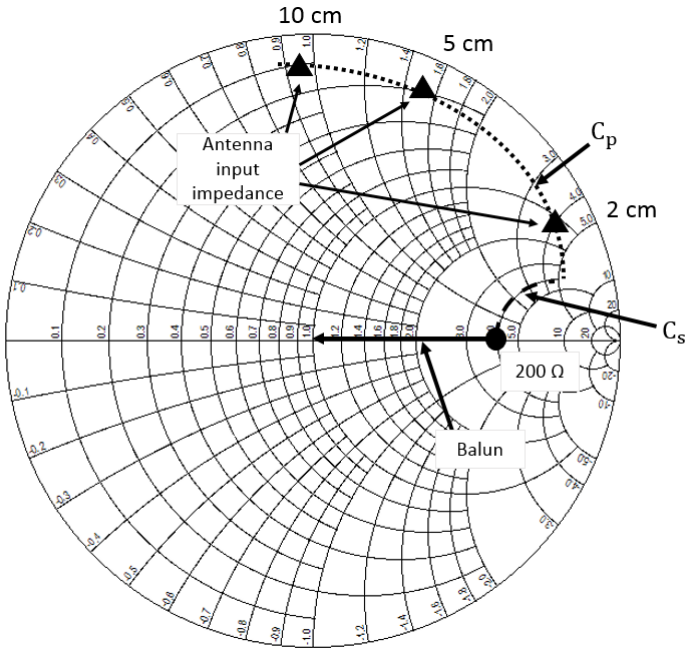

Figure 1.2: Variations of the antenna input impedance depending on the degree of proximity and impedance tuning method

The steepest gradient algorithm is employed in an adaptive tuning technique for achieving the automatic control of the antenna input impedance variations. Coaxial cable is attached to the helical antenna working in balanced operation mode through U type balun with two series and two parallel varactor diodes. As shown in Figure 1.2, the antenna input impedance including the effects of human interaction is first

tuned in the equi-conductance circle by parallel connected varactor from the points represented by black rectangles to a impedance point located on 200 Ω constant resistance circle with an inductive reactance. Then, the series connected varactors provide a pure resistance of 200 Ω by eliminating the inductive reactance. The U type 1:4 balun is utilized as an ideal transformer to obtain impedance transformation from 200 Ω to 50 Ω. Automatic tuning unit is composed of a directional coupler and the rectifier unit including a diode, a resistor and a capacitor. Reflected signal is detected by the directional coupler whose coupling port which dynamically monitors the reflections from the antenna is connected to the rectifier circuit. The output of the rectifier circuit is used as a control voltage for the steepest gradient algorithm. Estimation function is defined as the absolute value of the difference of the rectifiers output voltage with exponent q in the case of perfect match and mismatch conditions. Experimental results show that helical antenna has a resonance frequency at 160 MHz for free space condition and the resonance frequency of the antenna moves to low frequencies due to the presence of human body at a certain distance. Initially, all control voltages are adjusted to the respective values corresponding to the free space condition. Convergent responses obtained for control voltages and output voltage of the rectifier circuit are plotted for a certain distance (2.5 cm) between human body and the helical antenna by increasing the number of iterations. The control unit running the steepest gradient algorithm sets the control voltages based on the rectifier output voltage. This automatic tuning unit gives a good impedance matching at 160 MHz.

An automatically controlled tunable impedance matching network designed based on the Planar Inverted F Antenna (PIFA) measurements is presented in [13]. It offers tuning capability for multiband applications in a cell phone system. The presence of body in the vicinity of the PIFA leads to the resonance frequency shifting to a lower frequency which results in an increase in the imaginary part of the antenna feed impedance. In this study, series LC tunable impedance matching network consisting of a fixed inductor and MEMS based switched capacitor array is proposed to remove the effects due to the user interaction. Since series LC network contains only one tunable element connected in series to antenna feed impedance, it can not improve the real part impedance variations.

Capacitor tuning ratio is derived for RF MEMS switch array by taking into consider-

ation both minimum and maximum operating frequencies in the multiband operation. The input impedance phase information of the network connected to the output of the power amplifier is used for tuning the reactive part variations. Output voltage and current of the power amplifier unit is utilized to determine the phase difference between the voltage and current at the input side of the impedance tuner. They are fed to phase detection unit including the limiter and mixer circuit to obtain phase information. Then, phase detector output is passed through the limiter to derive sign of the phase difference whose polarity adjusts the counter unit to change the capacitance state of the impedance tuning unit. Each element in the capacitor array is controlled by high bias voltages applied from a high voltage generator. The bias resistor and DC blocking capacitors connected in series to RF MEMS switches prevent the mixing up of the RF and DC control voltages, and provide RF isolation. Loss resistance of the fixed inductor and bias resistors predominantly causes degradation in the efficiency of the transmitter. Insertion loss of the automatic tuning unit (ATU) is measured at both high and low band operation modes which is nearly 0.5 dB. With reasonable insertion loss, ATU compensates for the extreme case impedance variations arising from the mismatch effects coming from the interaction between the antenna and the user. Figure 1.3 depicts the load impedances simulated with the automatic impedance tuning network and tuning method along the constant R circle on the Smith Chart. Once automatic impedance tuning is accomplished, tuned impedances are accumulated on the real axis of the Smith Chart.

An automatic impedance tuning system for the cell phone antennas consisting of a tunable impedance matching circuit, an impedance sensing unit and two controller units is presented in [14]. Tunable impedance matching circuit is composed of a tunable transformer and a variable reactance circuit connected to each other in cascade. It offers tuning in the real and imaginary impedance domain, respectively, as depicted in Figure 1.4. In this application, two step impedance transformation requires a controller unit including two separate integrators whose outputs produce control voltages for both real and imaginary part tuner sections. Impedance sensing unit consisting of two identical reactances connected to each other in series and three RF peak detectors generates the signals related to both real and imaginary part fluctuations. Three log peak detectors are connected to the common node and uncommon nodes of two

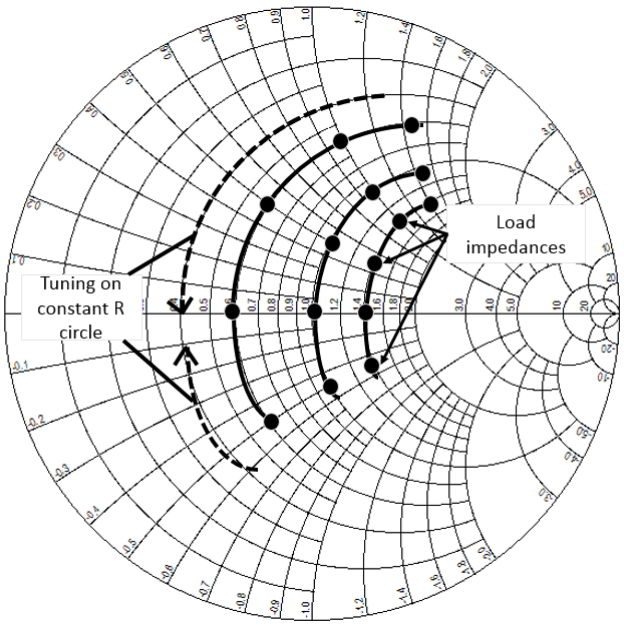

Figure 1.3: Impedance tuning with series LC tuner

series inductors which produce the amplitude information of RF signals. Log peak detectors include a few passive components (resistor, capacitor), and a schottky diode providing detection of RF signal magnitudes. An opamp and simple diode circuitry take the logarithm of the magnitude of RF signal. Since the log peak detectors pull very small currents from the common node and uncommon nodes of two series inductors and approximately the same current passes through the two series inductors, the outputs of the log peak detectors are proportional to the impedances seen from those nodes. The output voltages of the log peak detectors attached to the uncommon nodes are subtracted from each other to generate the signal setting the imaginary part of the tuned impedance to zero. The log peak detectors connected to the leads of the first inductor generate the output voltages subtracted from each other to obtain conditional information about the real part of the tuned impedance.

A control system is composed of two nested loops tuning the real and imaginary part of the antenna feed impedance. The outer loop adjusts the reactive part to zero, which controls a shunt or series connected tunable element. The inner loop controls a T-matching network (tunable transformer) including three tunable reactive branches connected in T type configuration. The overall system is tested using a PC running control algorithm and Maury tuner. The measurement results are plotted on the Smith

Chart for complex antenna feed impedances whose real and imaginary parts vary between 5Ω to 100Ω and -60Ω to 100Ω, respectively.

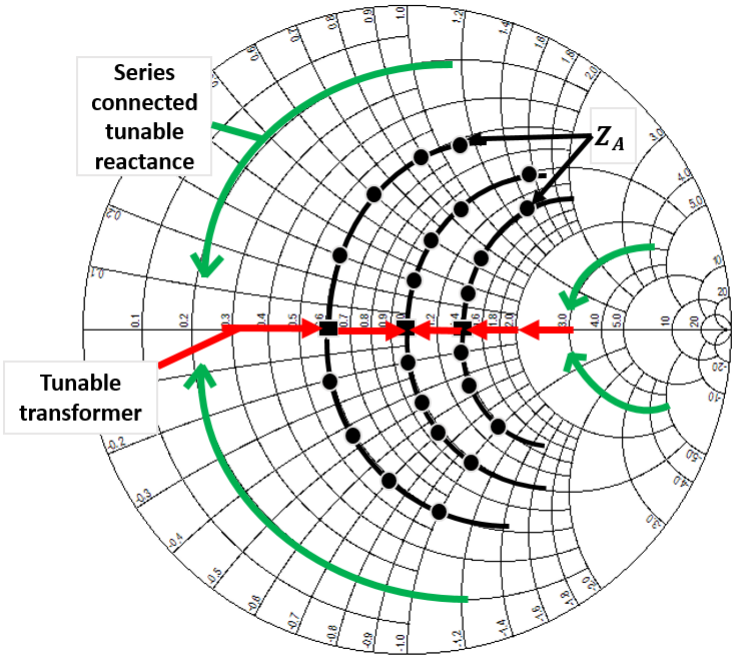

Figure 1.4: Impedance tuning with tunable transformer and series connected tunable reactance

The automatic impedance matching system adopting impedance tuning based on the phase difference between incident and reflecting waves is presented in [15]. The automatic impedance unit basically consists of an impedance tuner, a control block and a mismatch detector capable of measuring the sign of the phase difference between the incident and reflected waves. Since the presence of a body in the vicinity of the antenna significantly increases the reactive part of the antenna input impedance, a fixed inductor connected in series to a capacitor bank including RF MEMS switches and capacitors is used in the impedance tuner circuit. Directional coupler is fixed between power amplifier (PA) and the impedance tuner unit, which detects the incident and reflected waves. These waves are fed to the mismatch detector unit including a 90 degree phase shifter, limiters and a Gilbert Cell mixer. The output of the mismatch detector is connected to the limiter in order to obtain the sign of the phase difference. Based on the sign of the phase difference, the level shift unit produces high voltages in order to tune the mismatches by actuating RF MEMS switches in the capacitor bank. Since series tunable reactance unit is employed for tuning, it can only compensate for

the reactive part variations in antenna feed impedance.

Automatic impedance tuning network utilizing two step impedance transformation with analog tuning method is presented in [10]. Impedance tuner is composed of a 180 degree phase shifter and a variable transformer which tune the phase and the magnitude of the reflection coefficient. Firstly, 180 degree phase shifter dynamically changes the reflection coefficient phase on the constant VSWR circle as depicted with a green line in Figure 1.5 until the normalized magnitude of the load impedance is set to 1. Then, variable transformer adjusts the phase of the input impedance of

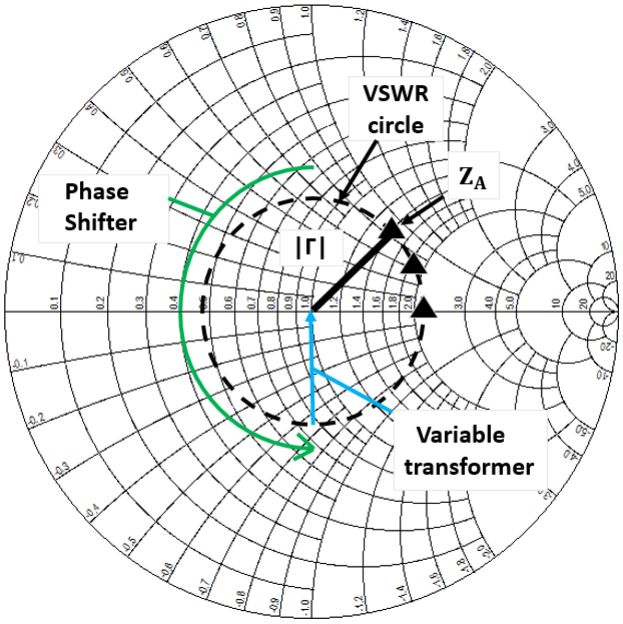

Figure 1.5: Impedance tuning with phase shifter and variable transformer

180 degree phase shifter to zero without affecting its magnitude as shown with a blue line in Figure 1.5. Two step transformation demands two control voltages for both impedance magnitude and phase tuning. A log amplifier, a mixer and a quarter wavelength transmission line are used in the impedance sensing unit to detect the impedance magnitude and phase variations. The quarter wave length transmission line is fixed between power amplifier and the impedance tuner to sense voltage magnitudes and phases at each end of the transmission line. The log amplifier is utilized to compare the signal magnitudes that is available at both ends of the $\lambda/4$ transmission line. It produces the error voltage for impedance magnitude variations. Each end of the transmission line is connected to the mixer in order to detect the phase of the

load impedance. When the input impedance of the impedance tuning unit is set to 50 Ω, the output voltages of log amplifier and mixer circuit become zero, which are fed to the opamp integrator circuits.

This section is devoted to the brief study of automatic impedance tuner systems proposed in the literature. The various types of automatic impedance tuning units designed based on analog and digital tuning techniques are discussed in detail. Since antenna input impedance variations can exist in both real and imaginary domain due to user interaction between cell phone and body, automatic impedance tuning units compensating for the effects of reactance fluctuations can not improve the real part impedance variations. In this thesis, the automatic impedance tuning units offering an independent control capability in real/imaginary and magnitude/phase domain of the antenna input impedance is employed to compensate for impedance fluctuations due to these interactions. Using MEMS based switched capacitor array in impedance tuner unit requires high control voltages to turn on MEMS switches. Since cell phone battery supplies limited tuning voltage (0-3.3 V), high voltage generation brings up extra power consumption and compactness problems. However, impedance tuners designed based on semiconductor type varactors are very suitable for cell phone applications. Since there is a small space for automatic impedance tuner unit in a cell phone, the circuit dimensions of impedance tuner, detection and sensing units should be kept as small as possible. This requirement restricts the usage of some proposed tuner configurations in GSM band. Thus, the design of automatic impedance tuning units using lumped components seems to be more reasonable than using stub based tuners. The insertion of a directional coupler between the transmitter/receiver and the antenna is the most common technique for sensing the variations of the reflection coefficient in practice. The amount of mismatch is monitored with this device by comparing coupled signals on the transmitter/receiver and the antenna side. Moreover, this device is commercially available as a chip component from various manufacturers at low costs. Besides, these chip couplers offer many advantages in terms of compact size, low insertion loss, and high directivity. The compact size feature of chip couplers makes it very attractive for cell phone RF front end applications where the available space is limited. Instead of using many components to achieve impedance detection, in practice the usage of single off shelf chip device

implementing impedance detection functionality is reasonable. Various manufacturers offer suitable electronic chip components capable of operating in the cell phone battery supply range (0-3.3 V). Besides, these components are able to meet power consumption requirements of a cell phone and functionality of impedance detection unit. Thus, it is more reasonable to employ an off shelf component capable of implementing impedance detection rather than the design of each sub block in detection unit separately. In this thesis, automatic impedance tuner circuits are designed and implemented by using lumped components, semiconductor type varactors, couplers and offshelf chip detector. The following section is devoted to the design objectives and limitations related to the automatic impedance tuning system.

1.3 Design Objectives and Organization of the Thesis

This section mainly focuses on the design objectives and general overview of the thesis. The basic goal of this thesis is to design and fabricate an automatic impedance matching network using semiconductor based (also known as Si varactor) varactor technology with an analogue tuning mechanism. The design objectives of this thesis are given as follows:

1. Impedance tuner which is used as a part of RF front end should be designed to have a low insertion loss and low insertion loss variation in the tuning range.
2. Since impedance tuner is placed in a cell phone, impedance tuner size should be very small for RF front end usage.
3. Due to the fact that maximum supply voltage of cell phone is 3.3 V, the tuning range of the impedance tuner should be sufficient enough to be able to compensate for the antenna input impedance variations with the control voltage range of 3.3 V or less.

An automatic impedance tuning network consisting of a directional coupler, an envelope detector, a simple integrator circuit with an opamp and a single varactor connected in series to the antenna input is proposed in this thesis. Reflected signal from the antenna terminals due to the mismatch is detected by the directional coupler. The

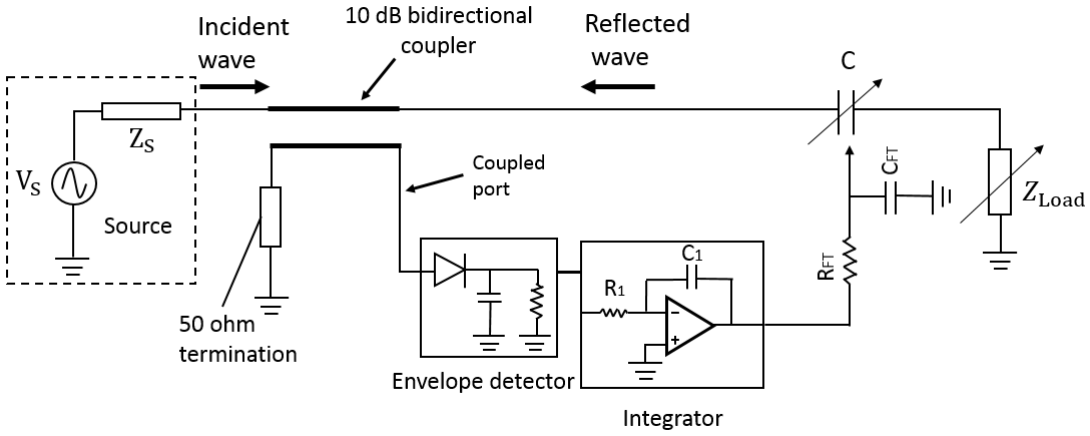

Figure 1.6: General block diagram of the automatic impedance tuner

port to which the reflected signal is coupled is connected to the envelope detector whose output can be used as a control voltage for the varactor as shown in Figure 1.6. The control unit is composed of an opamp, a resistor, and a capacitor which provides analog tuning with time varying control voltage based on the output voltage of the envelope detector (i.e error signal). Since the impedance tuner circuit includes a single varactor connected in series to the antenna terminals, it can only compensate for the mismatches of the reactive part as depicted in Figure 1.7. Although this automatic tuning unit offers advantages in terms of simplicity of detection and control circuit, compactness, and low cost, it provides real time tuning in a limited coverage region. Thus, it is required to design tunable circuits which offer reconfigurability in real and imaginary domain of antenna feed impedance to cover a wide impedance region on the Smith Chart.

Another automatic impedance tuner adopting the combination of two step impedance transformation is proposed in this study. To achieve two step transformation with circuit blocks, a tunable phase shifter and a T-matching sub-blocks including fixed inductors and varactors are connected to each other in cascade as shown in Figure 1.8. As depicted in Figure 1.9, detuned antenna impedances (black triangles) located at an arbitrary point on the Smith Chart can be moved along constant VSWR circle to a point which resides in the horizontal axis of the Smith Chart as shown with green arrows. Then, the real impedance can be moved along the horizontal axis to the center point of the Smith Chart as shown in Figure 1.9.

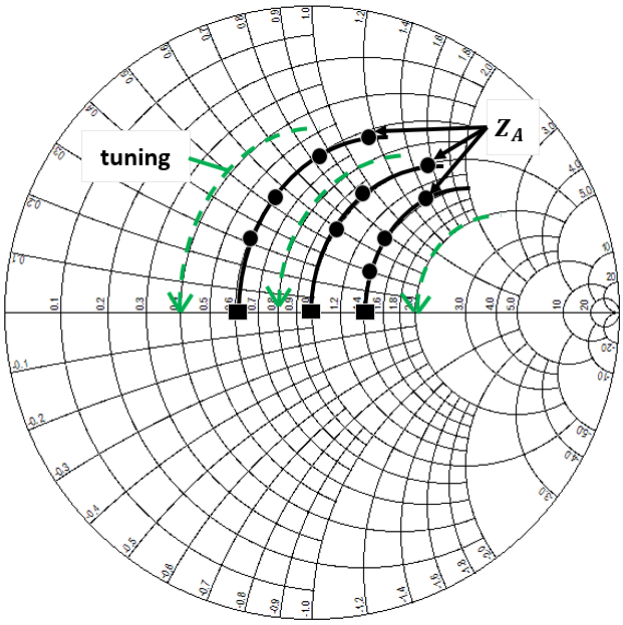

Figure 1.7: Impedance tuning with single series connected varactor

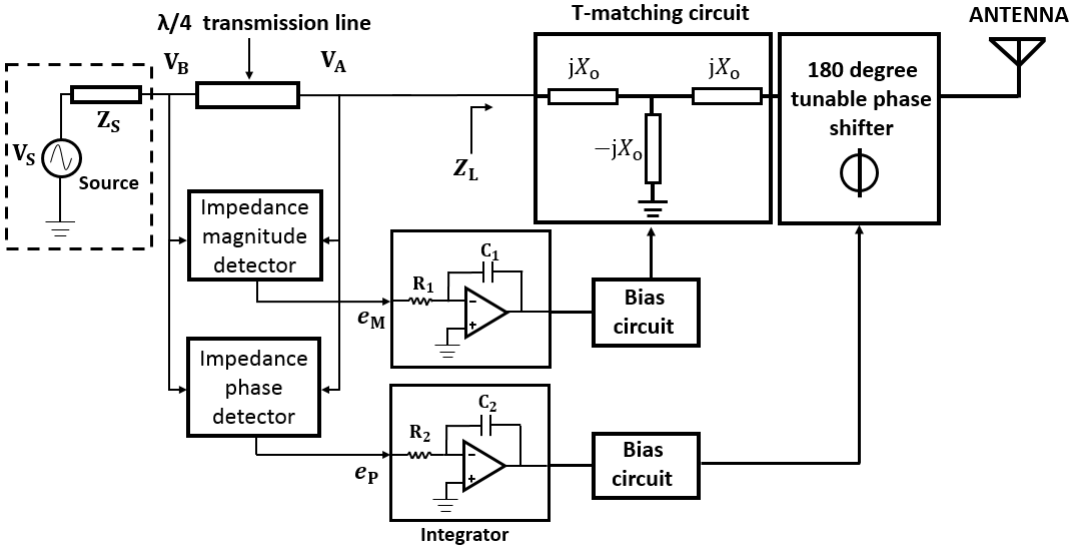

Figure 1.8: General block diagram of the automatic impedance tuner adopting two step impedance transformation

The tunable phase shifter changes continuously the phase of the reflection coefficient of antenna feed impedance on constant VSWR circle with applied bias voltage until the impedance phase is set to 0. T-matching circuit consisting of tunable series and shunt branches can transform the real part impedance when series and shunt reactances are set to the identical inductive and capacitive reactance values, respectively. In addition, the tuning range of each branch and phase tuning range of tunable phase shifter determine the limits of impedance coverage region and the insertion loss introduced by this configuration.

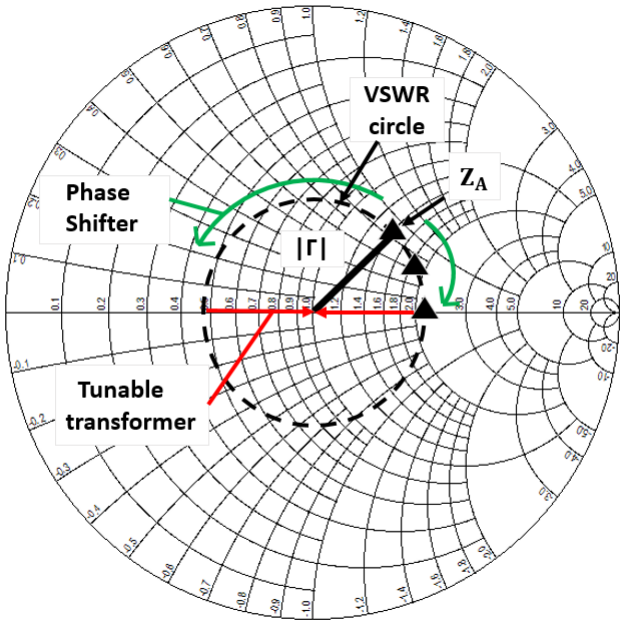

Figure 1.9: Impedance tuning with tunable transformer and phase shifter

A Planar Inverted F Antenna (PIFA) will be used to showcase the functionality of the system. In the second section, PIFA composed of shorting pins, tapered patch and ground plane is designed with WIPL-D Pro 3D electromagnetic simulation software based on Method of Moments technique [16]. Return loss variation is plotted with respect to frequency in GSM band to determine the bandwidth and resonance frequency of the PIFA. Besides, antenna radiation patterns in azimuth and elevation plane are plotted on the polar coordinate system. Since the user interaction between antenna and human body affects mainly the antenna input impedance depending on the proximity between them, PIFA is implemented based on simulated dimensions to investigate this interaction in GSM band.

An impedance detection and control approach similar to the one studied in [10] is presented in Chapter 3. Two envelope detectors and a logarithmic amplifier are used for impedance magnitude detection. The cascade connection of a mixer and a low pass filter is utilized for impedance phase detection. Impedance tuners are simulated in a closed loop impedance tuning system with magnitude and phase detection units for various antenna input impedances. Reflection coefficient variations with time are plotted on the Smith Chart and the rectangular coordinate system.

Impedance sensing, detection circuit with simple control network are implemented and measurement results are given in Chapter 4. Impedance tuner consisting of a 90 degree tunable phase shifter and a variable transformer is designed based on semiconductor varactor technology. Moreover, two identical 10 dB directional couplers are connected to each other in series in order to sense the magnitude and the phase of the reflection coefficient. AD8302 is utilized as a reflectometer with attenuators and bidirectional couplers. The output voltages of AD8302 are fed to simple integrator circuits to control both magnitude and phase of the reflection coefficient. The automatic impedance tuner consisting of the impedance tuner and the impedance detection and sensing unit is tested for various fixed load impedances connected to the antenna port. In order to measure the efficiency of impedance tuner, relative transducer gain which accounts for both the source/load mismatch and the dissipation loss of the impedance tuner is plotted for different load impedances in GSM band.

Chapter 5 is devoted to the conclusion of the thesis and some future improvements about the impedance tuning unit, insertion loss and power drawbacks of the impedance tuners.

CHAPTER 2

PLANAR INVERTED F ANTENNA

2.1 INTRODUCTION

In the last two decades, the rapid development of integrated chip technology enables electronic device manufacturers to fabricate low cost, small sized electronic devices such as cellular phones, laptop computers, PDAs, etc. Since these devices are small in size, portable and light in weight, new type of antennas must be designed to meet these requirements.

Planar Inverted F Antenna (PIFA) is the most widely used antenna in mobile communication industry due to its small size, compactness and low weight. Moreover, easy fabrication, simple structure, low manufacturing cost and easy feeding can be considered as other advantages which make this antenna a good candidate for mobile communication systems. Besides, it has a moderate gain in both vertical and horizontal polarizations, which makes it very popular in mobile communication systems where antenna position is not fixed and reflections exist from certain objects like buildings, cars, etc.

The Figure 2.1 depicts the general representation of the Planar Inverted F Antenna. PIFA is generally composed of a ground plane, a top metal plane or radiating patch, shorting plate or pins and a feeding wire which is connected to a coaxial feeding cable. The radiating patch and inner conductor of coaxial feed are connected through feeding wire. The outer conductor of coaxial cable is attached to the ground plane of the PIFA. The existence of the ground plane enhances the radiation characteristics of the antenna and reduces partially the harmful effects of electromagnetic power

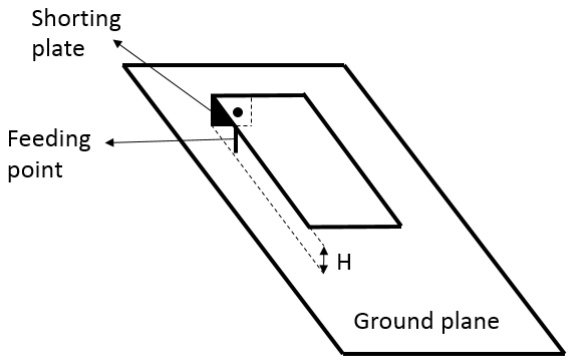

Figure 2.1: Representation of the general PIFA in free space

absorption by the body/head [17].

A typical PIFA antenna would have a very narrow bandwidth severely limiting its use in today's wide bandwidth applications. Several bandwidth enhancement methods can be used in PIFA design to achieve a wider bandwidth. The most common method is to increase the distance between the radiating patch and the ground plane. Unfortunately, this leads to an increase in the antenna volume. Bandwidth can also be improved by inserting a dielectric material having high permittivity, or by adding some loss to the antenna which results in degradation of antenna performance. Alternatively, a tapered patch proposed in [18] can be utilized to increase the bandwidth of PIFA. In spite of these short comings, PIFA is still a very good choice for many handheld applications. Thus, a tapered PIFA configuration is designed, simulated and implemented in the scope of this thesis work to measure human hand and head effects in GSM band. The following section focuses on the design, simulation and implementation of the tapered PIFA operating in GSM band. This is followed by the investigation of user interaction between the body and antenna.

2.2 Simulation and Measurement of PIFA in GSM Band

The designed PIFA in [19] which consists of a tapered patch, a ground plane, a feeding point, and shorting pins is simulated in free space at 900 MHz using WIPL-D Pro 3D EM simulation software based upon Method of Moments technique. Figure 2.2 shows the configuration of PIFA with a set of specific design parameters such as ground plane width and length, distance between tapered patch and ground plane,

patch width, and length, etc. The same design parameters proposed in [19] for the PIFA are given briefly as follows : L_a = 75 mm, W_a = 54 mm, H = 10 mm, W_b = 11 mm, W_a = 54 mm.

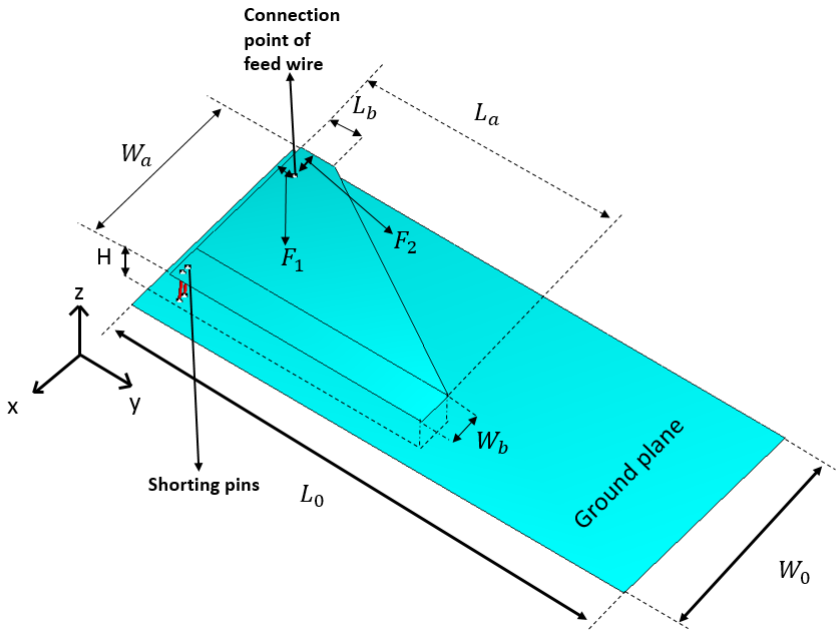

Figure 2.2: Configuration of the designed PIFA

The feeding wire is attached to the tapered patch at a point whose distance from the edges of tapered patch is F_1 = 4.4 mm and F_2 = 9 mm as shown in Figure2.2. The ground plane width and length are taken as W_o = 66 mm, L_o = 146.5 mm, respectively. There is no solid dielectric material between the tapered patch and the ground plane. The gap between them is air-filled.

Simulation results show that return loss is below -10 dB between 840 MHz and 960 MHz as shown in Figure 2.3. The resonance frequency of tapered PIFA is 900 MHz and at that frequency the simulated input impedance is 39-11jΩ. To verify the simulation results, tapered PIFA is fabricated using metal sheets and wires as illustrated in Figure 2.4. The inner conductor of the SMA connector is soldered to the tapered patch via a metal wire for the signal feed and the outer conductor of it is soldered to the ground plane of the antenna. The input return loss of the fabricated PIFA is measured in free space and compared with simulations in Figure 2.3. The simulated 3D radiation pattern is shown in Figure2.5. The radiation pattern of simulated antenna in the azimuth and elevation plane are plotted in Figures 2.6 and 2.7, respectively. In

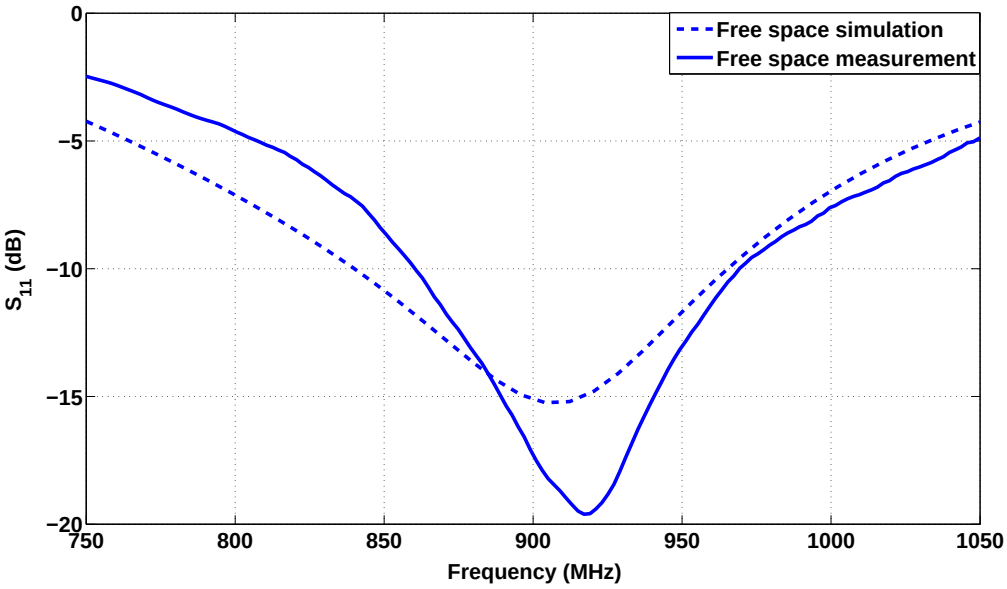

Figure 2.3: Return loss variation in GSM band

Figure 2.4: Photograph of the implemented PIFA

this section, proposed PIFA which resonates at 900 MHz is simulated and fabricated. The main objective in this section is to fabricate tapered PIFA to analyse human body effects in the GSM band. In the following section, the user interaction between PIFA and the body is discussed briefly based on the previous studies. The return loss of the fabricated PIFA is measured for various holding positions to investigate the amount of the antenna input impedance mismatch introduced by the body.

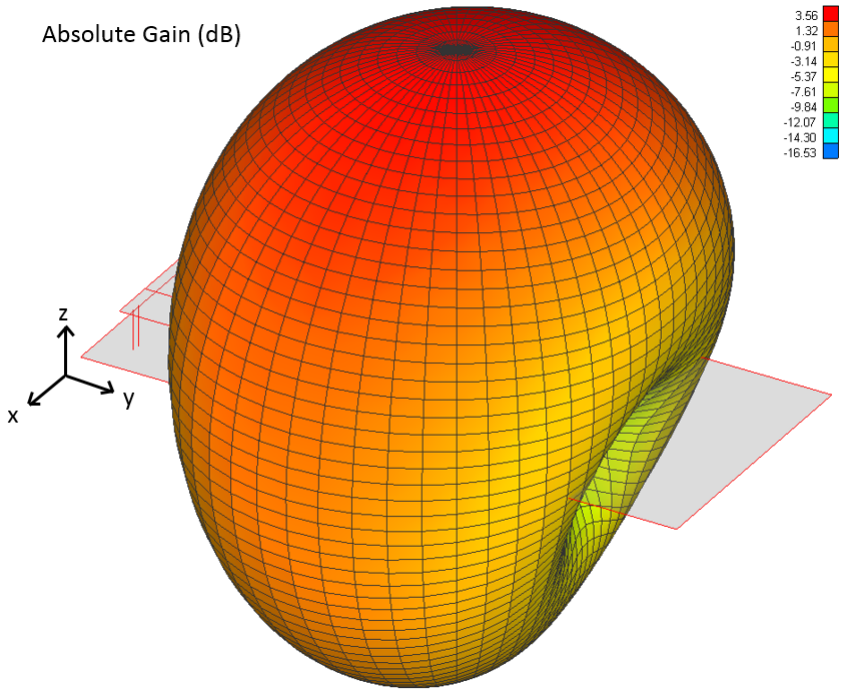

Figure 2.5: 3D radiation pattern of the simulated PIFA at 900 MHz

2.3 User Hand and Head Effects on PIFA in GSM Band

It is well documented in the literature that the input impedance of a PIFA varies depending on the degree of interaction between the user and the antenna [20], [21]. It is also known that this interaction detunes the antenna resonance frequency which affects mainly the reactive part of the PIFA input impedance [14]. Moreover, according to [14], reactive part of the antenna input impedance is typically much more sensitive to handling positions than real part of the antenna input impedance. Antenna input impedance variations occurring due to user and cell phone interaction cause an impedance mismatch between antenna and the RF Front end. In case of transmission,

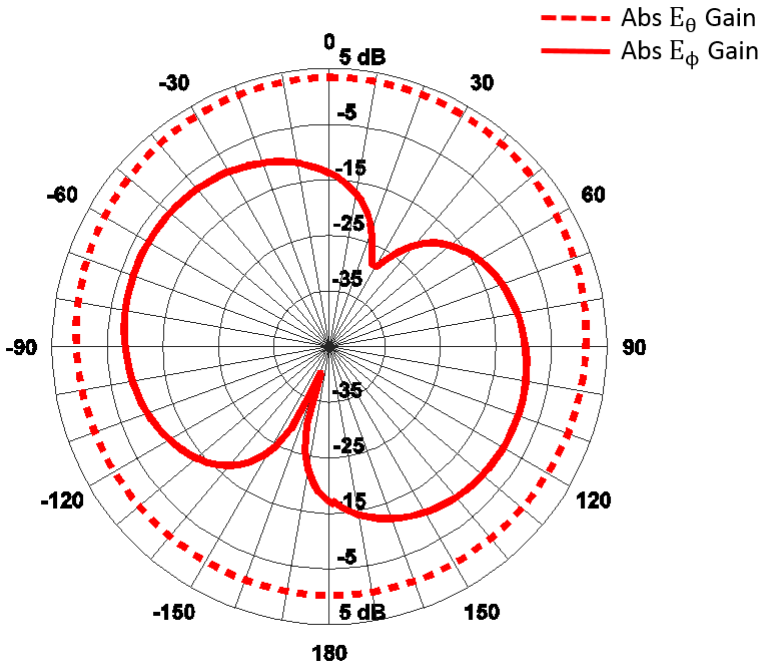

Figure 2.6: 2D radiation pattern in azimuth plane (xz plane) at 900 MHz

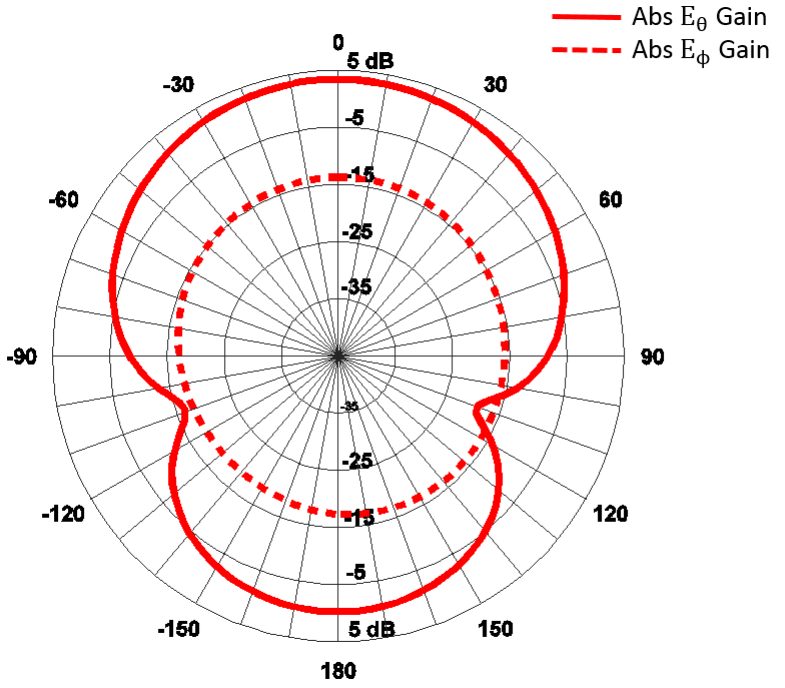

Figure 2.7: 2D radiation pattern in elevation plane (yz plane) at 900 MHz

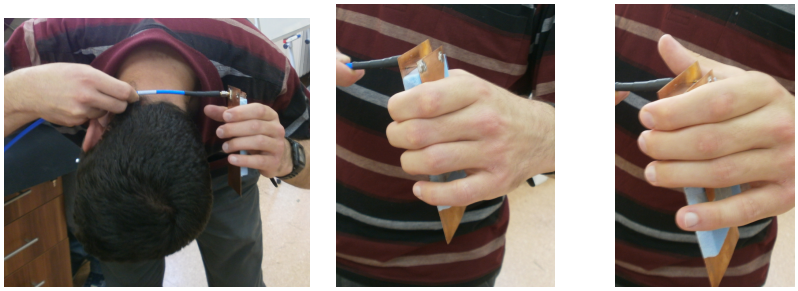

Figure 2.8: Representation of various holding positions of PIFA

such impedance mismatch leads to the increase of the reflected power from the antenna which reduces the link quality. Besides, it causes a shorter battery lifespan due to excessive power consumption [22]. In the receive path, it leads to degradation in the signal to noise ratio (SNR) which results in low data transmission rate in a certain bandwidth.

Since the user hand and head compose of different kinds of body tissues whose dielectric constants vary considerably, it is hard to model them in the simulation environment. To design a suitable impedance tuner which compensates for impedance variations occurring due to the presence of user hand and head in the vicinity of PIFA, the antenna input impedance is measured for various holding positions as shown in Figure 2.8. Figure 2.9 depicts the PIFA input impedance detuning region on the Smith Chart in GSM band due to the user hand and head effects. The measurement results show that the interaction between the user and PIFA causes dramatic changes in the imaginary part of its input impedance which is in agreement with the measurement results of the previous studies[14]. It can be easily seen from Figure 2.9 that user interaction mainly increases the reactive part of the antenna input impedance.

In this section, the return loss of the fabricated PIFA is measured for different holding positions to detect the mismatched impedances due to the body in the frequency band of 880-920 MHz. These measurements show that the mismatched impedances are accumulated on the first quadrant of the Smith Chart. User interaction primarily increases the reactive part of the antenna input impedance which reduces the resonance frequency of it. In the following chapter, automatic impedance tuning circuits are designed and simulated to dynamically compensate for these mismatches by using analog impedance tuning techniques.

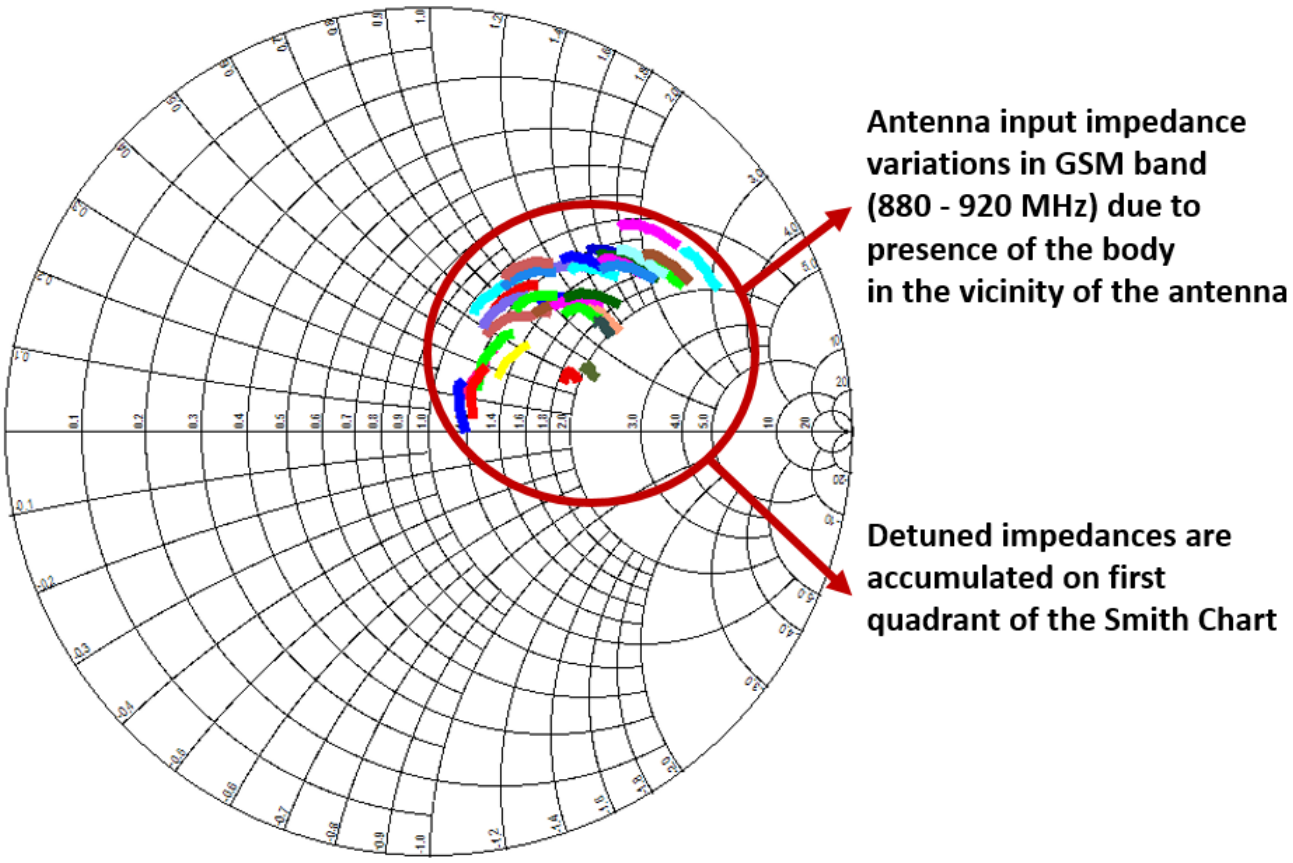

Figure 2.9: Antenna input impedance measurements in GSM band for various holding positions of PIFA

CHAPTER 3

AUTOMATIC IMPEDANCE TUNING CIRCUITS

This chapter is devoted to the design and simulation of automatic impedance tuning networks which dynamically compensate for the antenna input impedance variations by using analog tuning techniques. User interaction between the cell phone and the body substantially causes the impedance fluctuations, which mainly affects the operating conditions of RF front end units. These fluctuations degrade the power efficiency of a cell phone, and the maximum radiated power [23]. Automatic impedance tuning units are necessary in GSM systems because they can dynamically remove the effects of impedance fluctuations by using a reconfigurable tuner.

The automatic impedance tuning unit proposed in Section 3.1 utilizes the reflected power from the antenna to remove the inductive mismatches. It consists of a directional coupler, an envelope detector, an integrator, and a varactor. Since a single varactor is connected to the antenna in series, it can only compensate for the inductive mismatches. A closed loop tuning system is simulated with commercially available software to investigate the time variation of the reflection coefficient and the control voltage for the varactor in the automatic tuning process.

In Section 3.2, two different impedance tuning techniques are employed to tune dynamically both the magnitude and phase of the antenna input impedance in a sequential manner. Each of these tuning techniques is realized as two separate reconfigurable circuit blocks connected to each other in cascade. Since each tuning unit requires feedback information about the impedance magnitude and phase variation to maintain real time tuning, the design of impedance magnitude and phase detection units is also discussed in detail. Then, each impedance tuning unit is combined with the

impedance detection and control blocks to implement overall automatic tuning circuit. This is followed by the simulation of the overall automatic impedance tuning unit with these tuners.

3.1 Reflection Coefficient Magnitude Detection and Minimization

This section focuses on the design and simulation of an automatic impedance matching circuit which measures the amount of mismatch by using the reflected power level. It is composed of a simple impedance detection and a control circuit which provide an opportunity to design a low cost and compact circuit for cell phone applications. A general block diagram of the proposed automatic impedance tuning unit is depicted in Figure 3.1. It consists of a 10 dB directional coupler, an envelope detector, a single varactor, a simple control, and a bias unit. The main objective of this tuning unit is to

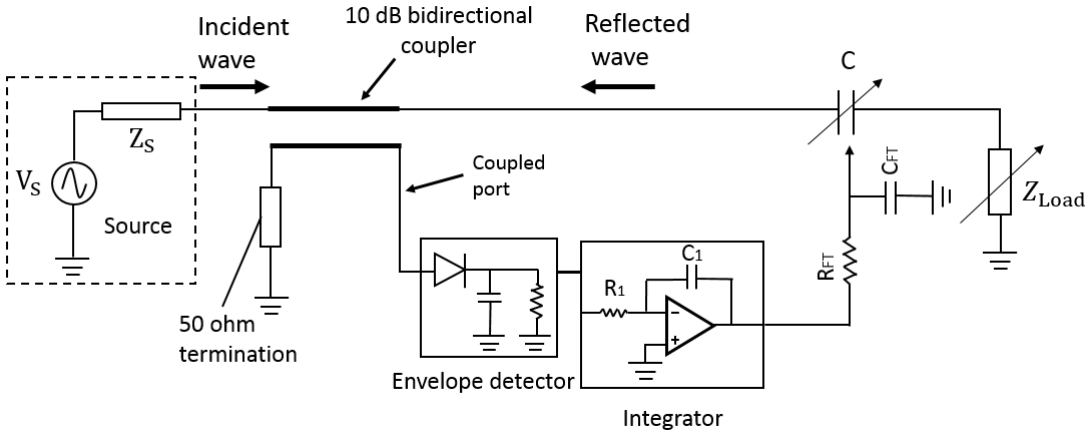

Figure 3.1: General block diagram of the automatic impedance tuner

reduce the reflections from the antenna due to inductive mismatches. It provides an impedance correction in imaginary axis of the antenna feed impedance and employs only one varactor connected to the antenna in series. The amount of mismatch can be determined by the output signal level of the envelope detector. The output voltage of the envelope detector is sensitive to reflected power variations from the antenna, which can be used as a control parameter for real time tuning. Theoretically speaking, when the perfect matching condition is maintained, there is no available reflected power from the antenna side which results in zero output voltage at the output of the envelope detector. Therefore, the output of the envelope detector (i.e error signal) can

be fed to an integrator including an opamp, a capacitor and a resistor in order to obtain control voltage as shown in Figure 3.1. The simulation models of subunits consisting of the overall automatic impedance tuner and simulation results of this tuner are discussed in more detail as follows.

Directional couplers are widely used as passive components in RF and microwave control circuits for isolation, separation of signals etc. It is well documented in the literature that one of the most common methods to measure impedance mismatches is to fix a directional coupler between the transmitter/receiver and the antenna. It provides the samples of signals from both source and antenna side as a function of coupling ratio C, when it is fixed between antenna and source. The coupling ratio is the value that indicates how much power is transferred to the coupling port with respect to the incident power at the input port. The coupled power from the antenna side can be defined as shown below:

$$P_r = K|\Gamma|^2 P_i$$

in which K is a constant determined by coupling ratio. P_i and $|\Gamma|$ are the incident power from the source side and magnitude of the reflection coefficient of antenna input impedance, respectively. Ideal coupled transmission line in Advanced Design System (ADS) is utilized to model ideal characteristics of 10 dB directional coupler, which simply demands even-odd mode characteristic impedance, the electrical length of the line and operating frequency values for simulation. Even and odd mode characteristic impedance values are calculated for 10 dB ideal coupled transmission line based on the equations relating the coupling coefficient (k_c) and characteristic impedance (Z_o) as defined below :

$$C = 20 \log k_c \tag{3.1}$$

where k_c is the coupling ratio and C is the amount of coupling in dB.

$$Z_{oe} = Z_o \sqrt{\frac{1 + k_c}{1 - k_c}} \tag{3.2}$$

$$Z_{oo} = Z_o \sqrt{\frac{1 - k_c}{1 + k_c}} \tag{3.3}$$

where Z_{oe} and Z_{oo} are even and odd mode characteristic impedances, respectively. Since the previous studies and our PIFA measurements show that the user interaction between PIFA and the body significantly increases the reactive part of the antenna input impedance at GSM band, a single BST varactor connected to the antenna in series can be employed to dynamically compensate for the inductive variations in the imaginary domain as depicted in Figure 3.2. Tuning series capacitor value varies the reactive part of the mismatched impedance over circle segments of constant resistances as shown in Figure 3.2. C-V characteristic curve of a BST varactor is plotted as shown in Figure 3.3 based on its characteristic equation. It is modelled by using symbolically defined device (SDD) block in ADS.

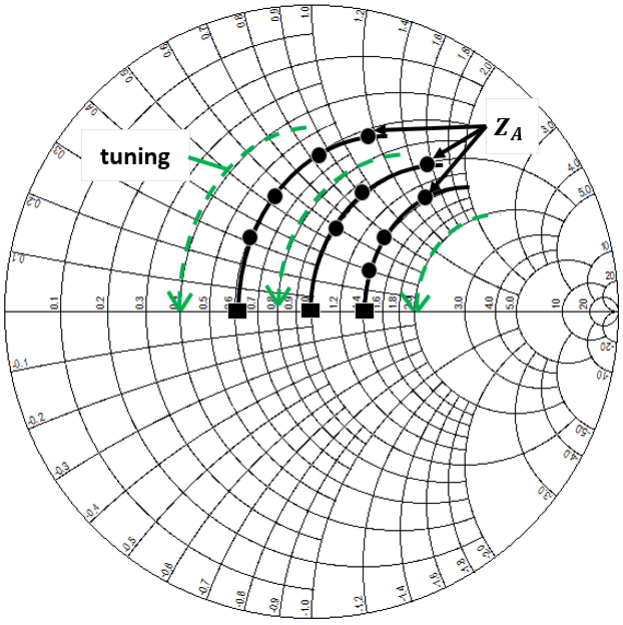

Figure 3.2: Impedance tuning with single varactor connected to the antenna in series

SDD blocks enable the designer to model equation based linear and non-linear components or circuits such as logarithmic amplifiers, mixers, various kinds of varactors, transistors etc. S-parameter analysis is performed on BST varactor model which is adopted to the specification of this study by sweeping DC bias voltages between -18 to 18 V to determine capacitance variation with bias voltage as depicted in Appendix Figure A.1. Bias circuitry including an RF choke inductor and a DC block capacitor is attached to the BST varactor model to perform S parameter simulation properly. The RF choke inductor and DC block capacitor are used to insert DC bias without affecting the RF signal.

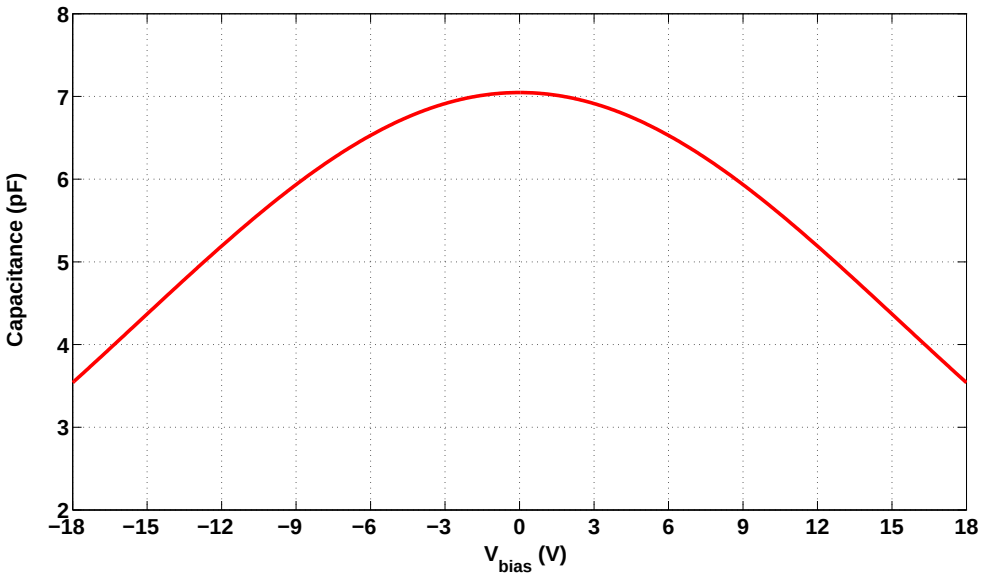

Figure 3.3: Capacitance variation of BST varactor model with DC bias voltage

Envelope detector including a diode, a capacitor, and a resistor is attached to the port where the reflections are coupled from the antenna side due to the inductive mismatches. The output of the envelope detector is fed to the simple inverting opamp integrator circuit which produces a control signal via simple RC bias circuit for BST varactor as illustrated in Figure 3.1. The input impedance (R_1) and feedback capacitance of inverting opamp integrator which controls the loop are set to 1 kΩ and 5 nF, respectively. Besides, the resistance (R_{FT}) and capacitance (C_{FT}) values of simple bias network are chosen as follows: R_{FT} = 10 kΩ, C_{FT} = 1 pF.

The overall impedance tuning system is simulated in ADS with Envelope simulator to monitor reflection coefficient variations with time. The circuit schematic of overall automatic impedance tuner system in ADS is illustrated in Appendix Figure A.2. Envelope simulator in ADS offers analysis flexibility of transient responses of the automatic gain controllers (AGC), phase locked loops (PLL), and adaptive impedance matching systems in the simulation environment. The reset switch connected parallel to the opamp capacitor as shown in Appendix Figure A.2 is an essential component to avoid divergence problems introduced by ideal opamp circuit in the envelope simulation. Since the ideal opamp having infinite gain at DC brings up divergence problems, it is short circuited at time t=0 by the reset switch to solve this problem in envelope simulation. Then, the switch automatically turns off to perform actual time domain

simulation (t > 0) [24]. To determine reflection coefficient variation with time, power probes are attached to each port of the coupled transmission line component except isolation port as depicted in Appendix Figure A.2. Simulation results show that the automatic impedance tuning unit dynamically compensates for the initial antenna input impedance ($Z_{ANT} = 50 + j113\,\Omega$) in less than $80\,\mu$sec as shown in Figure 3.4. Control voltage variation for BST varactor is also plotted with time as depicted in Figure 3.5.

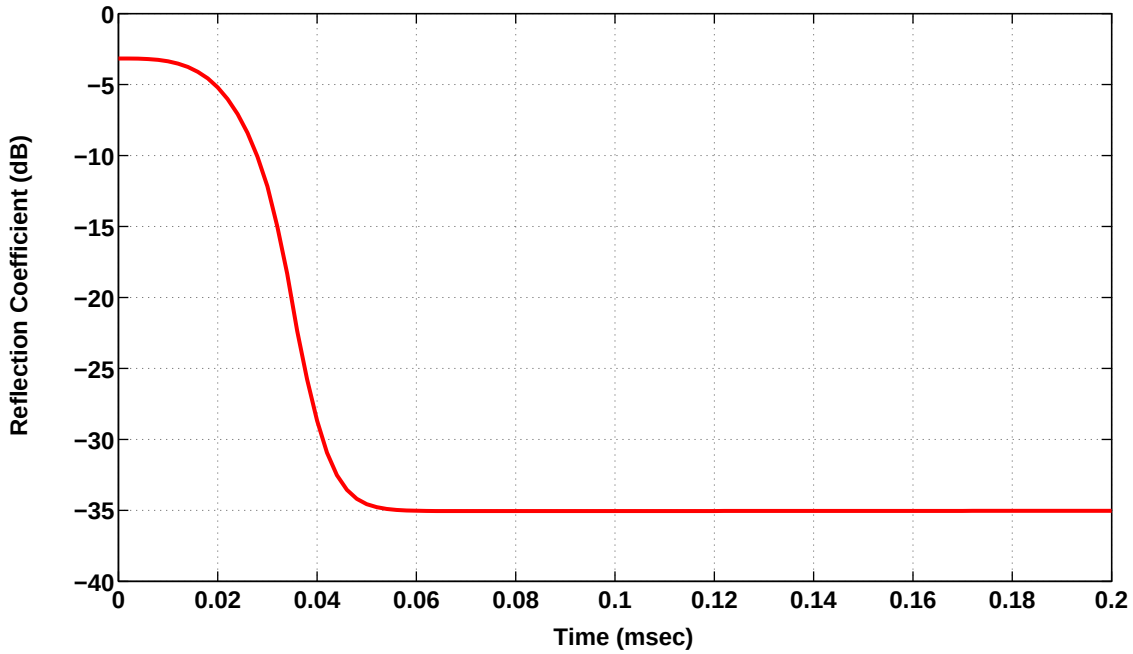

Figure 3.4: Variation of the reflection coefficient (dB) with time showing that the proposed automatic impedance tuning circuit tunes input impedance

This adaptive impedance tuning unit offers many advantages in terms of the simplicity of detection and the control unit, the compactness of overall tuning circuit and low cost. However, it can only change the inductive reactances along constant R circle on the Smith Chart which results in a limited impedance tuning region. Besides, in spite of the fact that the reactive part of the antenna feed impedance is much more susceptible to the presence of body in the vicinity of PIFA, the real part of it also varies within certain limits as previously illustrated in Figure 2.9. Therefore, it is required to design tunable circuits which offer reconfigurability in both real and imaginary parts of the antenna feed impedance. However, tuning algorithms which provide reconfigurability in both axis of the antenna feed impedance require complicated impedance

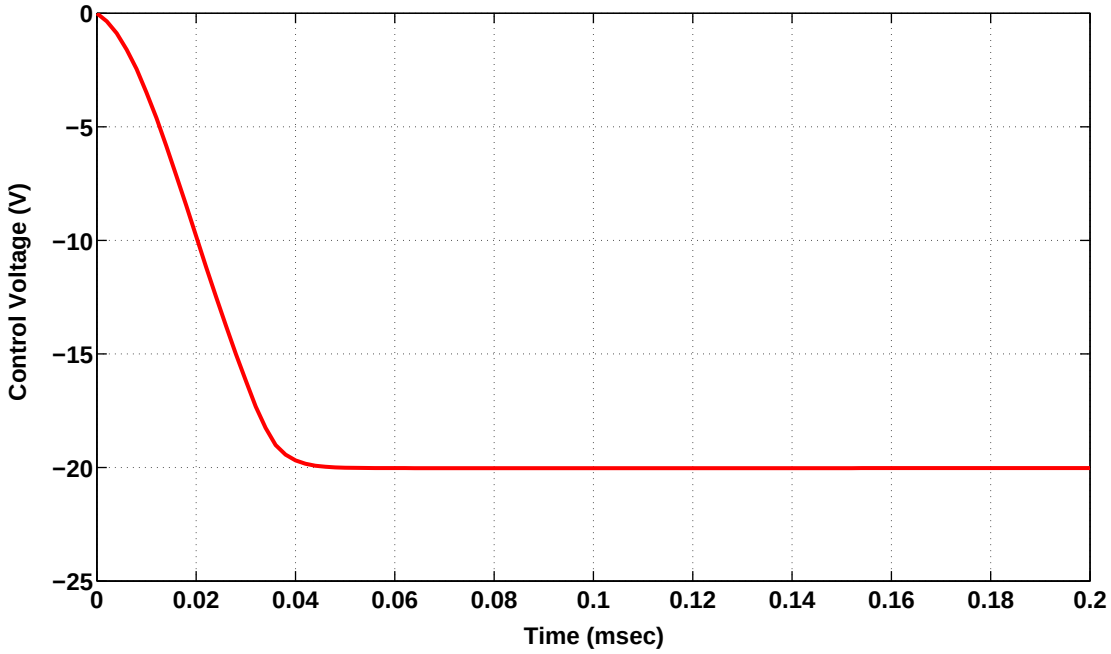

Figure 3.5: Control voltage variation of BST varactor model with time

tuner units.

3.2 Impedance Magnitude and Phase Tuning Techniques

Previous measurements show that the user interaction between PIFA and body mainly causes an increase in the imaginary part of the antenna feed impedance. Although the reactive part of the antenna feed impedance is much more sensitive to the body, this interaction also increases the real part of it. It can be inferred from the previous measurements that user interaction detunes the free space antenna input impedance to a certain region on first quadrant of the Smith Chart at GSM band. Mismatched impedances accumulated on a certain region of the Smith Chart can be transformed to 50Ω by applying two different tuning techniques. These techniques are realized by using separate impedance tuners connected in cascade. They are employed to remove real and imaginary part variations dynamically. The analysis and design of these impedance tuners are discussed in more detail in the following subsections.

3.2.1 Tuning in Magnitude and Phase Domain of Antenna Input Impedance

In this subsection, two step impedance transformation technique proposed in [10] is employed to eliminate the effects of mismatches arising from the user interaction between cell phone and body. It comprises of two stage tuning process, which offers tuning flexibility in the phase and magnitude domain of the antenna input impedance. As a first step, the mismatched antenna input impedance represented by black triangles is moved along constant VSWR circle to a point positioned on lower vertical axis of the Smith Chart as shown in Figure 3.6. The first step of this tuning technique

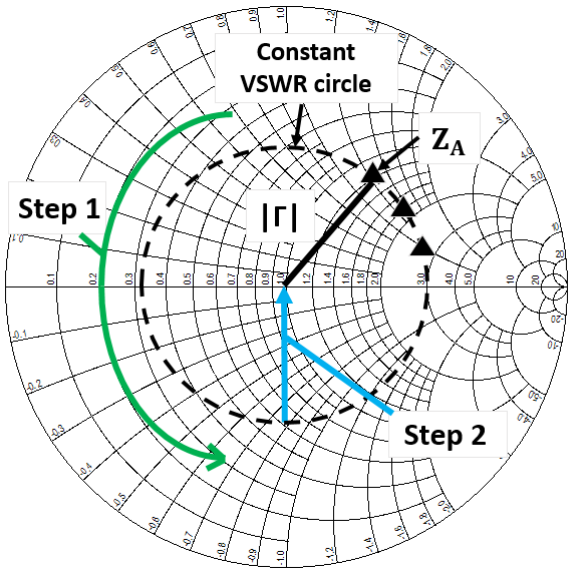

Figure 3.6: Impedance tuning with phase shifter(step 1) and variable transformer (step 2)

sets the magnitude of normalized antenna input impedance to 1. This transformation can be achieved by employing a tunable phase shifter. It can rotate the mismatched antenna input impedance around the center of the Smith Chart with fixed radius ($|\Gamma|$) to the desired point by varying the phase of the reflection coefficient. Then, the input impedance of the tunable phase shifter can be moved along the vertical axis of the chart by utilizing a variable transformer. Since only the phase of impedance changes along the vertical axis of the Smith Chart, it offers phase tuning capability without affecting its input impedance magnitude. Phase tuning can be considered as a second step of this tuning technique as shown in Figure 3.6. A tunable phase shifter and a variable transformer attached to each other in cascade can cover the mismatched re-

gion arising from the interaction between the cell phone and body depending on their tunable phase range. The phase shift introduced by the tunable phase shifter can be described as ϕ as illustrated in Figure 3.7. Since the incident wave passes through

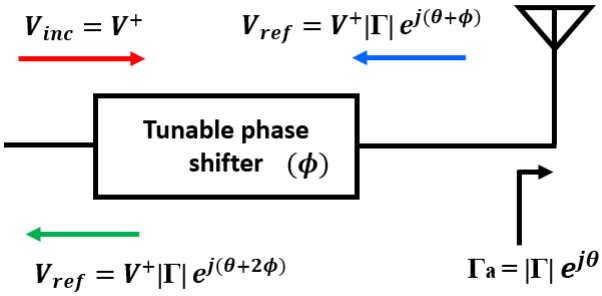

Figure 3.7: Insertion phase effect of tunable phase shifter on the reflection coefficient

the phase shifter and reflects back due to the mismatches, the reflected wave includes the phase of reflection coefficient of the mismatched load and the insertion phase of tunable phase shifter (ϕ). As the reflected wave passes through the tunable phase shifter again as shown in Figure 3.7, the reflected wave at the input of the tunable phase shifter contains multiple of 2 in front of the insertion phase term (ϕ).

In the following subsections, the design and simulation of a 90 degree tunable phase shifter and a variable transformer are performed by using lumped components.

3.2.1.1 90 Degree Tunable Phase Shifter

This subsection focuses on the design and simulation of a 90 degree tunable phase shifter by using fixed inductors and variable capacitances. A phase shifter is a two port microwave circuit which provides an opportunity to change the phase of RF signal. It has a wide variety usage within various applications such as phased array antenna, beamforming network, power divider, phase discriminator, communication and measurement systems [25],[26],[27]. Since the phase of the reflection coefficient needs to be changed continuously, the movement of the mismatched impedance on the constant VSWR circle can be achieved by using analog tunable phase shifters. It offers continuous phase tuning flexibility with an unlimited resolution. The most widely used component to accomplish reconfigurable phase altering is a semiconduc-

tor based varactor whose schematic is depicted in Figure 3.8. Capacitance voltage characteristic curve of a semiconductor type varactor diode is plotted as shown in Figure 3.9 based on the equation 3.4. It is modelled by using SDD block in ADS.

Figure 3.8: Circuit schematic of a semiconductor type varactor

$$C(V) = \frac{C_o}{(1 + \frac{V}{V_0})^n} \tag{3.4}$$

where V is the reverse bias voltage, V_o is the junction potential with no bias (which varies between 0.5-0.7 V), C_o is the capacitance value which corresponds to zero bias voltage and the n is an exponent factor (varies with respect to different doping profile). The exponent factor is approximately equal to 0.5 for uniformly doped diodes and is greater than 0.5 for hyperabrupt junction varactors [28]. The hyperabrupt junction varactors provide large capacitance variation in restricted tuning range.

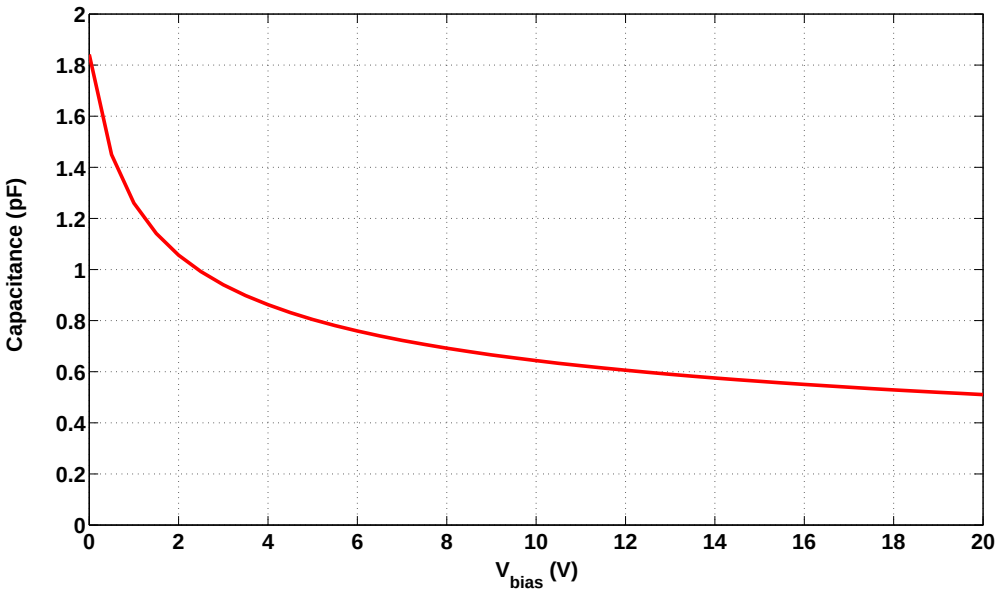

Figure 3.9: Capacitance variation of a semiconductor varactor model with reverse DC bias voltage

The capacitance value of a semiconductor type varactor can be continuously altered

by a reverse bias voltage as shown in Figure 3.9. The increase in the reverse bias voltage grows the volume of the depletion region which leads to decrease capacitance value between its leads. Semiconductor varactor technology offers numerous advantages in terms of low cost, fast tuning capability, high tuning ratio, being small in size and easy integration. These advantages make it very attractive for cell phone applications where the compactness and cost of the circuit are important. However, turn on and breakdown operation modes restrict the capacitance tuning ratio and its usage in high power applications. Since the tunable phase shifter circuit as a part of impedance tuning unit is integrated in a cell phone RF front end unit, the most convenient way to design it in small size is to use lumped components. Thus, the analog variable phase shifter proposed in the literature is adopted to obtain compact size circuit with tunable phase[10]. Figure 3.10 depicts the circuit schematic of tunable phase shifter consisting of fixed inductors and varactors. As the same analog variable phase shifter

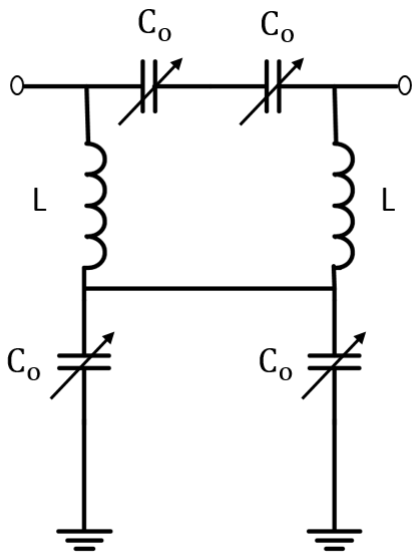

Figure 3.10: Circuit schematic of tunable phase shifter

configuration is employed in this subsection, the mathematical expressions given in [10] that define insertion phase and return loss variation in varactor tuning range is mentioned here briefly. Even and odd mode analysis is performed on circuit depicted in Figure 3.10 to derive S parameters in terms of even and odd mode reflection coefficients as defined in equations 3.5 and 3.6.

$$S_{11} = 0.5\left[\Gamma_e + \Gamma_o\right] \tag{3.5}$$

$$S_{21} = 0.5\left[\Gamma_e - \Gamma_o\right] \tag{3.6}$$

where Γ_e and Γ_o are even and odd mode reflection coefficients. Γ_e and Γ_o can be expressed in terms of W and z as given in equation 3.7 and 3.8, respectively.

$$\Gamma_e = \frac{jWz - 1}{jWz + 1} \tag{3.7}$$

$$\Gamma_o = \frac{1 - jWz}{1 + jWz} \tag{3.8}$$

where

$$W = \Omega - \frac{1}{\Omega} \tag{3.9}$$

$$\Omega = \omega\sqrt{LC} \tag{3.10}$$

and

$$z = \frac{1}{Z_o}\sqrt{\frac{L}{C}} \tag{3.11}$$

The square root of L over C must be equal to the characteristic impedance of line to satisfy perfect match between the transmission line and the phase shifter in the varactor tuning range. Thus, the tunable phase shifter requires variable inductances to sustain perfect matching condition while the variable capacitance changes continuously the insertion phase of the tunable phase shifter. Although a fixed inductor and a varactor connected in series provide an opportunity to design a tunable inductor in a certain tuning range, this solution brings up some drawbacks in terms of insertion loss and compactness of circuit due to an increase in the number of components. Besides, it is not easy to obtain electronically tunable inductor commercially available. In spite of the fact that fixed inductors degrade the performance of tunable phase shifter in terms of matching condition, it gives a reasonable impedance matching over varactor tuning range with fixed inductors [10]. It is assumed that L_o and C_o values are defined as follows:

$$L_o = \frac{Z_o}{w} \tag{3.12}$$

$$C_o = \frac{1}{wZ_o} \tag{3.13}$$

where Z_o is the characteristic impedance and ω is the angular frequency.

The fixed inductor value is defined as multiplication of L_o value with a coefficient whose value is calculated based on tunable phase range of phase shifter.

$$L = aL_o \tag{3.14}$$

There are two possible solutions (z = 1,W = 0) which satisfy the perfect matching condition ($S_{11} = 0$). Fixed inductor value ($L = aL_o$) is placed in equations 3.9, 3.10 and 3.11 for perfect matching conditions ($z = 1$ and $W = 0$) to derive maximum and minimum values of the varactors in terms of C_o and a. Furthermore, insertion phases of the phase shifter are defined as shown below for each matching condition by using the expressions from equation 3.6 to equation 3.8.

$$z = 1 \rightarrow C_{min} = aC_o \rightarrow \Phi = \pi - 2\arctan(W)$$

$$W = 0 \rightarrow C_{max} = C_o/a \rightarrow \Phi = 180$$

Mathematical expression defining tunable phase range of analog variable phase shifter can be obtained by subtracting the insertion phase value corresponding to C_{max} from the insertion phase corresponding to C_{min}. It can be described as follows:

$$\Delta\Phi = 2\arctan(W)$$

By setting the tunable phase range to 90 degree, a value can be easily calculated using 3.9 and 3.10. C_{min}, C_{max}, and fixed inductor values can be defined in terms of C_o and L_o, respectively as follows : $0.618C_o$, $1.618C_o$, and $0.618L_o$.

C_{min}, C_{max}, fixed inductor values calculated at 900 MHz are given as follows: $C_{min} = 2.185$ pF, $C_{max} = 5.722$ pF and $L = 5.464$ nH. Return loss ($S_{11}(dB)$) and insertion phase variation ($\angle S_{21}$) are plotted as depicted in Figures 3.11 and 3.12, respectively by sweeping capacitance values in the varactor tuning range.

In the varactor tuning range, the return loss variation of tunable phase shifter is below -10 dB as seen in Figure 3.11. As visualized from Figure 3.12, the insertion phase of the tunable phase shifter varies from -90 degree to -180 degree at 900 MHz as the capacitance value changes from 2.185 pF to 5.722 pF. It can be easily seen from these figures that 90 degree reconfigurable phase shift is achieved in this varactor tuning range with reasonable return loss.

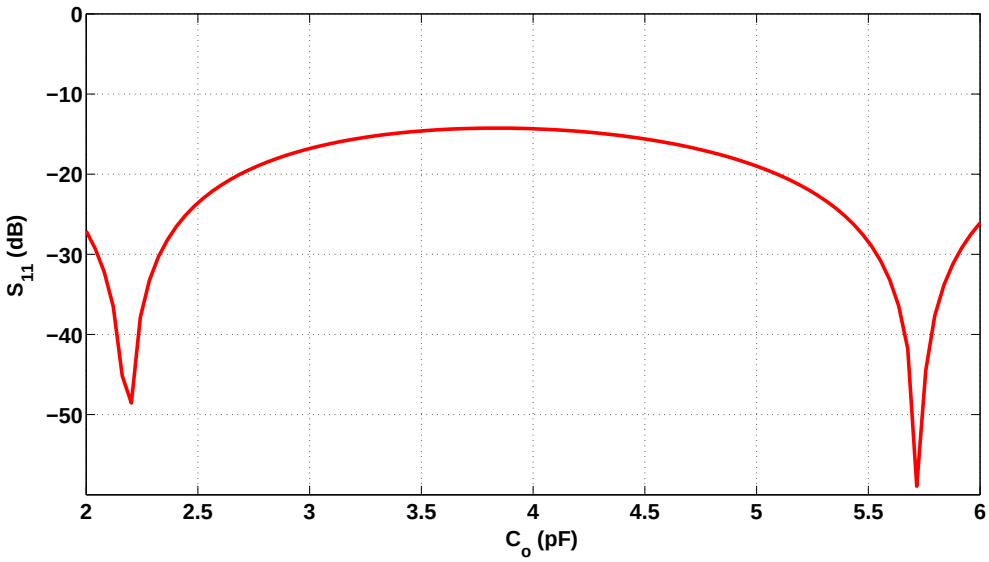

Figure 3.11: Return loss variation of 90 degree tunable phase shifter in the varactor tuning range at 900 MHz

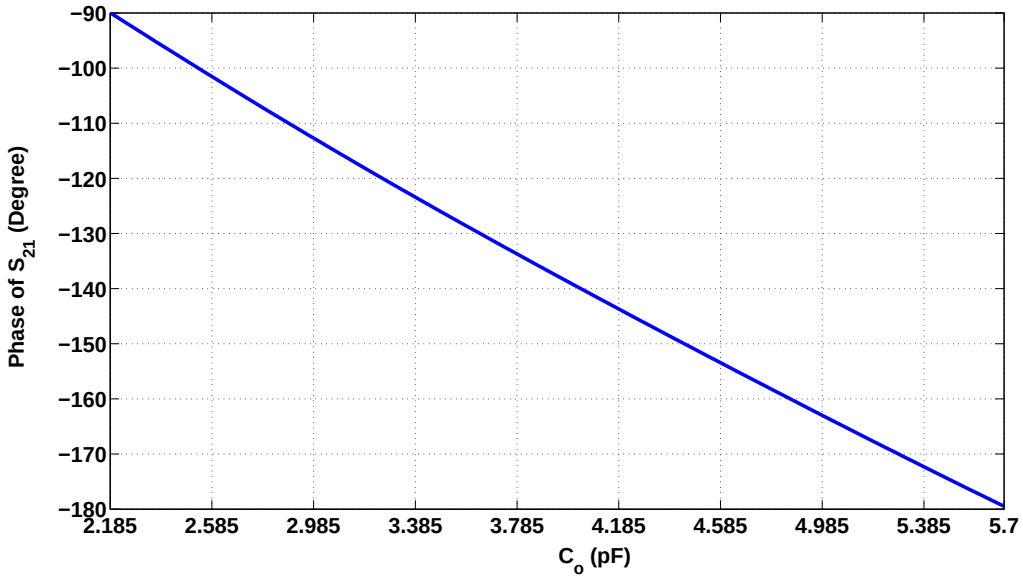

Figure 3.12: Insertion phase variation of 90 degree tunable phase shifter circuit from C_{min} to C_{max} at 900 MHz

3.2.1.2 Variable Transformer

This subsection elaborates on the design and simulation of the impedance tuner proposed in the literature whose topology is identical to the variable transformer circuit as shown in Figure 3.13[10]. It consists of fixed inductors, series and parallel connected varactors. This impedance tuner is employed to change continuously the phase of the impedance without affecting its magnitude. This tuning corresponds to the movement along the vertical axis of the Smith Chart. The same mathematical expressions utilized in [10] are mentioned here briefly to describe the tuning behaviour of the variable transformer. It is assumed that the fixed inductor value is defined as shown below.

$$L = L_o = \frac{Z_o}{w}$$

in which Z_o and w are the characteristic impedance and angular frequency, respectively. The continuous capacitance variation of the series (C_s) and parallel (C_p) connected varactors are expressed in terms of x and C_o in equation 3.15 and 3.16, respectively.

$$C_s = (x+1)C_o \tag{3.15}$$

$$C_p = \frac{C_o}{(x+1)} \tag{3.16}$$

where

$$C_o = \frac{1}{\omega(Z_o)} \tag{3.17}$$

x value determines the maximum and minimum capacitance values of series and parallel connected varactors. Even mode and odd mode analyses are performed on the circuit illustrated in Figure 3.13 by using C_s and C_p capacitances. S_{11} and S_{21} values of the variable transformer can be easily derived in terms of x by using the even-odd mode reflection coefficients. These values are given as shown below.

$$S_{21} = \frac{x^2-1}{x^2+1} \tag{3.18}$$

$$S_{11} = -j\frac{2x}{x^2+1} \tag{3.19}$$

The variation of x value from an arbitrary constant to zero moves the impedance along the vertical axis of the Smith Chart to its center as illustrated in Figure 3.14. It

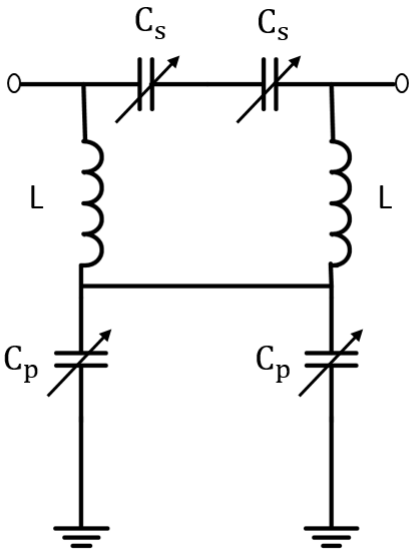

Figure 3.13: The circuit schematic of the variable transformer

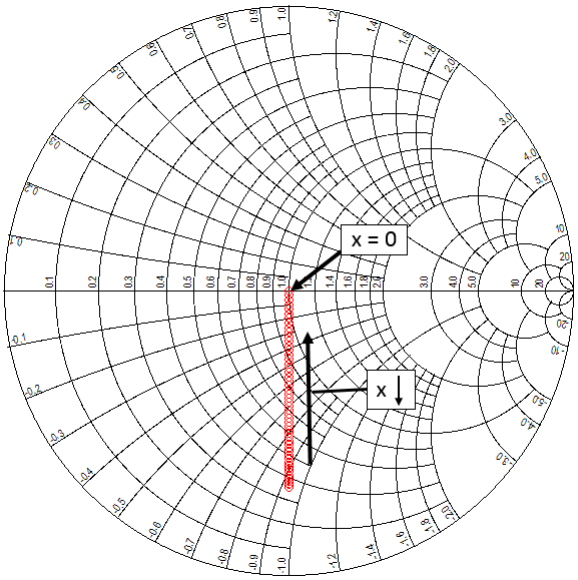

Figure 3.14: Variable transformer tuning on the Smith Chart by sweeping x value in a certain range

is obvious from equation 3.15 and 3.16 that the capacitance values of varactors connected to the variable transformer in series and parallel are inversely proportional to each other. This condition requires two separate control voltages for shunt and series varactors to achieve the impedance phase tuning properly. However, the maximum varactor tuning voltage for both C_s and C_p varactors can be applied to the common connection point of series varactors. It provides an opportunity to set the variable transformer by only a single control voltage as shown in Figure 3.15.

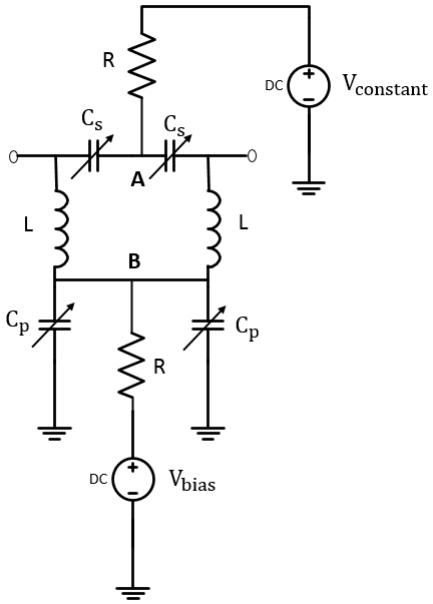

Figure 3.15: Representation of the variable transformer with bias voltages

In Figure 3.15, the cathodes of C_s's are attached to the common connection point, A, where the applied voltage is kept constant at maximum bias voltage level ($V_{constant}$). The cathodes of C_p's are attached to the common connection point, B, where the variable control (V_{bias}) is applied through a bias resistor. Therefore, the variation of a single control voltage between zero and maximum bias voltage leads to a change in C_p and C_s values in opposite way. In other words, the increase in the single bias voltage increases the value of C_s due to the reduction of reverse bias voltage between its anode and cathode. Since the anodes of semiconductor based varactors (C_p) are connected to ground, the increase in the bias voltage decreases the parallel capacitance value. For each bias voltage, the capacitance values of varactors connected in series and parallel must be chosen carefully to satisfactorily meet capacitance variations described in equations 3.15 and 3.16. Besides, it can be mathematically proved

that variable transformer only tunes the phase of the impedance having normalized magnitude 1 which corresponds to the movement along vertical axis as shown in Figure 3.14. It is assumed that Z_L is the impedance connected to the variable transformer as shown in Figure 3.16.

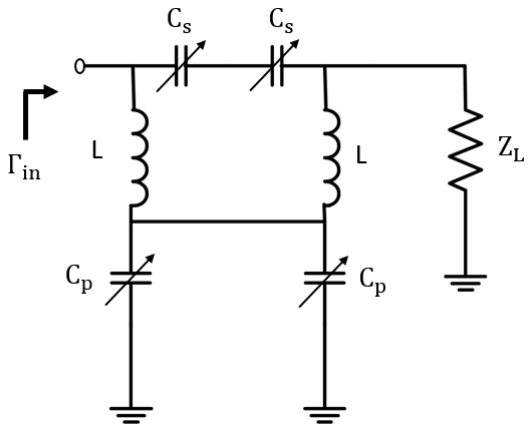

Figure 3.16: Variable transformer connection with input impedance of the phase shifter (Z_L)

Since this network is reciprocal,

$$S_{12} = S_{21} = \frac{x^2 - 1}{x^2 + 1} \tag{3.20}$$

$$S_{11} = S_{22} = -j\frac{2x}{x^2 + 1} \tag{3.21}$$

Input reflection coefficient (Γ_{in}) of the circuit depicted in Figure 3.16 can be described in terms of S parameters of the variable transformer and the load reflection coefficient (Γ_L) as shown below.

$$\Gamma_{in} = S_{11} + \frac{S_{12}S_{21}\Gamma_L}{1 - S_{22}\Gamma_L} \tag{3.22}$$

where S_{11}, S_{21}, S_{12}, and S_{22} are S parameters of the variable transformer and Γ_L is the reflection coefficient of the input impedance (Z_L) positioned on the vertical axis of the Smith Chart. Since the 90 degree tunable phase shifter sets the magnitude of normalized antenna input impedance to 1 with an arbitrary phase, Z_L resides in the vertical axis of the Smith Chart. It is described as follows:

$$Z_L = 1\angle(\alpha) \tag{3.23}$$

The normalized impedance at the input of circuit illustrated in Figure 3.16 can be easily calculated by using the input reflection coefficient of it (Γ_{in}) as shown below.

$$z_{in} = \frac{1 + \Gamma_{in}}{1 - \Gamma_{in}} \tag{3.24}$$

The magnitude of the normalized input impedance ($|z_{in}|$) can be expressed in terms of x and the phase of Z_L by using equations from 3.20 to 3.24 as shown below.

$$|z_{in}| = \frac{\sqrt{4 - \frac{16x\sin(\alpha)}{x^2+1} + \frac{16x^2}{(x^2+1)^2}}}{\sqrt{4 - \frac{16x\sin(\alpha)}{x^2+1} + \frac{16x^2}{(x^2+1)^2}}} = 1 \tag{3.25}$$

The magnitude of the normalized impedance seen at the input of the variable transformer does not depend on x value and the phase of $Z_L(\alpha)$ as defined in equation 3.25. It is clearly seen from equation 3.25 that the variable transformer does not affect the normalized magnitude of the impedance at the input of the phase shifter. Variation of x from 0 to 1 leads to an inverse change in the value of varactors connected in series (C_s) and parallel (C_p) (from C_o to $2C_o$ and from $C_o/2$ to C_o, respectively). The maximum value of x determines the tunable phase range of the variable transformer. When x value is chosen very close to 1, the insertion loss introduced by the variable transformer is very high, which means that there is a significant compromise between the phase tuning range and insertion loss of the variable transformer. The fixed inductor value, C_{min} and C_{max} values of C_s and C_p varactors are calculated based on equations from 3.15 to 3.17 at 900 MHz as follows:

$L = 8.841\,\text{nH}$, $C_o = 3.536\,\text{pF}$, $C_{smin} = 3.536\,\text{pF}$, $C_{smax} = 7.072\,\text{pF}$, $C_{pmin} = 1.718$ pF, $C_{pmax} = 3.536\,\text{pF}$.

3.2.2 Tuning in Real and Imaginary Parts of Antenna Input Impedance

New impedance tuning technique which offers independent tuning capability in real and imaginary parts of the antenna feed impedance is proposed in this section. Impedance tuning in both real and imaginary axes of the antenna feed impedance can be achieved by using two stage impedance transformation as illustrated in Figure 3.17. The mismatched antenna input impedance represented by black triangles is moved along constant VSWR circle to the points which reside in the horizontal axis of the Smith Chart

as shown in Figure 3.17 (Step 1). The first stage of this tuning technique sets the phase of the antenna feed impedance to 0 by changing the phase of the reflection coefficient of the antenna feed impedance. The phase variation of the reflection coefficient can be achieved by employing a 180 degree tunable phase shifter. It moves the mismatched antenna input impedances along the constant VSWR circle to the points located in the horizontal axis of the Smith Chart as shown in Figure 3.17. Then, to obtain the perfect matching condition, the real impedance seen at the input of the tunable phase shifter needs to be moved along the horizontal axis to center of the Smith Chart (Step 2). The second step transformation requires a tunable transformer (T-matching) circuit which provides an opportunity to tune real impedances with a single control voltage. The details of two separate tunable circuits consisting of fixed inductors and varactors are discussed in more detail in the following subsections.

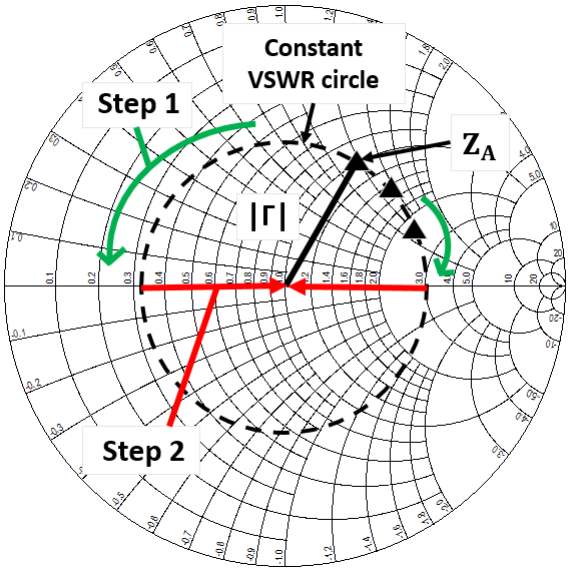

Figure 3.17: Impedance tuning with phase shifter (Step1) and tunable transformer (Step2)

3.2.2.1 180 Degree Phase Shifter

This section focuses on the design and simulation of a 180 degree tunable phase shifter by using fixed inductors and variable capacitances. This tuner is employed to move the mismatched impedances along constant VSWR circle to the points which reside in the horizontal axis of the Smith Chart as illustrated in Figure 3.17. Two

stage circuit configuration as depicted in Figure 3.18 is used to achieve 180 degree phase tuning with reasonable insertion loss.

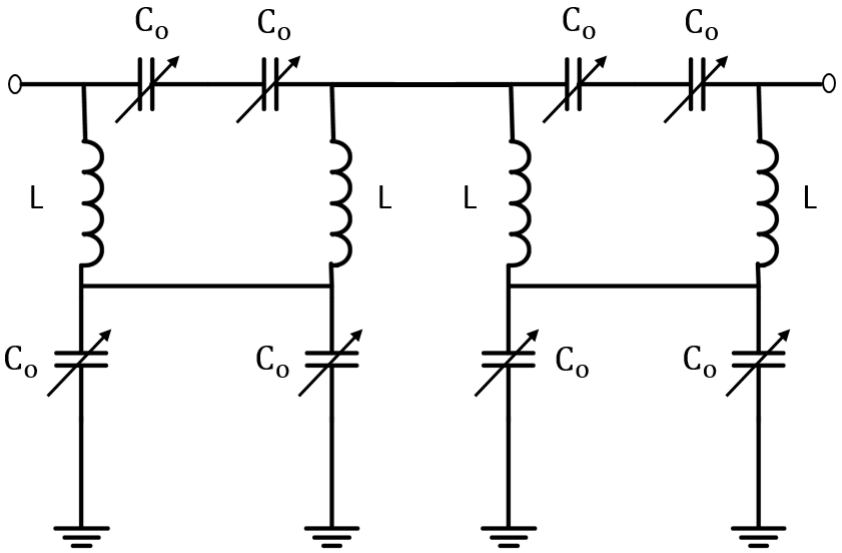

Figure 3.18: Circuit schematic of the 180 degree tunable phase shifter consisting of two single stage circuit connected in cascade

Since it is impossible to achieve 180 degree tunable phase shift by a single stage configuration [10], even if varactors have infinite varactor tuning range, the most common method to increase reconfigurable phase range is to connect individual single stage blocks in cascade as shown in Figure 3.18. However, this solution brings up an increase in the insertion loss which degrades the performance of overall tuner. As the wave travels back from the antenna due to the mismatches, reflection coefficient at the input of the 180 degree tunable phase shifter includes multiple of 2 in front of the insertion phase term (ϕ). Therefore, it offers tuning capability in all quadrants of the Smith Chart. It is a good candidate for the general purpose tuner applications where adaptive impedance control is required. Besides, it is important to note that the mismatched impedance region due to the user interaction between the cell phone and the body can also be covered by using impedance tuner designed based on this tuning technique. S parameter analysis of tunable phase shifter consisting of a two stage circuit is performed based on chain scattering matrix (a.k.a transmission matrix or T- matrix). S parameters of each identical single stage circuit is converted to chain

scattering matrix as shown below [29].

$$\begin{bmatrix} T_{11} & T_{12} \\ T_{21} & T_{22} \end{bmatrix} = \begin{bmatrix} \frac{1}{S_{21}} & \frac{-S_{22}}{S_{21}} \\ \frac{S_{11}}{S_{21}} & S_{12} - \frac{S_{11}S_{22}}{S_{21}} \end{bmatrix}$$

The chain scattering matrix of the two stage circuit can be derived based on known S parameters of the single stage circuit by multiplying the chain scattering matrix of each identical block as shown below.

$$\begin{bmatrix} T'_{11} & T'_{12} \\ T'_{21} & T'_{22} \end{bmatrix} = \begin{bmatrix} \frac{1}{S_{21}} & \frac{-S_{22}}{S_{21}} \\ \frac{S_{11}}{S_{21}} & S_{12} - \frac{S_{11}S_{22}}{S_{21}} \end{bmatrix} \times \begin{bmatrix} \frac{1}{S_{21}} & \frac{-S_{22}}{S_{21}} \\ \frac{S_{11}}{S_{21}} & S_{12} - \frac{S_{11}S_{22}}{S_{21}} \end{bmatrix}$$

Then, S parameters (S') of the overall circuit illustrated in Figure 3.18 can be defined by using conversion as shown below.

$$\begin{bmatrix} S'_{11} & S'_{12} \\ S'_{21} & S'_{22} \end{bmatrix} = \begin{bmatrix} \frac{T'_{21}}{T'_{11}} & T'_{22} - \frac{T'_{21}T'_{12}}{T'_{11}} \\ \frac{1}{T'_{11}} & \frac{T'_{12}}{T'_{11}} \end{bmatrix}$$

To obtain the return loss of the overall circuit (S'_{11}), T'_{21} and T'_{11} are expressed in terms of the S parameters of the single stage network as follows:

$$T'_{21} = \frac{S_{11} - S_{11}^2 S_{22} + S_{11}S_{12}S_{21}}{S_{21}^2} \tag{3.26}$$

$$T'_{11} = \frac{1 - S_{11}S_{22}}{S_{21}^2} \tag{3.27}$$

The return loss of the overall circuit (S'_{11}) can be expressed as shown below:

$$S'_{11} = \frac{T'_{21}}{T'_{11}} = \frac{S_{11} - S_{11}^2 S_{22} + S_{11}S_{12}S_{21}}{1 - S_{11}S_{22}} \tag{3.28}$$

Since the single stage network depicted in Figure 3.10 is reciprocal (i.e $S_{11} = S_{22}$ and $S_{12} = S_{21}$) S'_{11} and S'_{21} can be expressed respectively as follows:

$$S'_{11} = \frac{S_{11}(1 - S_{11}^2 + S_{21}^2)}{1 - S_{11}^2} \tag{3.29}$$

$$S'_{21} = \frac{1}{T'_{11}} = \frac{S_{21}^2}{1 - S_{11}^2} \tag{3.30}$$

There are two possible solutions ($S_{11} = 0$, $(1 - S_{11}^2 + S_{21}^2) = 0$) which satisfy the perfect matching condition ($S'_{11} = 0$) for two stage phase shifter configuration.

$$S_{11} = 0 \rightarrow z = 1\, W = 0$$

$$(1 - S_{11}^2 + S_{22}^2) = 0 \rightarrow W\pm = 1$$

It is assumed that L_o and C_o values are expressed in terms of the characteristic impedance and frequency as given in equation 3.12 and 3.13, respectively. Fixed inductor value is expressed in terms of a coefficient (a) and (L_o) as shown below.

$$L = aL_o$$

The fixed inductor value (aL_o) is placed in equations 3.7 and 3.8 to find C_{min} and C_{max} values of the identical varactors in terms of a and C_o for $z = 1$ and $W = 0$. C_1 and C_2 capacitance values are expressed in terms of C_o and a for these solutions as shown below.

$$z = 1 \rightarrow C_1 = aC_o \rightarrow \Phi = 0$$

$$W = 0 \rightarrow C_2 = \frac{C_o}{a} \rightarrow \Phi = 0$$

The second perfect matched condition ($1 - S_{11}^2 + S_{21}^2 = 0$) gives two different values for W as shown below.

$$W = \pm 1 \tag{3.31}$$

For $W = 1$

$$\Omega^2 - \Omega - 1 = 0 \tag{3.32}$$

which gives

$$\Omega_{1(1,2)} = \frac{1 \pm \sqrt{5}}{2} \tag{3.33}$$

For $W = -1$

$$\Omega^2 + \Omega - 1 = 0 \tag{3.34}$$

which gives

$$\Omega_{2(1,2)} = \frac{-1 \pm \sqrt{5}}{2} \tag{3.35}$$

Equation 3.10 and positive solutions of equation 3.32 and 3.34 are used to find the capacitance values in terms of a and C_o. Inductor value is taken as aL_o for each solution. The capacitance values corresponding to $W = -1$ and $W = 1$ are described as shown below.

$$W = 1 \rightarrow C_4 \rightarrow \frac{C_o}{a}(\frac{\sqrt{5}+1}{2})^2 \rightarrow \Phi = 0$$

$$W = -1 \rightarrow C_3 \rightarrow \frac{C_o}{a}(\frac{\sqrt{5}-1}{2})^2 \rightarrow \Phi = 180$$

C_2 and C_3 varactor tuning expressions are chosen to obtain 180 degree phase variation. Besides, by setting a = 0.786, nulls for return loss (S_{11}) can be distributed evenly in varactor tuning range [10]. The calculated values for the inductor and varactors at 900 MHz are given as follows: $L = 6.949$ nH, $C_{min} = 1.718$ pF, $C_{max} = 4.497$ pF. S parameter analysis is performed in ADS by sweeping the capacitance values in varactor tuning range. The return loss ($S_{11}(dB)$) and the insertion phase variation ($\angle S_{21}$) are plotted as illustrated in Figures 3.19 and 3.20, respectively. It can easily be seen from Figure 3.19 that return loss of 180 degree tunable phase shifter is less than -20 dB in varactor tuning range. Besides, as visualized from Figure 3.20 insertion phase of tunable phase shifter varies from 0 degree to 180 degree at 900 MHz as capacitance value changes from 1.718 pF to 4.497 pF. The simulation results show that 180 degree maximum reconfigurable phase shift can be achieved in this varactor tuning range with reasonable return loss.

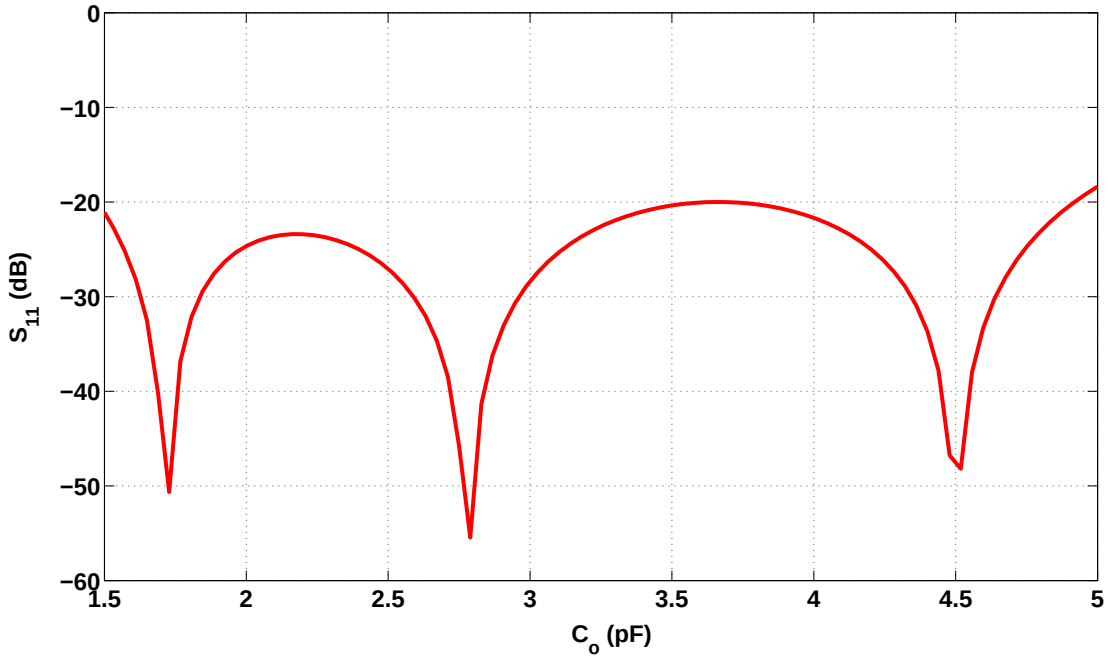

Figure 3.19: Return loss variation of 180 degree tunable phase shifter in varactor tuning range

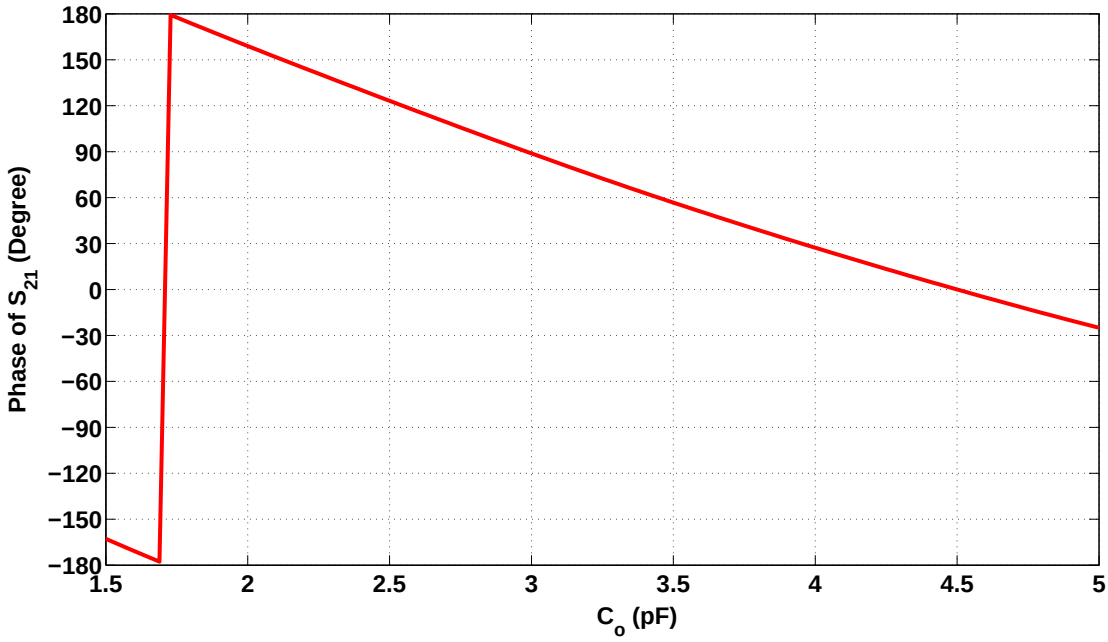

Figure 3.20: Insertion phase of 180 degree tunable phase shifter in varactor tuning range

3.2.2.2 T-matching Circuit

In the previous section, 180 degree tunable phase shifter is designed to tune the phase of reflection coefficient on the constant VSWR circle. This tuner dynamically changes the phase of the reflection coefficient of the mismatched impedance to 0 or 180 degree. This movement corresponds to an impedance located in the horizontal axis of the Smith Chart with a certain distance away from the center point as previously illustrated in Figure 3.17. To obtain a perfectly matched impedance, the real impedance must be tuned dynamically to the center point of the chart by a reconfigurable tuner. This tuner should offer tuning capability in the real axis of the impedance with a single bias voltage. Moreover, it is also desirable that it should meet the compact circuit design requirements of a cell phone at low costs. T-matching circuit including varactors and identical fixed inductors can transform the real impedance by a single bias voltage without adding a reactive impedance. After setting the phase of the reflection coefficient of the mismatched impedance to 0 or 180 degree, the input impedance seen at the input of tunable phase shifter (Z_p) can be described as shown below. It is clearly seen from equation 3.36 that Z_p has no

imaginary component.

$$Z_p = Z_o \frac{1 \pm |\Gamma|}{1 \mp |\Gamma|} \tag{3.36}$$

To achieve the second step transformation, the real impedance tuning technique proposed in the literature is utilized [14].

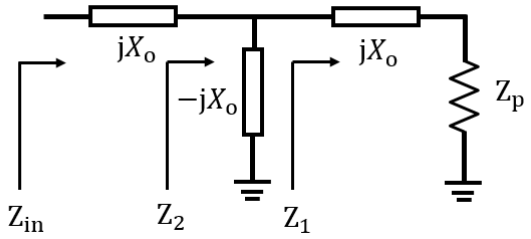

Figure 3.21: T-matching circuit connection with the input impedance of 180 degree tunable phase shifter

The input impedance of T-matching circuit can be derived by employing equations from 3.37 to 3.40.

$$Z_1 = Z_p + jX_o \tag{3.37}$$

$$Z_2 = Z_1 // - jX_o \tag{3.38}$$

$$Z_2 = \frac{X_o^2 - jX_o Z_p}{Z_p} \tag{3.39}$$

When the real impedance (Z_p) is attached to the T-matching circuit as depicted in Figure 3.21, the input impedance of the circuit illustrated in Figure 3.21 has only real part as defined in equation 3.40.

$$Z_{in} = \frac{X_o^2}{Z_p} \tag{3.40}$$

The magnitude of reactance value of each branch consisting of T-type circuit needs to be reconfigurable and identical to fulfil the real part transformation. Moreover, the shunt branch should be set to the capacitive reactance whose magnitude is identical with other branches to achieve the transformation correctly. One of the most common methods to realize variable reactance for each branch is to connect a fixed inductor and a varactor to each other in series as illustrated in Figure 3.22.

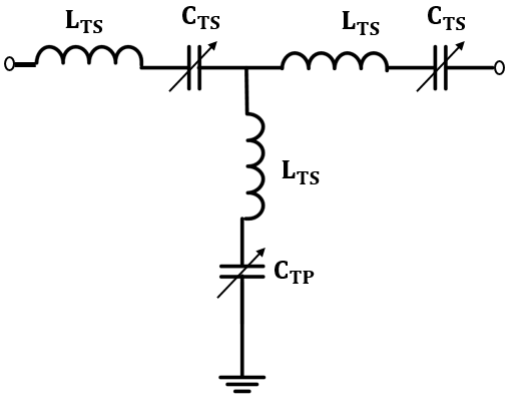

Figure 3.22: Realization of a T-matching circuit with varactors and fixed inductors

However, the main problem in this configuration is to adjust continuously each tunable branch to a desired reactance value with a single bias voltage. To overcome this problem, the capacitance values of varactors corresponding to single bias voltage should be chosen carefully so that the identical capacitive and inductive reactances are obtained for the shunt and series branches of T matching circuit. The fixed inductor value and varactor tuning ratio mainly determine the reactance tuning range of each branch, which also affects the transformation ratio of tunable transformer. The fixed inductor value is chosen as 50 nH and it is assumed that the reactance of each branch (X_o) varies between [16Ω, 160Ω]. These boundaries define the maximum and minimum tunable reactance values of series branches. Since the fixed inductor and the varactor are connected to each other in series for each branch, C_{min} and C_{max} values for each varactor can be found easily by using the minimum and maximum values of tunable reactance range. C_{min} and C_{max} values of the varactors connected to series branches are calculated at 900MHz as follows:

$$L_{TS} = 50\,\text{nH} \tag{3.41}$$

$$wL_{TS} - \frac{1}{wC_{TSmax}} = \text{X}_{\text{max}} \tag{3.42}$$

$$wL_{TS} - \frac{1}{wC_{TSmin}} = \text{X}_{\text{min}} \tag{3.43}$$

$$C_{TSmin} = 0.662\,\text{pF} \tag{3.44}$$

$$C_{TSmax} = 1.44\,\text{pF} \tag{3.45}$$

As the reactance value of the shunt branch varies between [-16Ω, -160Ω] to achieve the real part tuning, the minimum and maximum capacitance values of the varactor

in the shunt branch are calculated as shown below:

$$L_{TS} = 50\,\text{nH} \tag{3.46}$$

$$wL_{TS} - \frac{1}{wC_{TPmax}} = \text{-16} \tag{3.47}$$

$$wL_{TS} - \frac{1}{wC_{TPmin}} = \text{-160} \tag{3.48}$$

$$C_{TPmin} = 0.399\,\text{pF} \tag{3.49}$$

$$C_{TPmax} = 0.591\,\text{pF} \tag{3.50}$$

Although this tuner offers numerous advantages in terms of low cost, compactness, and reconfigurability with a single bias, it suffers from tradeoff between transformer tuning ratio and insertion loss. The block diagram of T-matching circuit and 180 degree phase shifter connected in cascade which summarizes the second tuning method is depicted in Figure 3.23.

In this subsection, the theory and realization of real impedance transformation with lumped components have been discussed in detail. It is important to note that this tuner is capable of covering a wide range of mismatched impedances in the horizontal axis of the Smith Chart as long as varactor tuning requirements are satisfactorily met. However, while its coverage region enlarges in the horizontal axis, the loss introduced by this tuner increases rapidly. Thus, this tradeoff should be taken into consideration for this tuning unit.

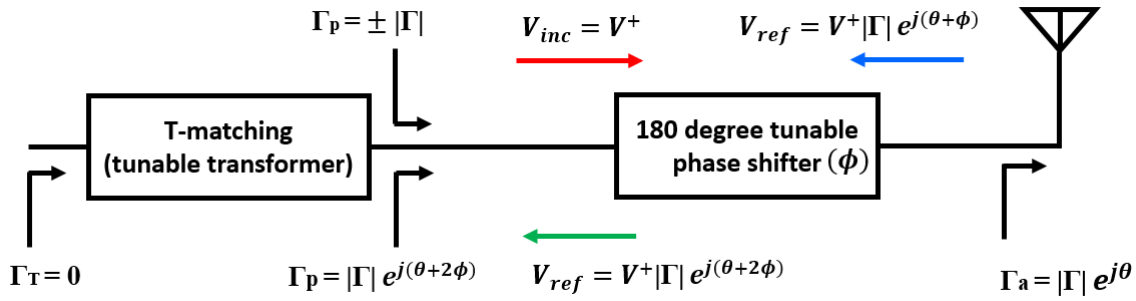

Figure 3.23: Cascade connection of T-matching circuit and 180 degree phase shifter

3.3 Mismatch Detection in Magnitude and Phase Domain of Impedance

This section focuses on the theory and design of impedance magnitude and phase detection units proposed in [10]. It is employed to test the adaptive tuning capability of two different tuners discussed in the previous sections. Since the impedance tuners designed based on two different analog tuning techniques utilize two step impedance transformation, each impedance tuning block requires two separate control voltages related to the magnitude and phase variations of antenna input impedance. To determine these variations, the quarter wavelength transmission line is fixed between the impedance tuner and the source as shown in Figure 3.24.

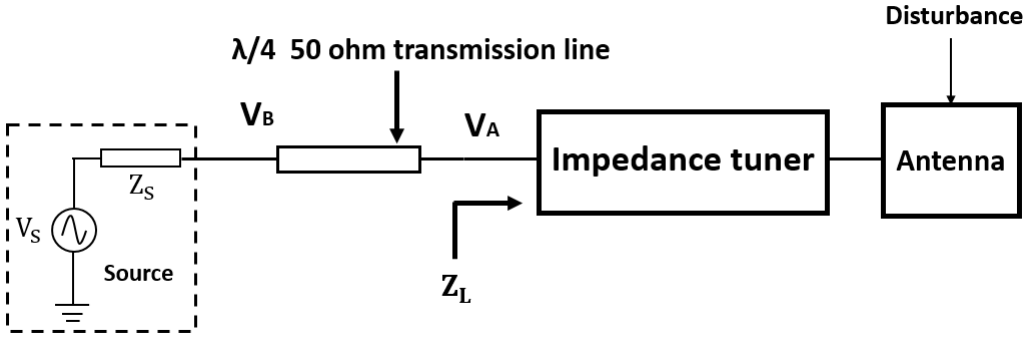

Figure 3.24: Impedance tuner with a quarter wavelength transmission line

The magnitudes and phases of node voltages positioned at each end of the quarter wavelength transmission line can be compared to check whether perfect matching condition is achieved or not. When the impedance at the input of the impedance tuner (Z_L) is set to 50Ω, each node has an identical voltage magnitude and there is a 90 degree phase difference between the node voltages due to the quarter wavelength transmission line as shown in Figure 3.25. Envelope detectors are attached to buffers to determine the peak values of the voltages at the connection points of the quarter wavelength transmission line as shown in Figure 3.26. In order to produce an error voltage for impedance magnitude variations, the outputs of the envelope detectors are applied to a log amplifier which takes the logarithm of the magnitude ratio of these two signals as depicted in Figure 3.26. Since each node has an identical voltage magnitude when perfect matching condition is achieved as illustrated in Figure 3.25, the logarithm of magnitude ratio is zero (i.e. error voltage for impedance magnitude

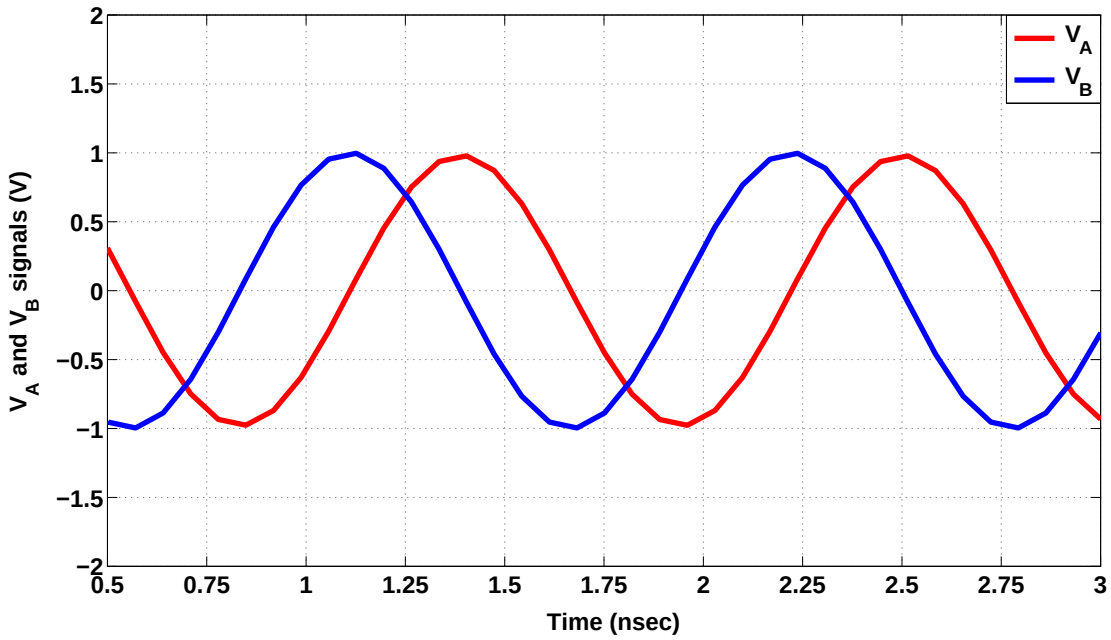

Figure 3.25: V_A and V_B waveforms when $Z_L = 50\,\Omega$

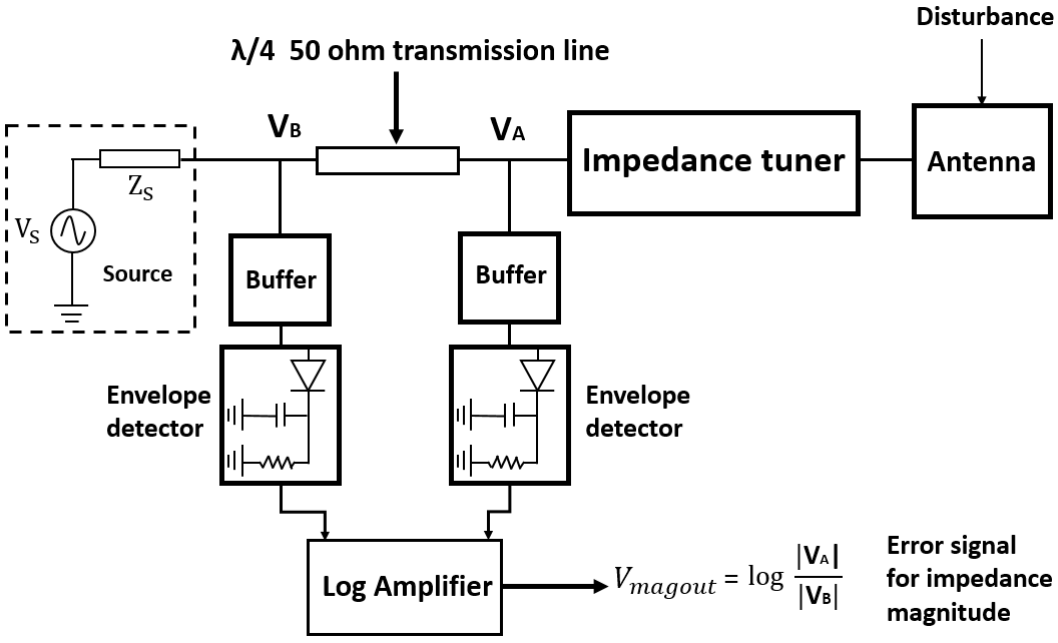

Figure 3.26: Block diagram of impedance magnitude detection unit

variation).

Let us assume that $V_A = A_1 \cos(wt + \phi_A)$ and $V_B = B_1 \cos(wt + \phi_B)$, if V_A and V_B signals are applied to the inputs of the mixer as shown in Figure 3.27, then, the output

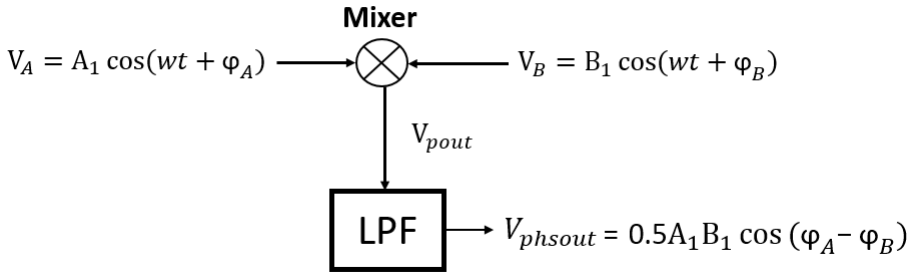

Figure 3.27: Block diagram of a mixer and a lowpass filter configuration

of the mixer can be defined mathematically as follows:

$$V_{pout} = 0.5A_1B_1 \cos(2wt + \phi_A + \phi_B) + 0.5A_1B_1 \cos(\phi_A - \phi_B) \tag{3.51}$$

V_{pout} is fed to the input of the low pass filter in order to obtain the second term in equation 3.51. The second term of the equation is extracted from the output of the mixer by the low pass filter whose cut-off frequency is below the frequency of the first term. Since 90 degree phase difference exists between V_A and V_B when the perfect matching condition (Z_L= 50Ω) is achieved at the input of the impedance tuner, the output voltage of the mixer-low pass filter configuration is zero (i.e. error voltage for impedance phase variation). The output of the low pass filter is a cosine function of the phase difference with a constant. The output of the low pass filter can be used as the error signal for the integrator to control the phase of the impedance.

$$V_{phsout} = 0.5A_1B_1 \cos(\phi_A - \phi_B) \tag{3.52}$$

The detection of phase difference can be simply done by using a mixer and a low pass filter as shown in Figure 3.28. Error voltages are fed to simple opamp integrator circuits including resistors and capacitors to obtain control voltages for tuning phase and magnitude of impedance. Non-inverting and inverting type opamp integrators can sum up the error voltages to produce control voltages until the best matching condition is achieved. Figure 3.29 and 3.30 depict the non inverting and inverting type opamp integrators, respectively. Since semiconductor based (Si) varactors require only reverse bias voltages for capacitance tuning, transfer function between the

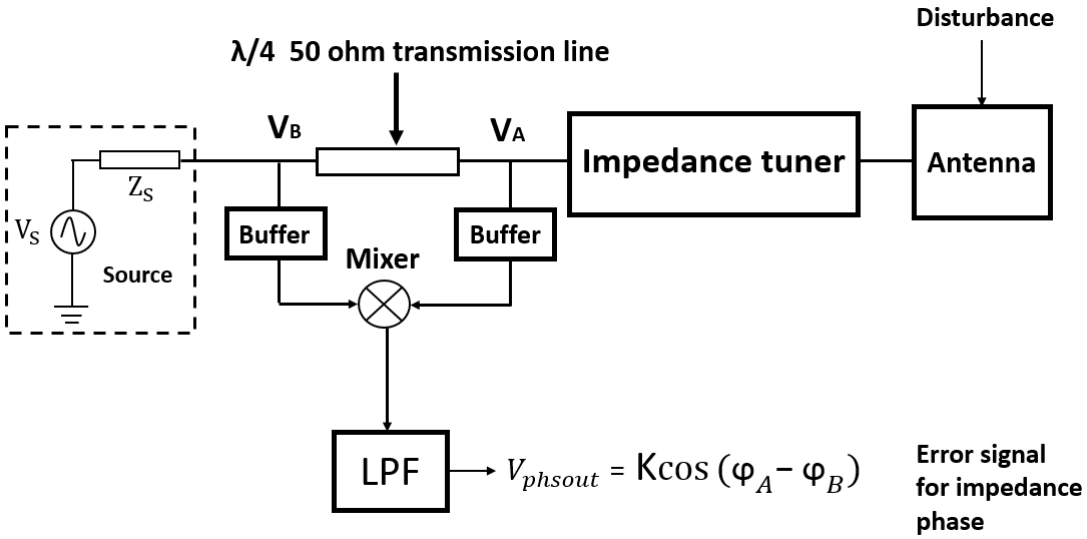

Figure 3.28: Block diagram of impedance phase detection unit

impedance detection and tuner units must be carefully specified to keep semiconductor varactors in reverse bias in adaptive tuning process.

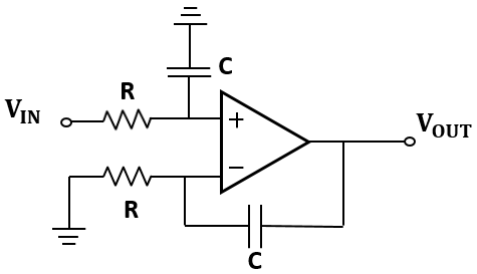

Figure 3.29: Circuit schematic of a non-inverting type opamp integrator

3.4 Adaptive Impedance Matching with T-matching Circuit and 180 Degree Phase Shifter

This section is devoted to the design and simulation of an automatic impedance matching circuit which dynamically compensates for the mismatched impedances by using magnitude and phase detection units with an impedance tuner consisting of a T-matching circuit and a 180 degree tunable phase shifter. It consists of a quarter wavelength transmission line, an impedance detection unit, inverting type opamp integrators, a T-matching and a 180 degree tunable phase shifter connected in cascade as illustrated in Figure 3.31. Since 180 degree tunable phase shifter is utilized

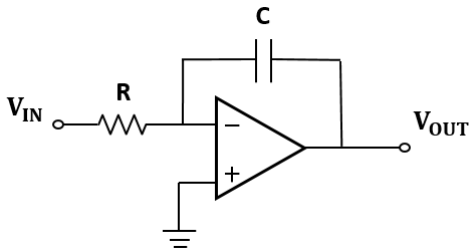

Figure 3.30: Circuit schematic of an inverting type opamp integrator

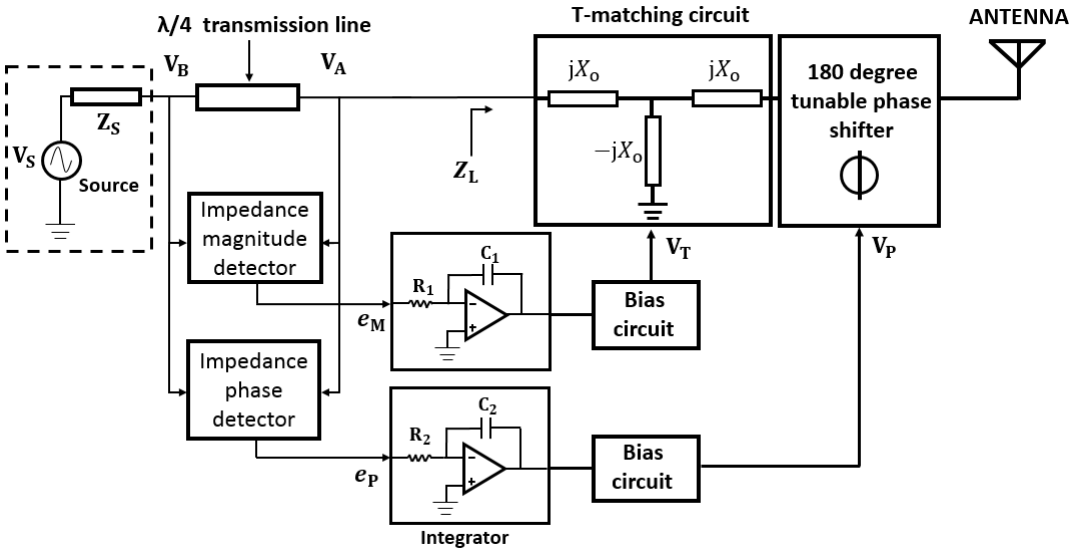

Figure 3.31: Block diagram of the automatic impedance tuner with the impedance magnitude and phase detection units including T-matching and 180 degree tunable phase shifter

to eliminate the reactive part variations, the output of the impedance phase detection unit is fed through an inverting opamp integrator to 180 degree tunable phase shifter as depicted in Figure 3.31. The output of phase detection unit produces the error signal related to the reactive part variations. It is connected to an inverting integrator in order to generate control signal for the tunable phase shifter which changes continuously the phase of the reflection coefficient until the output voltage of phase detector becomes zero (i.e error signal). When the phase detector produces zero error voltage, the input impedance of tunable phase shifter is set to an impedance point located in the horizontal axis of the Smith Chart. After setting the phase of the impedance to zero, T-matching circuit can tune dynamically the mismatches in real impedance domain. To achieve the dynamic tuning in real impedance domain, the inverting type opamp integrator which is fed by the output of the magnitude detector is attached to T-matching circuit as illustrated in Figure 3.31. As the overall tuning unit performs the automatic tuning process in a sequential manner with two nested loops, the outer loop setting the 180 degree tunable phase shifter needs to converge faster than the inner loop. Thus, in order to achieve this sequential tuning process, the feedback capacitance of outer loop integrator is chosen smaller than the feedback capacitance of the inner loop integrator. The input resistance (R_1) and the feedback capacitance (C_1) values of the opamp integrator which dynamically controls tunable phase shifter are set to $1\,\mathrm{k}\Omega$ and $5\,\mathrm{nF}$, respectively. The input resistance (R_2) and the feedback capacitance (C_2) values of the opamp integrator which adjusts tunable transformer (T-matching circuit) for real part tuning are set to $1\,\mathrm{k}\Omega$ and $50\,\mathrm{nH}$, respectively. Besides, the capacitor and resistor values of the simple bias networks for both integrators are chosen as follows : C_{FT} = 100 pF, R_{FT} = 5 kΩ, respectively. T-matching circuit and 180 degree tunable phase shifter are composed of BST varactor models and fixed inductors whose values are calculated in the previous sections. S parameter analysis is performed based on previously calculated C_{min}, C_{max} and the fixed inductor values for both T-matching circuit and 180 degree tunable phase shifter to determine the impedance coverage region of this tuner. Figure 3.32 depicts the impedance coverage region of this tuner at 900 MHz. As long as the mismatched impedance falls into the coverage region of this impedance tuner, the antenna feed impedance can be matched dynamically to $50\,\Omega$ by using this automatic impedance tuning unit. The outer loop adjusts the phase of the antenna input impedance to zero by changing the phase of the

reflection coefficient on constant VSWR circle.

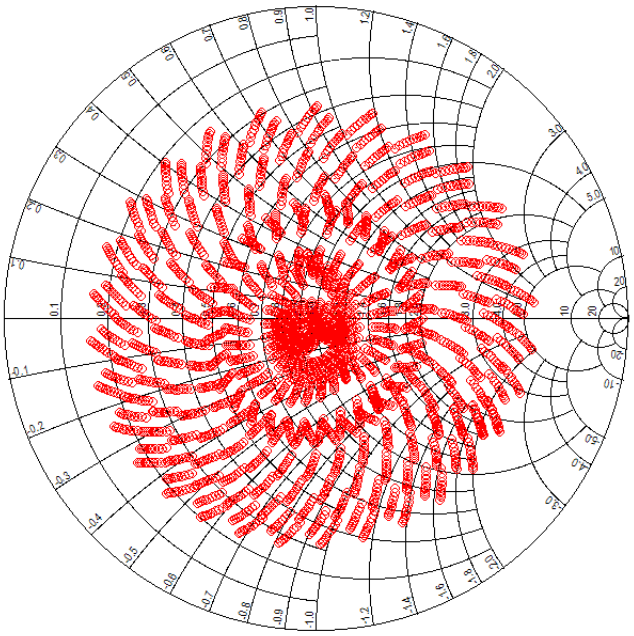

Figure 3.32: Impedance coverage region of T-matching circuit and 180 degree tunable phase shifter on the Smith Chart

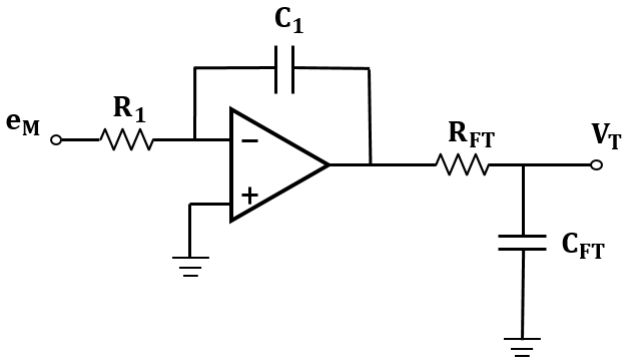

Figure 3.33: Circuit schematic of an inverting integrator with RC bias circuit for the impedance magnitude control

Loop equations that governs the outer and inner loop tuning process are expressed in equations 3.53 and 3.54 based on input-output relation of the inverting integrator as shown in Figures 3.33 and 3.34.

$$R_1 R_{FT} C_1 C_{FT} \frac{d^2 V_T}{dt^2} + R_1 C_1 \frac{dV_T}{dt} + e_M = 0 \tag{3.53}$$

$$R_2 R_{FT} C_1 C_{FT} \frac{d^2 V_P}{dt^2} + R_2 C_2 \frac{dV_P}{dt} + e_P = 0 \tag{3.54}$$

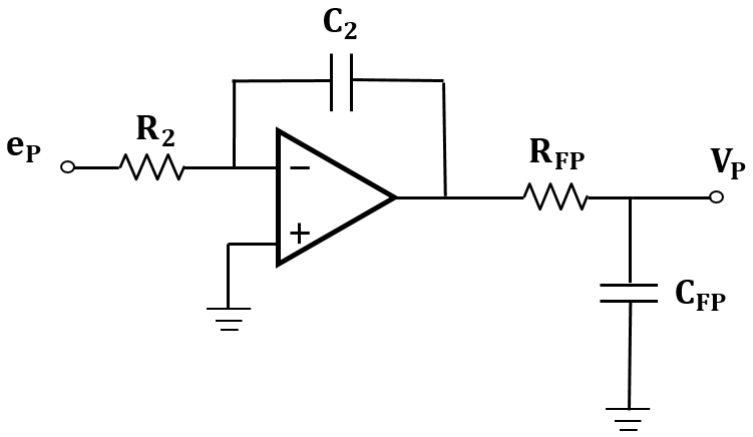

Figure 3.34: Circuit schematic of an inverting integrator with RC bias circuit for the impedance phase control

V_P and V_T can be described as control voltages for the 180 degree phase shifter and the tunable transformer, respectively. The automatic impedance tuner is simulated in ADS with the envelope simulator engine at 900 MHz to test the dynamic performance of the impedance tuner consisting of T-matching circuit and 180 degree phase shifter. Reflection coefficient (dB), antenna input impedance variations with time are plotted for different mismatched antenna impedances ($Z_{mismatched}$) in rectangular plots and the Smith Chart as shown in Figures 3.35 to 3.40. The simulation results show that the automatic impedance tuning unit dynamically compensates for the mismatches in less than 5 msec. The reflection coefficient magnitude is below -20 dB in less than 2 msec after the initiation of the adaptive tuning process as illustrated in Figures 3.36, 3.38, 3.40.

3.5 Adaptive Impedance Matching with Variable Transformer and 90 Degree Phase Shifter

This section focuses on the design and simulation of an automatic impedance matching circuit which dynamically removes the effects of the mismatched impedances by using magnitude and phase detection units with a variable transformer and a 90 degree tunable phase shifter. The automatic impedance tuning circuit is composed of a quarter wavelength transmission line, impedance magnitude and phase detection units, noninverting integrators, a variable transformer and a 90 degree tunable phase

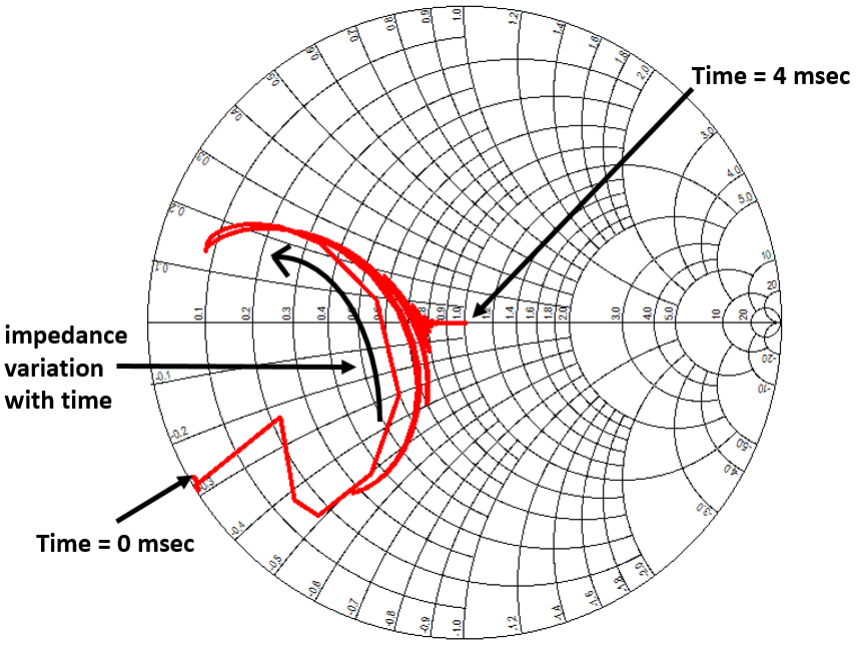

Figure 3.35: Impedance variation with time on the Smith Chart when the mismatched antenna input impedance $Z_{mismatched} = 50 - 100j\,\Omega$ is tested with the automatic impedance tuner

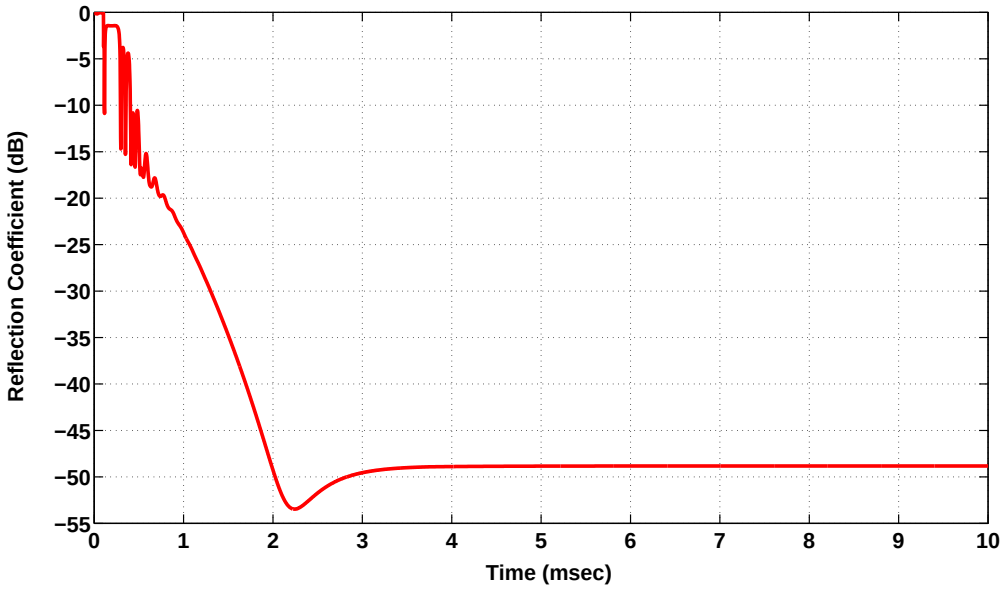

Figure 3.36: Reflection coefficient variation with time when the mismatched antenna input impedance $Z_{mismatched} = 50 - 100j\,\Omega$ is tested with the automatic impedance tuner

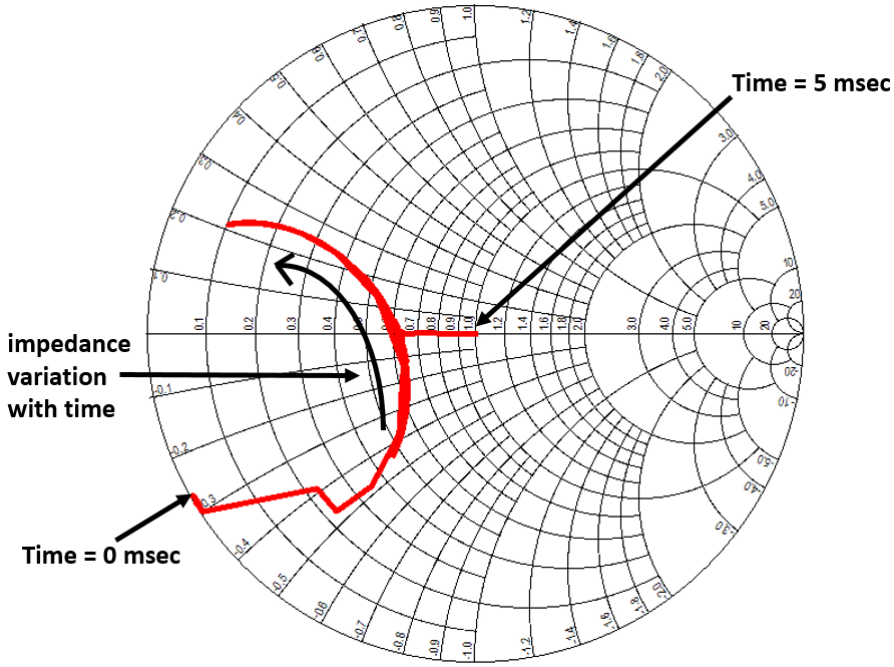

Figure 3.37: Impedance variation with time on the Smith Chart when antenna the mismatched input impedance $Z_{mismatched} = 30 - 50j\,\Omega$ is tested with the automatic impedance tuner

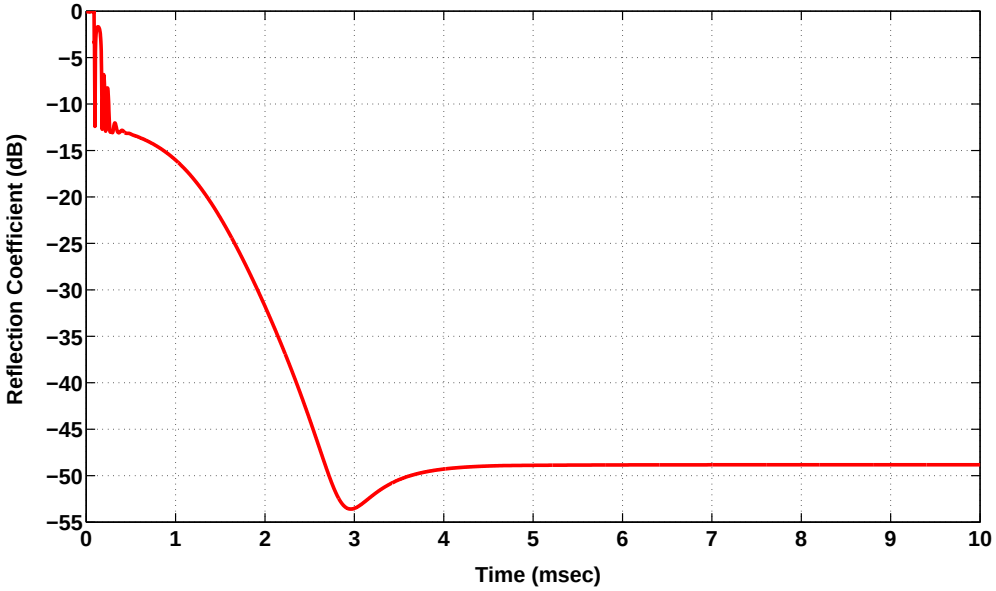

Figure 3.38: Reflection coefficient variation with time when the mismatched antenna input impedance $Z_{mismatched} = 30 - 50j\,\Omega$ is tested with automatic impedance tuner

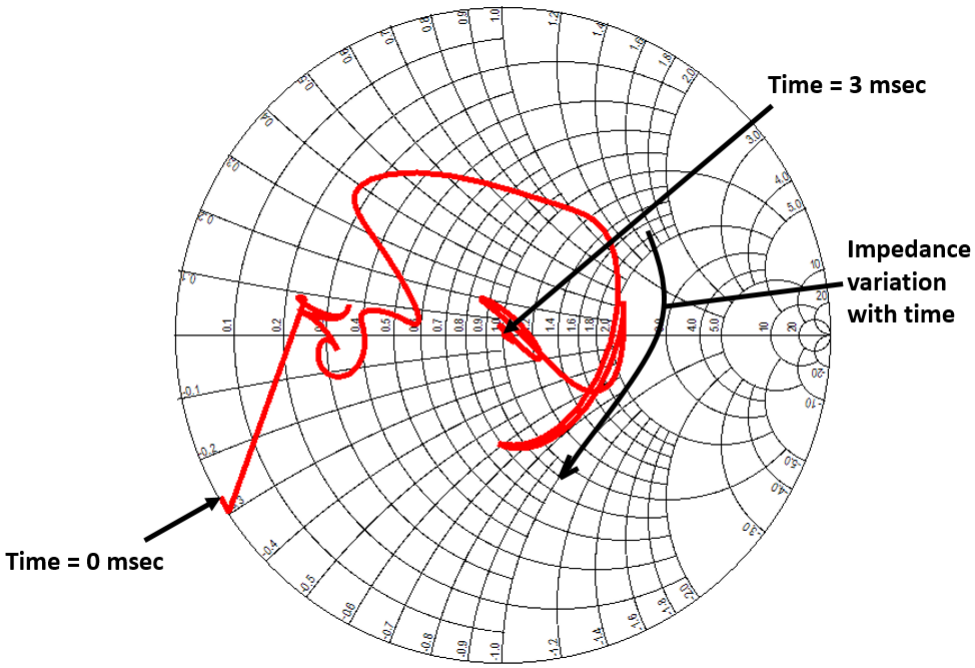

Figure 3.39: Impedance variation with time on the Smith Chart when the mismatched antenna input impedance $Z_{mismatched} = 100 - 10j\,\Omega$ is tested with the automatic impedance tuner

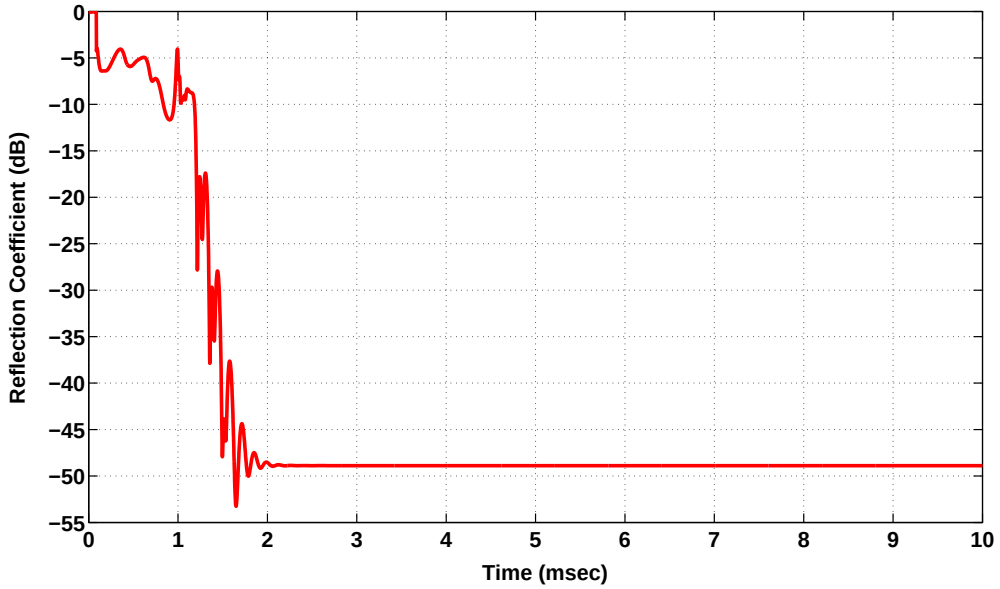

Figure 3.40: Reflection coefficient variation with time when the mismatched antenna input impedance $Z_{mismatched} = 100 - 10j\,\Omega$ is tested with the automatic impedance tuner

shifter connected in cascade as illustrated in Figure 3.41. Since 90 degree tunable

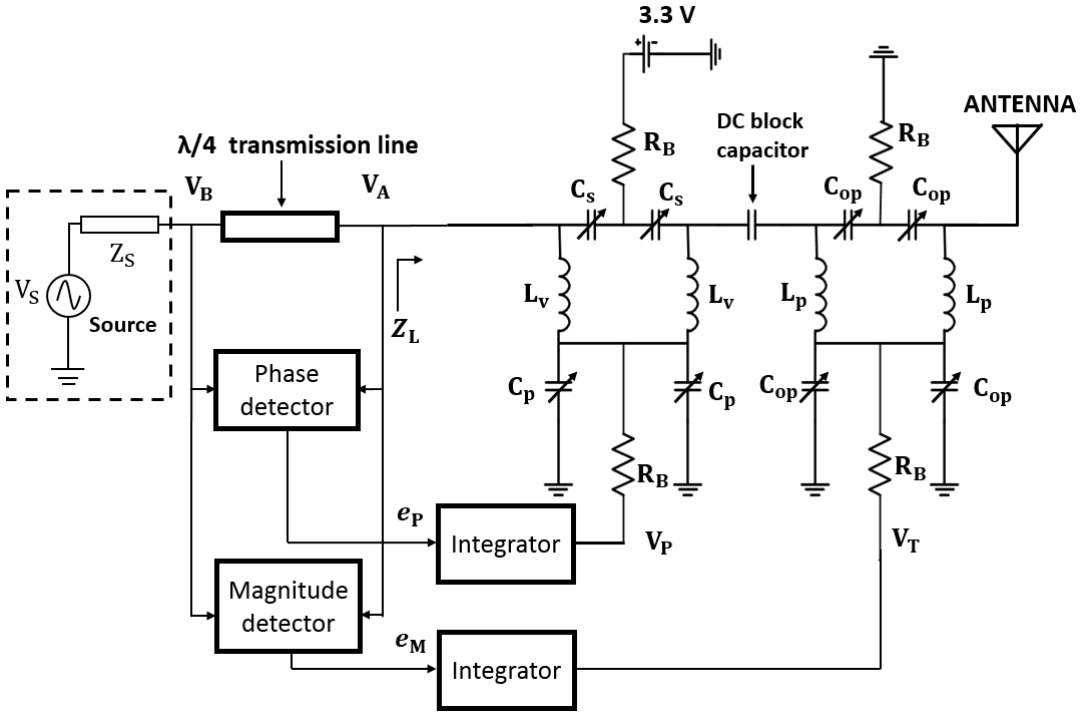

Figure 3.41: Block diagram of the automatic impedance tuner with impedance magnitude and phase detection units including variable transformer and 90 degree phase shifter

phase shifter is utilized to set the magnitude of normalized antenna input impedance to 1, the output of the impedance magnitude detection unit is fed through a non inverting opamp integrator to the tunable phase shifter as depicted in Figure 3.41. The output of the magnitude detection unit produces an error signal to check whether impedance magnitude tuning is achieved or not. It is connected to an non inverting integrator in order to generate a control signal for tunable phase shifter which changes continuously the phase of the reflection coefficient until the output voltage of magnitude detector becomes zero (i.e error signal). When the magnitude detector produces zero error voltage, the input impedance of tunable phase shifter is set to the impedance point which resides in the lower vertical axis of the Smith Chart (i.e. impedance magnitude tuning). After setting the magnitude of normalized antenna input impedance to 1, the variable transformer sets the phase of the input impedance of tunable phase shifter to zero without affecting its magnitude. To accomplish the impedance phase tuning, noninverting integrator which is fed by the output of phase detector is attached to the variable transformer circuit as illustrated in Figure 3.41.

Since the overall tuning unit performs the automatic tuning process in a sequential manner with two nested loops, the outer loop controlling the tunable phase shifter needs to converge faster than the inner loop. Therefore, in order to achieve this sequential tuning process, the feedback capacitance of the outer loop integrator is chosen smaller than the feedback capacitance of the inner loop integrator. The input resistance (R_1) and the feedback capacitance (C_1) values of the noninverting opamp integrator which dynamically controls the variable transformer are set to 1 kΩ and 10 nF, respectively. The input impedance (R_2) and the feedback capacitance (C_2) values of the opamp integrator which adjusts tunable phase shifter for impedance magnitude tuning are set to 100 kΩ and 4.7 nH, respectively. Besides, the capacitance value at the output of the integrators are chosen as: C_{FT} = 3 pF. The impedance tuning unit is composed of semiconductor based varactor models and fixed inductors whose values are calculated in the previous sections. S parameter analysis is performed based on previously calculated C_{min}, C_{max} and fixed inductor values for both variable transformer and 90 degree tunable phase shifter to determine the impedance coverage region of this tuner. Figure 3.42 depicts the impedance coverage region of this tuner at 900 MHz. As long as the mismatched impedance falls into the coverage region of this impedance tuner, the antenna feed impedance can be matched perfectly to 50 Ω by this automatic impedance tuning unit. Loop equations that govern the adaptive tuning process are defined in equations 3.55 and 3.56 based on the input output relation of the noninverting opamp integrator depicted in Figures 3.44 and 3.43.

$$R_1 C_1 \frac{dV_T}{dt} - e_M = 0 \tag{3.55}$$

$$R_2 C_2 \frac{dV_P}{dt} - e_P = 0 \tag{3.56}$$

in which V_P and V_T is described as control voltages for the 90 degree phase shifter and variable transformer, respectively. The automatic impedance tuner is simulated in ADS with the envelope simulator engine (commercially available) at 900 MHz to test the dynamic performance of the impedance tuner consisting of the variable transformer and 90 degree phase shifter. The reflection coefficient magnitude (dB), the antenna input impedance, and the control voltage variations with time are plotted for different mismatched antenna input impedances ($Z_{mismatched}$) from Figure 3.45 to

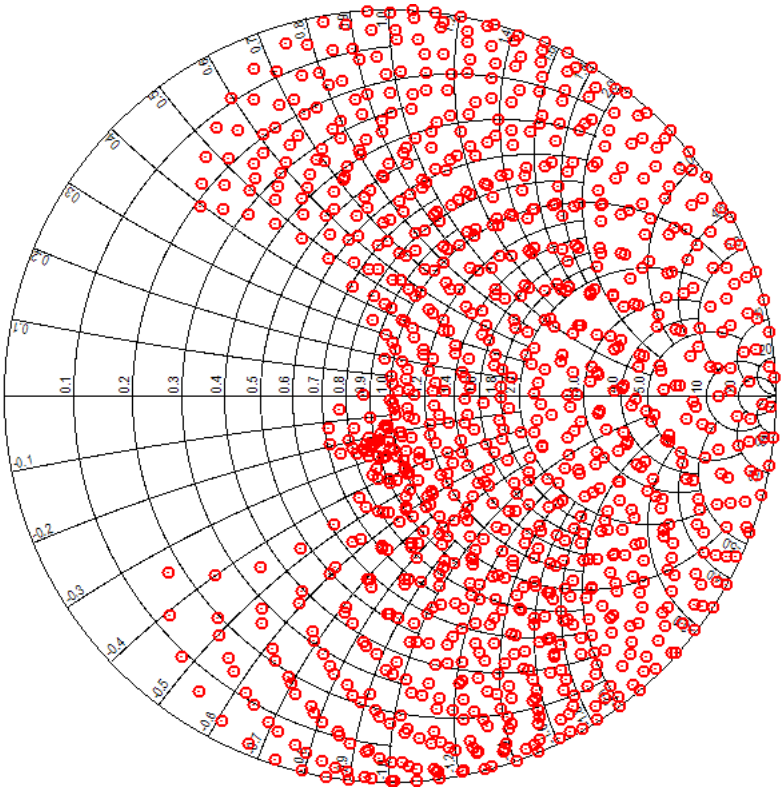

Figure 3.42: Impedance coverage region of impedance tuner including the variable transformer and 90 degree phase shifter

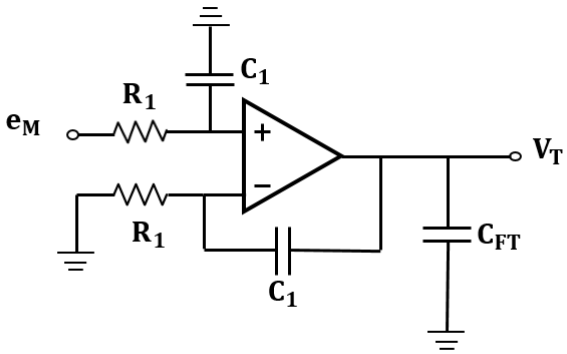

Figure 3.43: Circuit schematic of noninverting opamp and shunt capacitance for impedance magnitude control

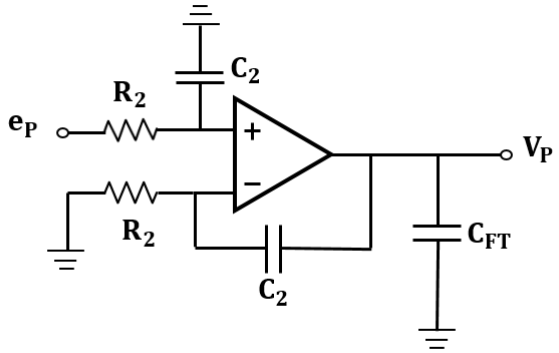

Figure 3.44: The circuit schematic of a noninverting opamp and a shunt capacitance for the impedance phase control

3.60. The simulation results show that the automatic impedance tuning unit dynamically compensates for the mismatches in less than 6 msec, which is suitable for tuning cell phone impedance variations due to interaction between cell phone and the body. Since control voltages for the tunable phase shifter and variable transformer varies between 0 - 3.3 V, this impedance tuner can satisfactorily meet the cell phone battery requirements.

3.6 Overall Assessment of Designed Tuned Circuits

In previous sections, two impedance tuner circuits offering independent control capability in magnitude and phase domain of antenna input impedance are tested with the automatic impedance tuning unit. These circuits can be compared in different ways such as control voltage level, coverage region, compactness, and insertion loss. Since impedance tuning unit including T-matching circuit and 180 degree phase shifter requires high control voltages beyond the maximum cell phone battery supply voltage, it is not appropriate for cell phone applications. Although this circuit offers tuning capability in a wide coverage region, it may bring up some problems in terms of compactness, and insertion loss. However, impedance tuner consisting of a variable transformer and a 90 degree phase shifter is more suitable than this tuner for such applications. Although its coverage area is limited compared to the impedance tuner including T matching circuit and 180 degree phase shifter, it is sufficient for

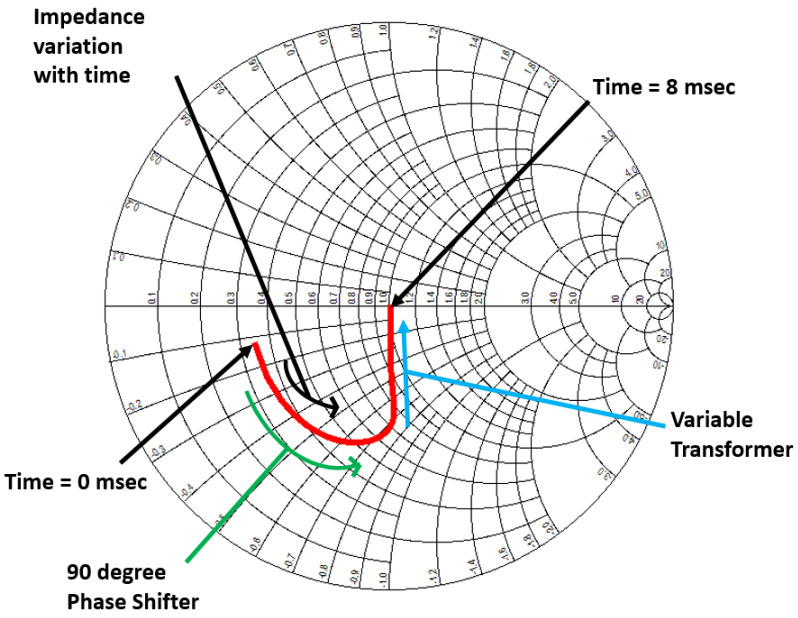

Figure 3.45: Impedance variation with time on the Smith Chart when the mismatched antenna input impedance $Z_{mismatched} = 120 + 90j\,\Omega$ is tested with the automatic impedance tuner

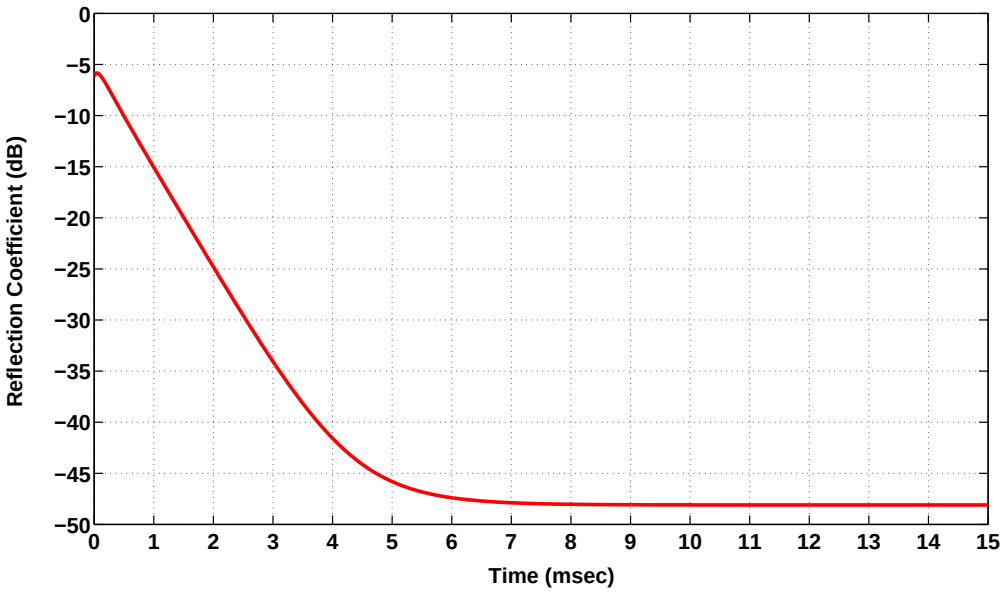

Figure 3.46: Reflection coefficient variation with time when the mismatched antenna input impedance $Z_{mismatched} = 120 + 90j\,\Omega$ is tested with the automatic impedance tuner

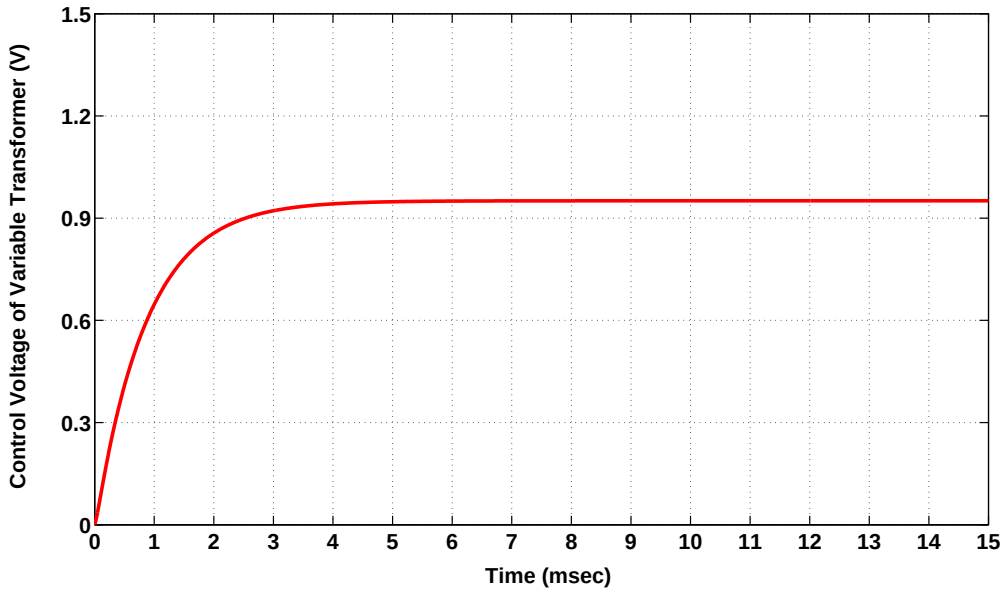

Figure 3.47: The control voltage variation of the variable transformer as a function of time when the antenna input impedance $Z_{mismatched} = 120 + 90j\,\Omega$ is tested with the automatic impedance tuner

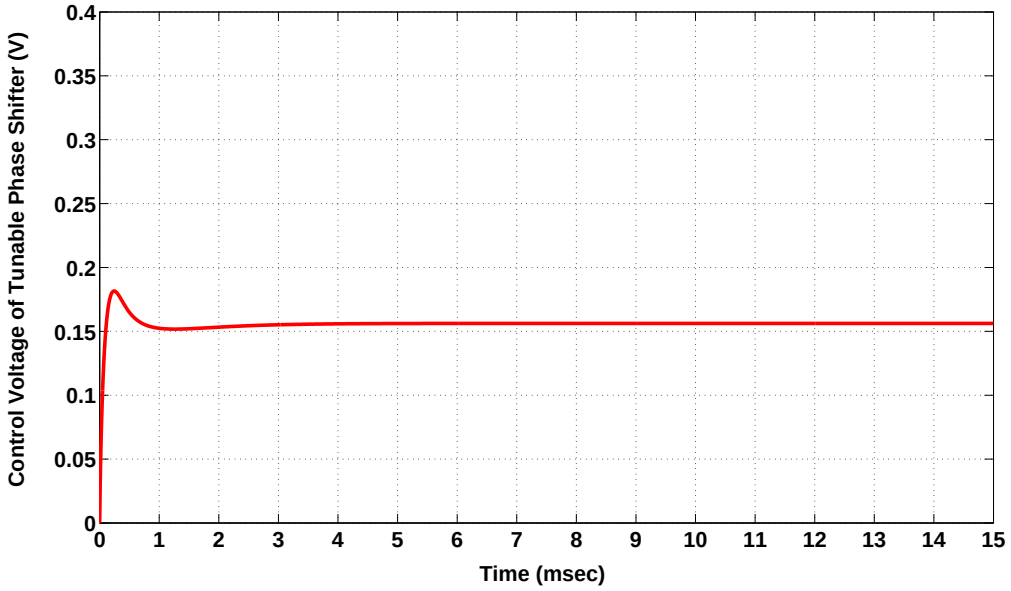

Figure 3.48: The control voltage variation of the 90 degree phase shifter with time when the antenna input impedance $Z_{mismatched} = 120 + 90j\,\Omega$ is tested with the automatic impedance tuner

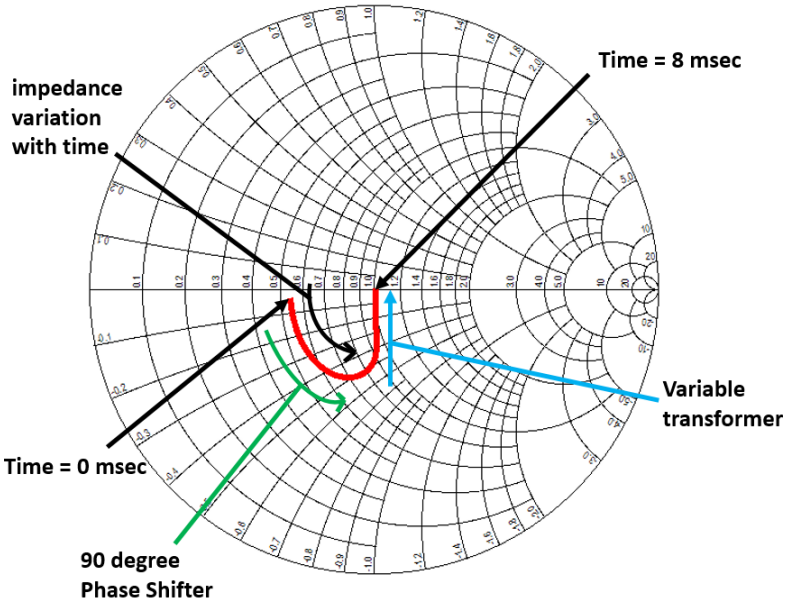

Figure 3.49: Impedance variation with time on the Smith Chart when the mismatched antenna input impedance $Z_{mismatched} = 100 + 20j\,\Omega$ is tested with the automatic impedance tuner

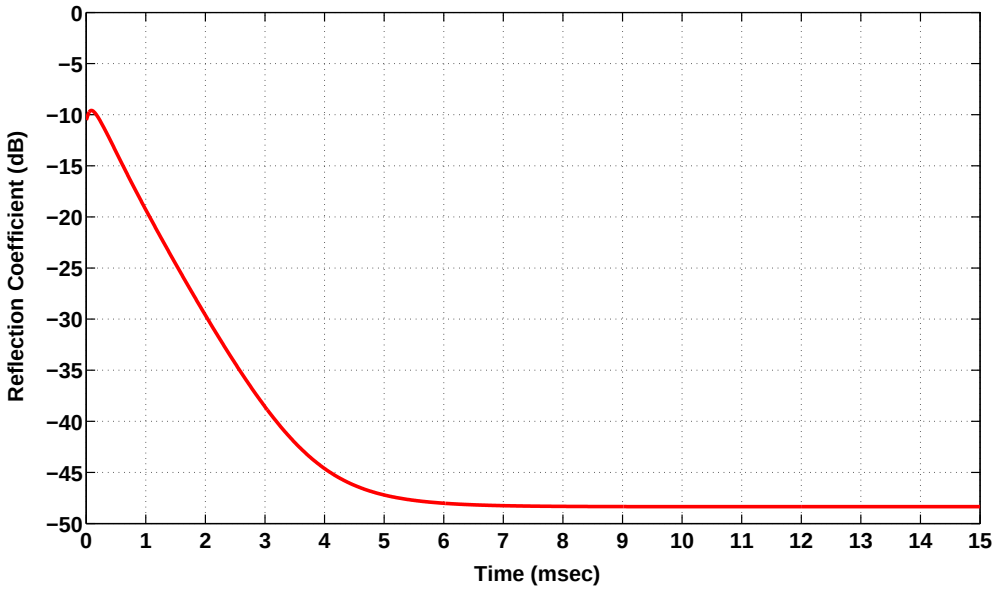

Figure 3.50: Reflection coefficient variation with time when the mismatched antenna input impedance $Z_{mismatched} = 100 + 20j\,\Omega$ is tested with the automatic impedance tuner

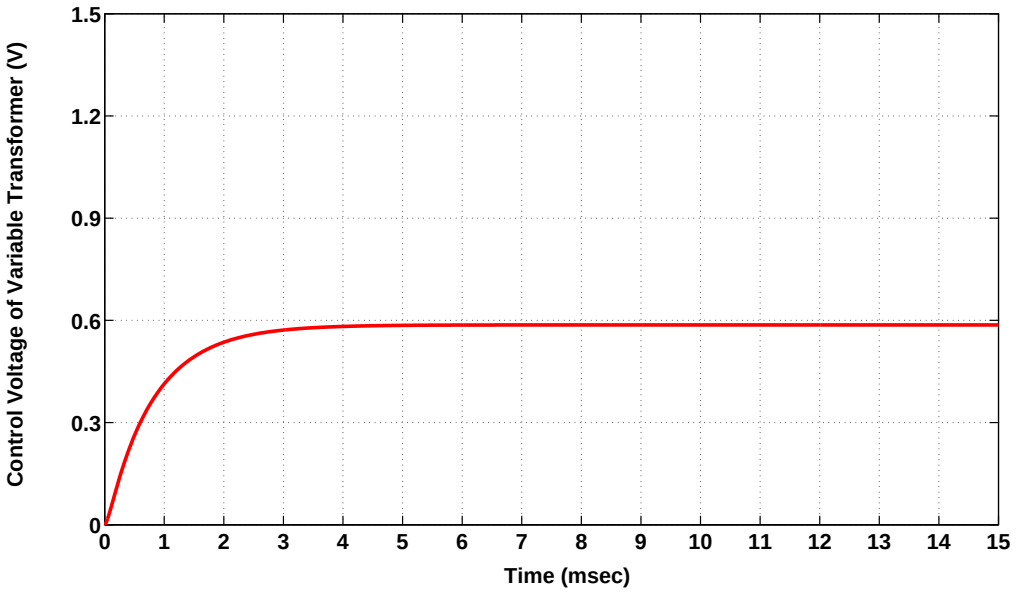

Figure 3.51: The control voltage variation of the variable transformer with time when the mismatched antenna input impedance $Z_{mismatched} = 100 + 20j\,\Omega$ is tested with the automatic impedance tuner

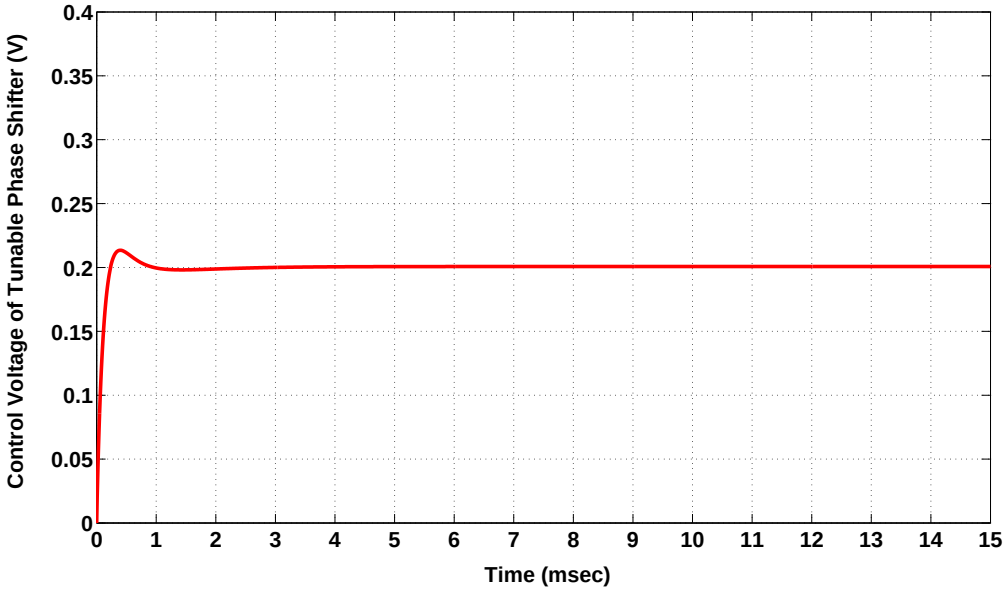

Figure 3.52: The control voltage variation of the tunable phase shifter with time when the mismatched antenna input impedance $Z_{mismatched} = 100 + 20j\,\Omega$ is tested with the automatic impedance tuner

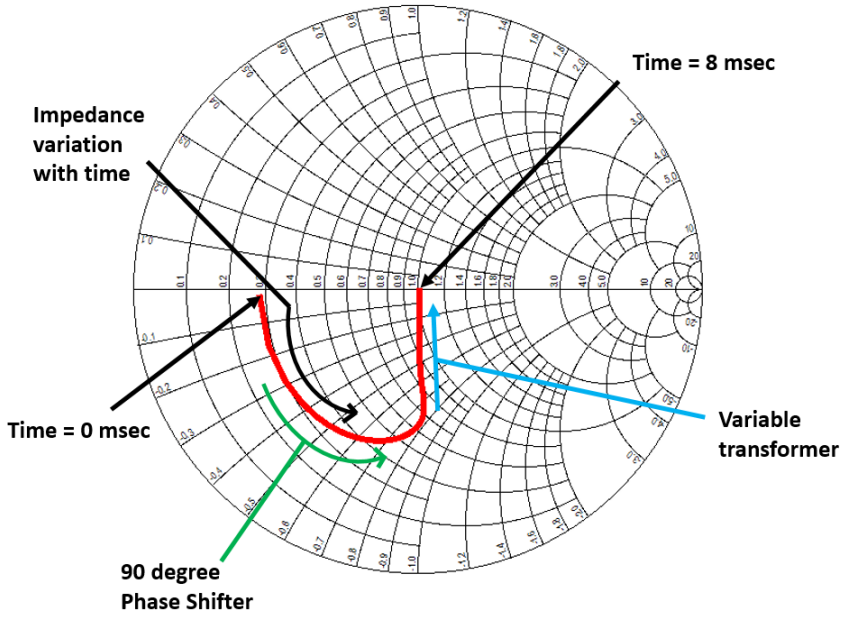

Figure 3.53: Impedance variation with time on the Smith Chart when the mismatched antenna input impedance $Z_{mismatched} = 200 + 100j\,\Omega$ is tested with the automatic impedance tuner

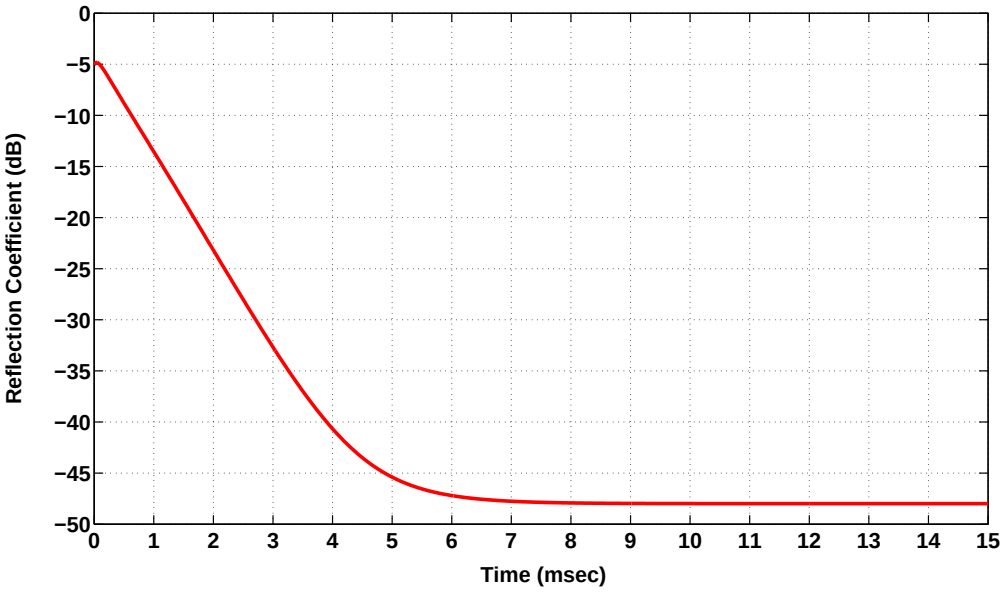

Figure 3.54: Reflection coefficient variation with time when the mismatched antenna input impedance $Z_{mismatched} = 200 + 100j\,\Omega$ is tested with the automatic impedance tuner

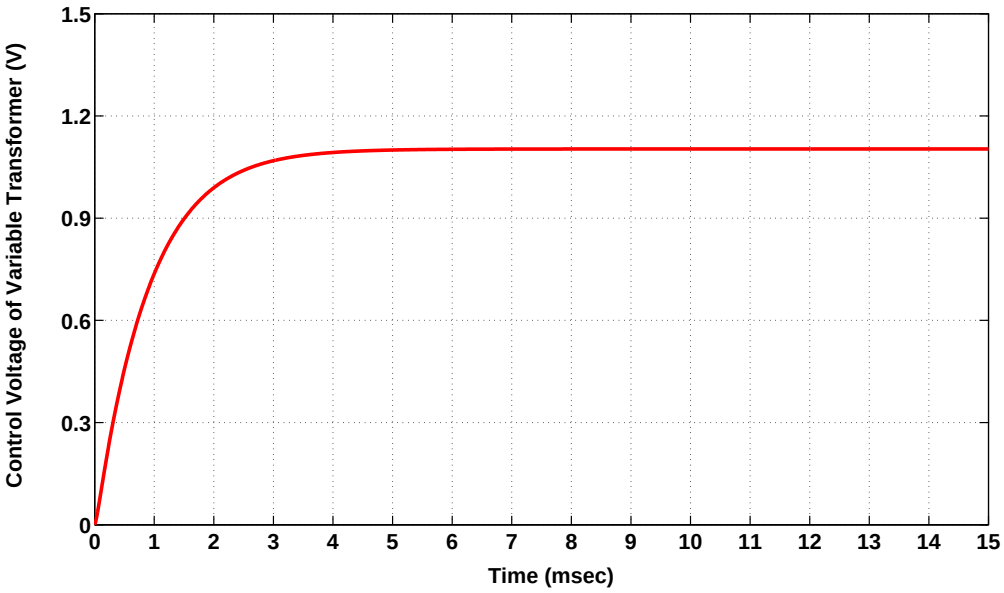

Figure 3.55: The control voltage variation of the variable transformer with time when the mismatched antenna input impedance $Z_{mismatched} = 200 + 100j\,\Omega$ is tested with the automatic impedance tuner

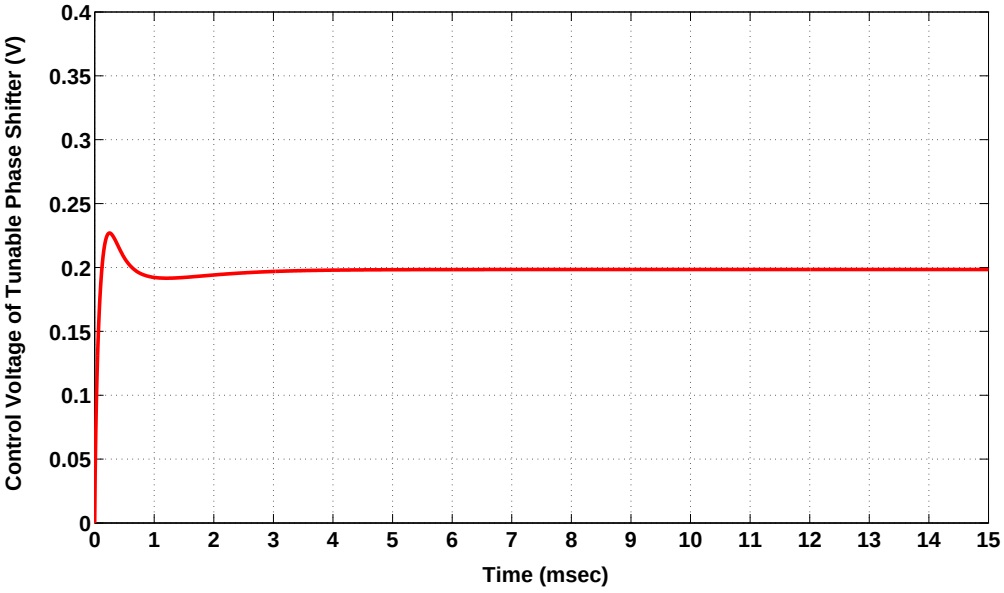

Figure 3.56: The control voltage variation of the 90 degree tunable phase shifter with time when antenna initial input impedance $Z_{mismatched} = 200 + 100j\,\Omega$ is tested with the automatic impedance tuner

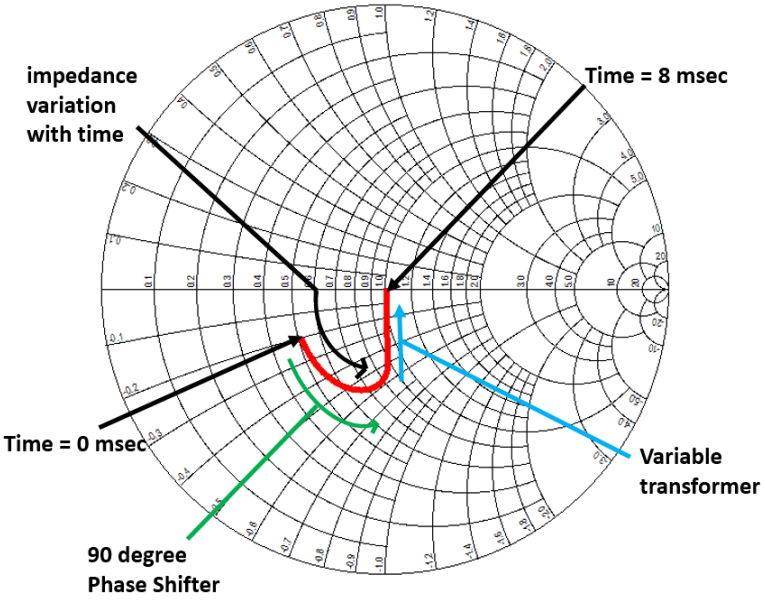

Figure 3.57: Impedance variation with time on the Smith Chart when the antenna input impedance $Z_{mismatched} = 80 + 50j\,\Omega$ is tested with the automatic impedance tuner

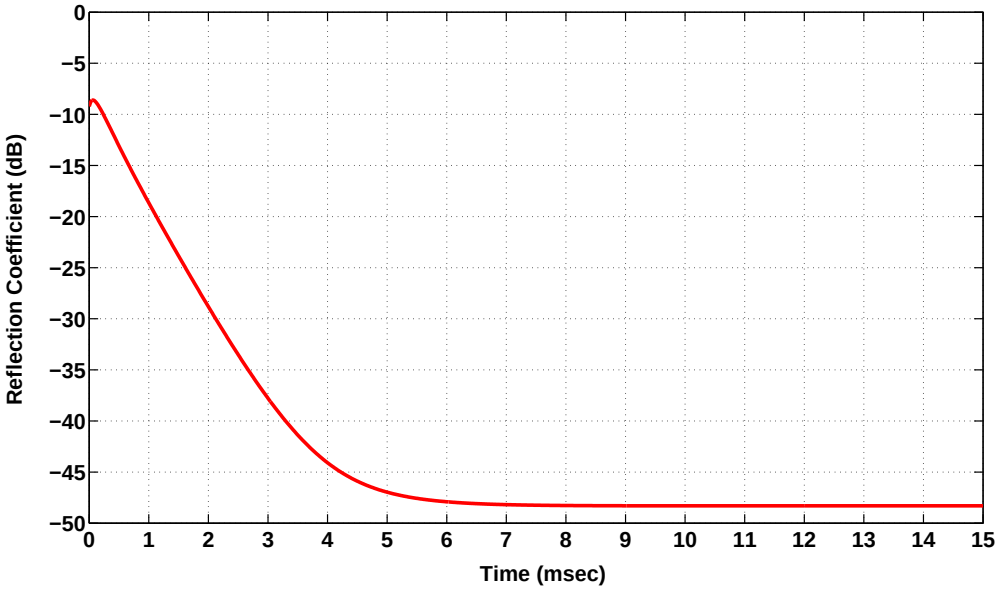

Figure 3.58: Reflection coefficient variation with time when antenna input impedance $Z_{mismatched} = 80 + 50j\,\Omega$ is tested with the automatic impedance tuner

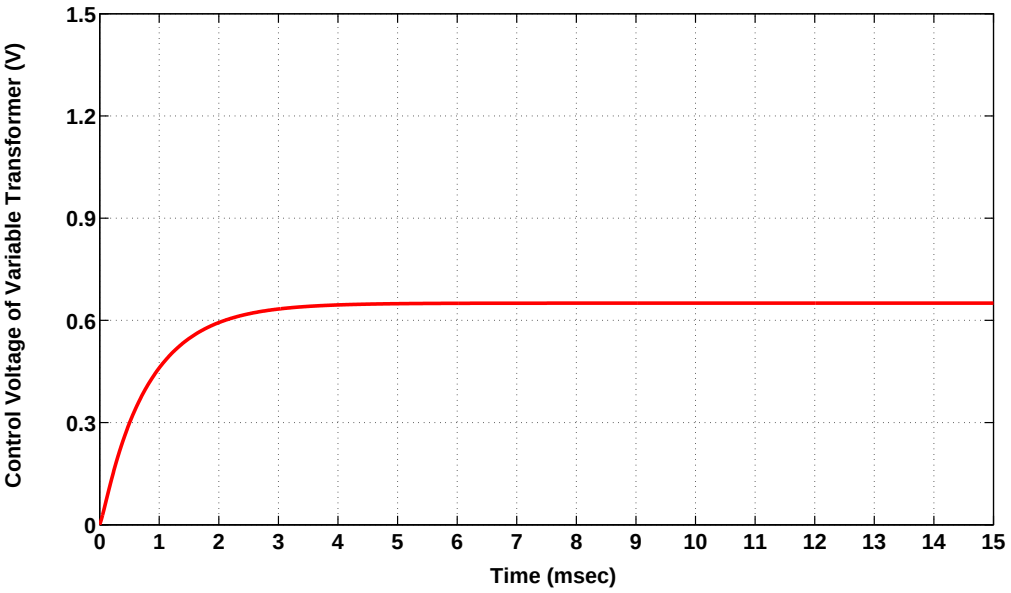

Figure 3.59: The control voltage variation of the variable transformer with time when the antenna input impedance $Z_{mismatched} = 80 + 50j\,\Omega$ is tested with the automatic impedance tuner

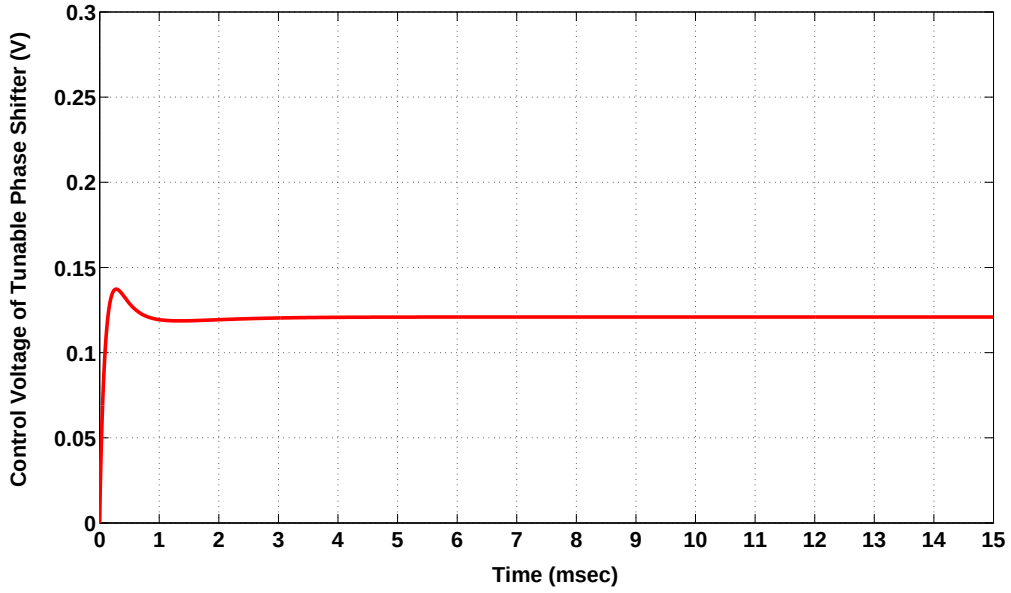

Figure 3.60: The control voltage variation of the 90 degree tunable phase shifter with time when the mismatched antenna impedance $Z_{mismatched} = 80 + 50j\,\Omega$ is tested with the automatic impedance tuner

cell phone applications. Besides, it provides tuning capability in cell phone battery supply range without requiring any extra circuit.

CHAPTER 4

MANUFACTURING AND MEASUREMENT

This chapter is devoted to the design and implementation of the automatic impedance tuning circuit consisting of the impedance tuner, an impedance detection, and control units. In the first section, a prototype of the impedance tuner composed of a 90 degree phase shifter and a variable transformer connected in cascade is implemented on an FR4 board. The design is based on the discussion detailed in the previous chapter. The limitations of impedance tuning units employing semiconductor varactor technology are also discussed in the same section. The impedance detection and control units composed of chip couplers, attenuators, and a gain and phase detector chip component (AD8302) are manufactured on an FR4 substrate and tested. In the final section, the automatic impedance tuning unit is fabricated to test the tuning performance of impedance tuner for various load impedances in GSM band. Load impedance variations on the Smith Chart with automatic tuning are plotted for different load impedances to investigate the impedance tuning capability of the automatic tuner. The VSWR values of load and tuned impedances are compared in the frequency band of 880-920 MHz. Besides, the relative transducer gain measurements are performed to assess the overall efficiency of the impedance tuner for different load impedances.

4.1 Implementation of Tunable Impedance Matching Circuit

In this section, a prototype of the impedance tuner consisting of cascade connected 90 degree tunable phase shifter and variable transformer based on semiconductor tech-

nology is implemented. The circuit schematics of the variable transformer and 90 degree phase shifter connected to each other in cascade is depicted in Figure 4.1

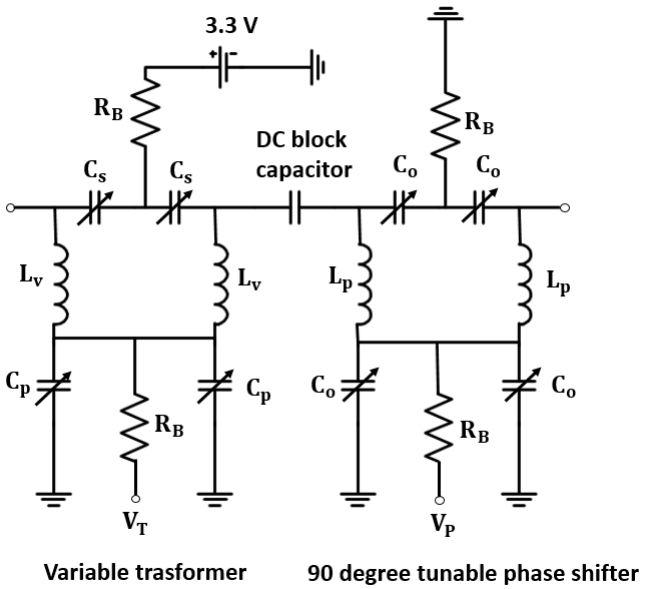

Figure 4.1: Cascade connection of variable transformer and 90 degree tunable transformer

Although tunable circuits offer flexibility to change the load impedance electronically, the usage of tunable circuits brings up some limitations and trade-offs in terms of insertion loss and impedance coverage. Variable capacitance can be achieved by using various technologies. Since semiconductor based varactor technology is utilized to implement this reconfigurable circuit, the basic limitations of semiconductor varactors for cell phone applications are given as follows:

1. The main factor which directly determines these limitations is the quality factor of the components (also known as the figure of merit). It is an important parameter for conventional and tunable circuits, which measures the energy storage capability of a component with respect to the dissipated energy on it. Since chip components (i.e. inductors and varactors) with finite Q values are available for real life applications, the tunable circuits composed of these components lead to losses and reduction in impedance tuning range.

2. Variation of junction capacitance due to reverse bias voltage leads to change in the quality factor of varactor. The increase in the applied reverse bias voltage

changes the junction capacitance inversely, which enhances the quality factor of the varactor.

3. Since impedance tuner including varactors and fixed inductors is integrated in a cell phone, the maximum voltage of the cell phone battery limits the varactor tuning range, which challenges the impedance tuner design.

4. Besides, as the decrease in the applied reverse bias voltage leads to reduction in the quality factor of the varactor, Q value of the varactor in the cell phone battery supply range (0-3.3 V) is lower than the reverse bias voltages close to breakdown condition. Thus, the maximum voltage of the cell phone battery restricts the effective usage of the impedance tuner due to low Q values in limited battery supply range.

As elaborated in the previous chapter, the inductor and varactor (C_{min} and C_{max}) values are calculated and simulated for the 90 degree phase shifter and the variable transformer at 900 MHz. Various manufacturers are investigated to find high Q inductors and varactors operating at GSM bands. SMV 1263 hyperabrupt junction tuning varactors from SKYWORKS are employed in the 90 degree phase shifter to achieve tuning range from 2.185 pF to 5.721 pF (C_o) within the control voltage range of 0-3.3 V. SMV 1233 and SMV 1234 hyperabrupt junction tuning varactors from SKYWORKS are chosen for variable transformer which provides capacitance tuning range from 3.536 pF to 1.718 pF (C_p) and from 7.072 pF to 3.536 pF (C_s), respectively. Moreover, coilcraft chip inductors of 0603CT-5N6 (L_p = 5.46 nH) and 0402HP-8N7 (L_v = 8.841 nH) are utilized in the 90 degree phase shifter and variable transformer, respectively [30]. The bias resistors of the variable transformer and 90 degree phase shifter (R_B) are chosen as 1 kΩ.

The impedance tuner is fabricated on a 1.6 mm -thick FR-4 board ($\epsilon_r = 4.4$, tanδ = 0.016) and the operating bandwidth is between 880 MHz-920 MHz. The photograph in Figure 4.2 depicts the manufactured impedance tuner. All the components including semiconductor varactors, inductors, DC block capacitors and bias resistors are mounted on FR4 substrate as shown in Figure 4.2. This fabricated impedance tuning unit design based on semiconductor varactors is tested for various load impedances with the impedance detection and the control circuit in section 4.4.

The fabrication of the impedance tuning unit composed of a cascade connecting the variable transformer and 90 degree phase shifter is presented in this section. The hyperabrupt junction tuning varactors from the manufacturer are chosen in order to ensure that they satisfactorily meet varactor tuning requirements of the 90 degree tunable phase shifter and variable transformer in limited supply range (0-3.3 V). In the following section, the high power effects on a impedance tuner designed based on semiconductor varactors are discussed in detail.

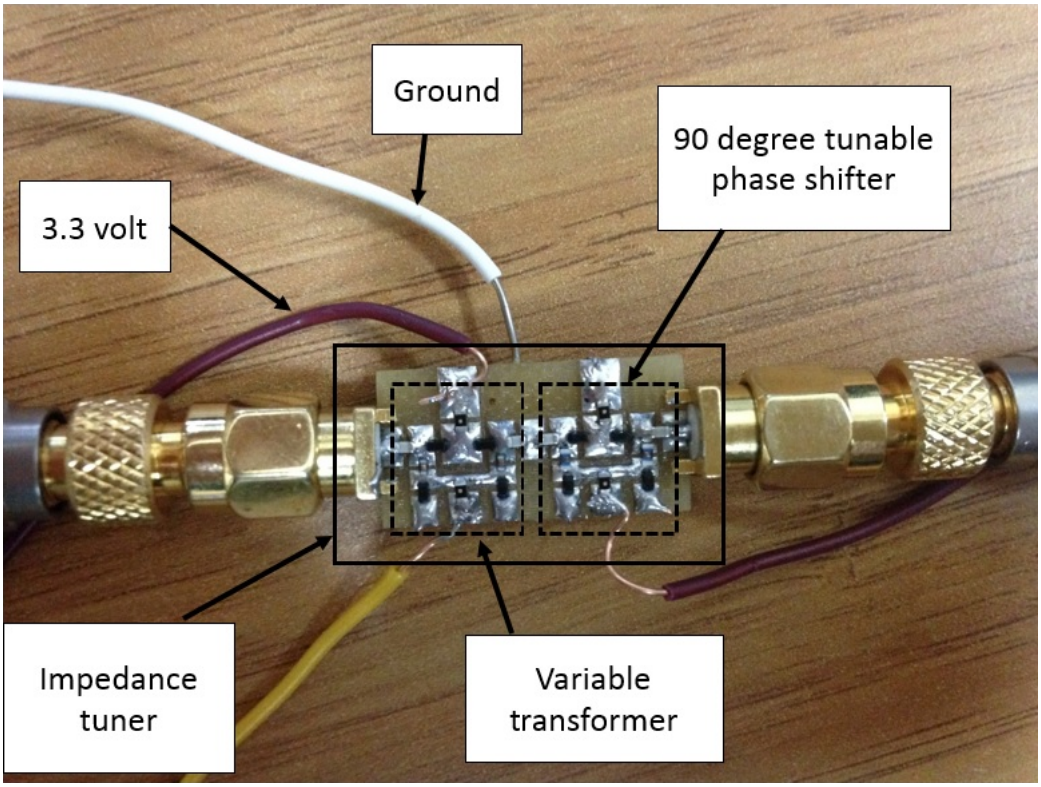

Figure 4.2: Photo of the fabricated impedance tuner circuit

4.1.1 Limitations of The Impedance Tuners

This section primarily investigates the effects of large RF swing across the semiconductor varactors due to the application of high powers to the impedance tuning unit. Semiconductor based varactor diodes are commonly utilized for tuning RF circuits electronically by a DC control voltage. Reverse biased control voltage changes the width of the depletion region which allows the control of the capacitance value introduced by the varactor. This component provides an opportunity to design compact

tunable RF circuits with a moderate capacitance tuning ratio. It also offers the advantages in terms of the low control voltage, high reliability and ease of integration. Besides, the continuous tuning capability with fast tuning speed makes it very attractive for adaptive impedance tuning circuits. However, high power applications mainly affect the maximum tuning range of the varactor and modulate the capacitance value due to the large RF swing across the varactor. The operating mode of the varactor which is a part of the impedance tuner can be changed depending on the total voltage (RF+DC) between its leads. To avoid destroying the varactor, the summation of the applied DC control voltage and the amplitude of the RF signal need to be lower than the breakdown voltage of varactor, $V_{Breakdown}$ [31]. Besides, minimum control voltage must be chosen carefully with applied specific power to avoid turn on mode as illustrated in Figure 4.3.

Equations 4.1 and 4.2 need to be satisfied in order to operate varactors in reverse biased mode,

$$V_{DC} + V_{RF} \leq V_B \tag{4.1}$$

$$V_{DC} - V_{RF} \geq 0 \tag{4.2}$$

Turn on limitation increases the minimum operating control voltage to avoid forward bias which leads to decrease the maximum tunable capacitance value. In other words, the peak value of V_{RF} must be lower than V_{DC} signal to keep the varactor in reverse biased mode. The topology of varactor connection and amount of power applied to the circuit determine the peak value of the RF swing across the varactor. A series connection of multiple varactors and high breakdown voltage varactors can be utilized to overcome these issues. By doing so, large RF swing is successfully divided across the multiple devices and the destructive effects for the varactor can be avoided. However, the increase in the varactor number brings up extra parasitics due to these connections. This trade off should be taken into consideration for high power applications. Quality factor of varactor can be defined as the ratio of the stored and dissipated energy on a varactor. The quality factor of the varactor is inversely proportional to operating frequency, junction capacitance and the summation of the undepleted epi

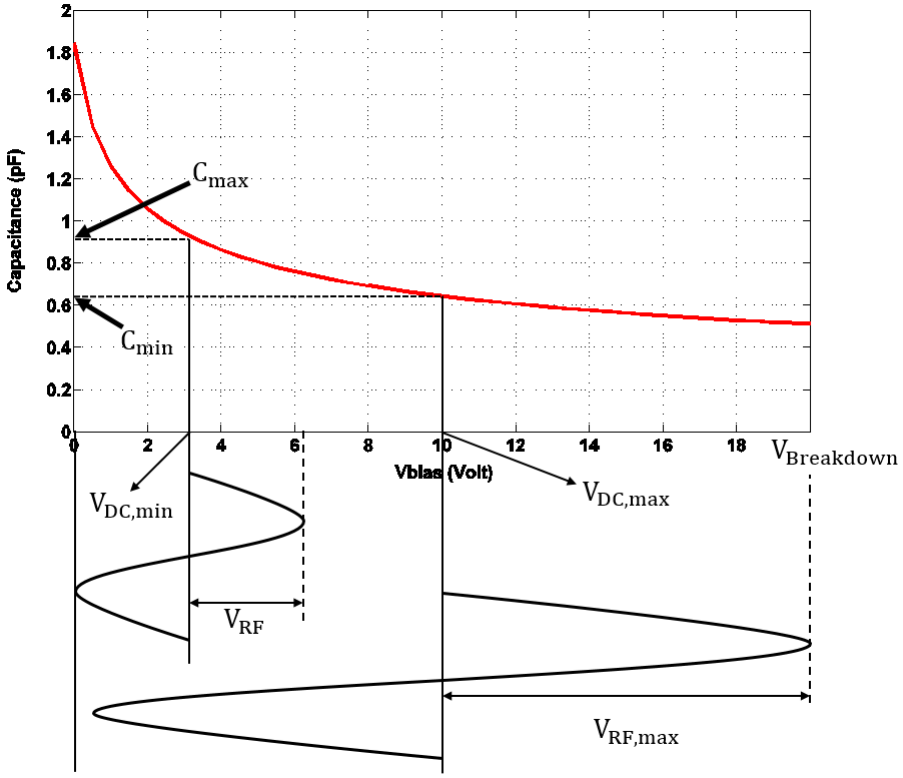

Figure 4.3: Typical varactor C-V characteristic with two extreme operating condition

and fixed contact resistance ($R_V = R_{epi} + R_{fixed}$) as defined in equation 4.3 [32].

$$Q = \frac{1}{wR_{(-V)}C_{(-V)}} \tag{4.3}$$

The increase in the reverse bias voltage reduces the junction capacitance and total resistance value which leads to enhance the quality factor of the varactor. Thus, the varactors require high DC voltages to reduce dissipation loss in tunable matching circuits. Besides, the loss introduced by the varactor becomes more pronounced in higher frequencies as stated in equation 4.3.

The cell phone battery supplies limited voltage (0-3.3 V) and RF swing across the varactors should be small to keep the varactors in their tuning range and to avoid turn on mode.

The effects of large RF swing on operating mode of the semiconductor varactors are discussed by taking into consideration both turn on and breakdown operation. The large RF swing across the varactor restricts the maximum and minimum tunable capacitance value of the varactor in reverse bias mode. Besides, since RF signal varies

continuously with time, the summation of DC and RF signal move back and forth between the minimum and maximum peak values of the overall signal in the horizontal axis of the Figure 4.3, which leads to the modulation of varactor capacitance value in such applications. Anti-series connection and the parameters which mainly affect the quality factor of varactors are also discussed in this section.

In the following section, the design and fabrication process of impedance sensing and detection unit which produces control voltages for the reflection coefficient magnitude and phase is discussed in detail.

4.2 Impedance Sensing and Detection

This section includes the design and implementation of impedance sensing and detection block as a part of overall automatic impedance matching system. Firstly, the general features, operating conditions, and the limitations of a commercially available electronic component (reflection coefficient detector) which provides an opportunity to measure reflection coefficient magnitude and phase is discussed. This is followed by a description of the coupling of the incident and reflected wave from the source and tuner side and measuring process of the reflection coefficient.

Since the variable transformer and the 90 degree phase shifter demand two separate signals to control both the magnitude and phase of the reflection coefficient, control voltages need to be produced by measuring the magnitude and the phase of the reflection coefficient at the input port of the impedance tuner. Analog Devices' wideband RF/IF Gain and Phase detector (AD8302) can be utilized as a reflectometer to measure the magnitude and the phase of the reflection coefficient [33]. The functional block diagram of the AD8302 is illustrated in Figure 4.4. It consists of log amps and a phase detector operating from -60 dBm to 0 dBm power range in a 50 Ω system. Besides, it can be used as a comparator, a controller, a gain and phase measurement of an amplifier or mixer with couplers and input circuitry.

The magnitude of the reflection coefficient is detected by comparing RMS voltage values of signals at the INPB and INPA ports of AD8302. It produces output voltages (V_{MAG}) and (V_{PHS}) based on the power ratio and the phase difference of the signals

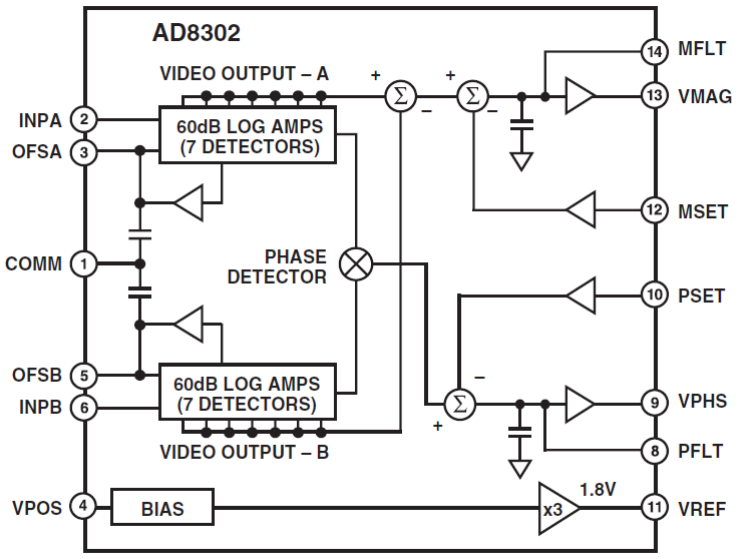

Figure 4.4: Functional block diagram of AD8302

that are available at the INPA and INPB ports. The transfer functions of AD8302 for both magnitude and phase detection are plotted based on measurement mode equations defined in its datasheet as depicted in Figure 4.5 and Figure 4.6, respectively [33]. Since the minimum measurable reflection coefficient in dB with AD8302 is -30 dB and the maximum value of it is never greater than 0 dB, the output of voltage of the AD8302 (V_{MAG}) varies between 0-0.9 V in ideal case. Operating of AD8302 as a reflectometer provides the diagnosis of the antenna mismatches that can cause severe problems in RF front end.

Since the magnitude and the phase detection of the reflection coefficient can be obtained at the same time, the use of AD8302 is very popular at reconfigurable RF front end systems. However, there are some requirements to use this off-shelf component effectively and correctly. For maximum dynamic range usage, -30 dBm reference power must be applied to INPB of AD8302. In order to operate AD8302 in maximum phase detection range, $\pm$90 degree phase difference must be set between the signals at INPA and INPB pins of the device in the perfect matched case. This reference phase shift must be introduced by the user to resolve the sign ambiguity and to avoid inaccuracies in the phase detector. Otherwise, the output voltage of V_{PHS} would be the same for -10 and 10 degree phase difference as shown in Figure 4.6. The incident and reflected waves coupled by using two identical 10 dB directional couplers from

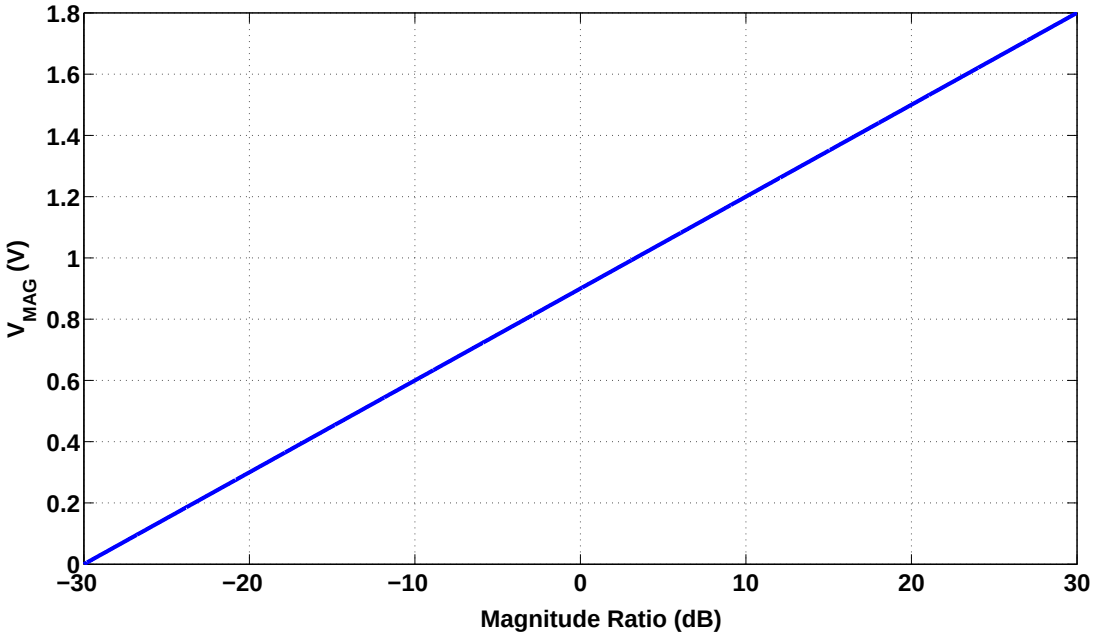

Figure 4.5: Output voltage (V_{MAG}) relation with magnitude ratio of the input signals

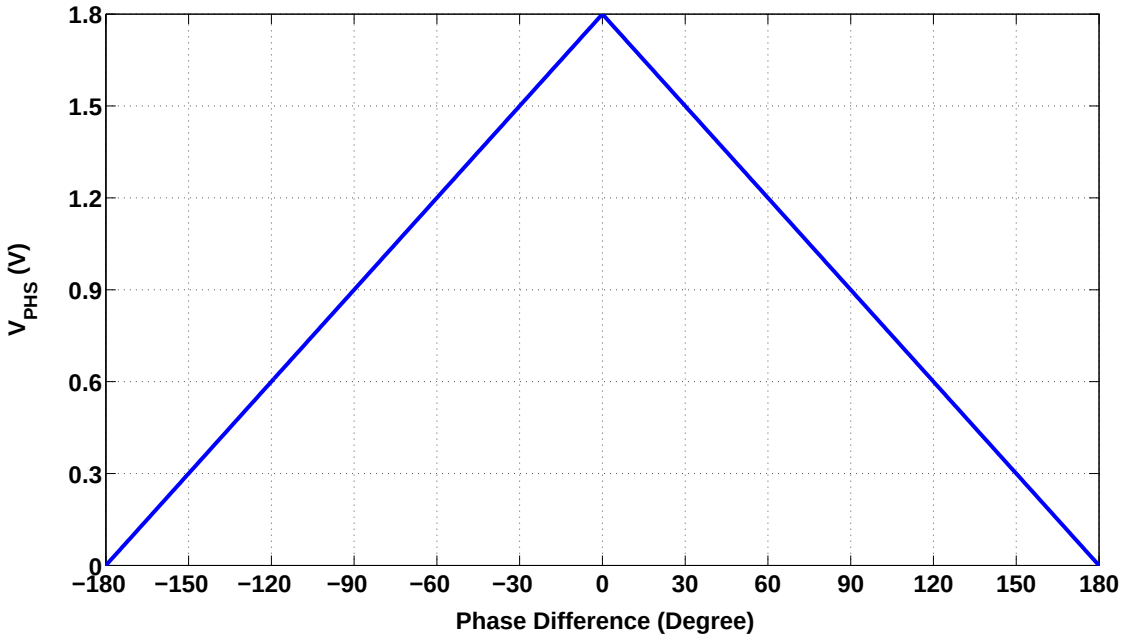

Figure 4.6: Output voltage (V_{PHS}) relation with phase difference of the input signals

ANAREN (model DC0710J5010AHF) are fed to the INPB and INPA of AD8302 through attenuators and the input circuitry of AD8302, respectively [34]. Since INPB is chosen for the reference port in reflectometer application, the coupled power from the source side is reduced to -30 dBm level using a attenuator. The connection of the couplers and the attenuators consisting of the impedance sensing unit is depicted on the Figure 4.7. In the previous chapter, the quarter wavelength transmission line is

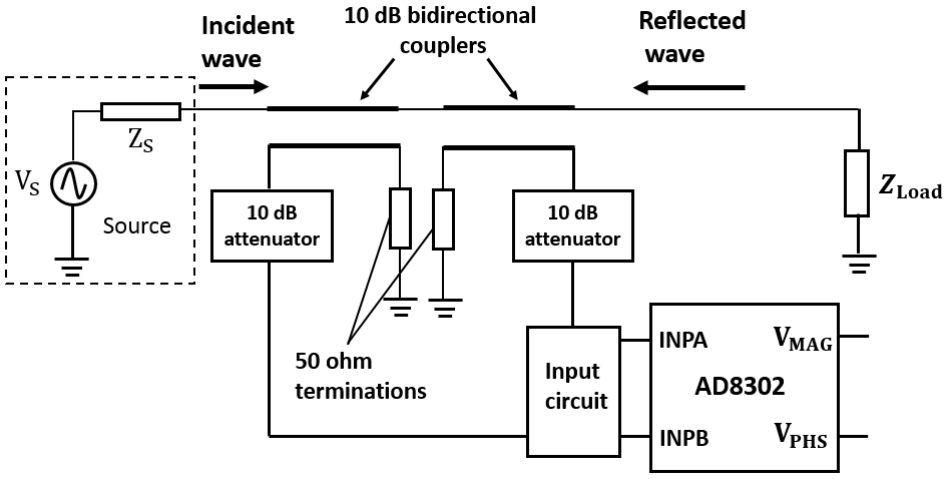

Figure 4.7: Block diagram of impedance sensing and detection unit

fixed between the impedance tuner and the generator in the simulation environment to sense impedance magnitude and phase variations. Since this technique is impractical for real life applications, instead of using the quarter wavelength transmission line, two bidirectional couplers are employed to diagnose impedance magnitude and phase variations independently. Matched loads are connected to the isolated ports of the bidirectional couplers. Impedance sensing unit is tested with AD8302 for open and short terminations that are connected as a load impedance to investigate the operation of impedance detection unit as depicted in Figure 4.7. Coupled signals from both source and load side are fed to the INPB and INPA of AD8302 through attenuators and input matching circuit, respectively. Since all the power reflects back from the load for open and short terminations, output voltage (V_{MAG}) is measured as 0.905 V and 0.929 V, respectively, which corresponds to the 0 dB magnitude ratio (reflection coefficient magnitude) as shown in Figure 4.5. The photographs of the impedance sensing and detection unit are depicted in Figures 4.8 and 4.9. The line impedances, the reference power and phase requirements must be addressed properly to avoid the

measurement inaccuracies of the reflection coefficient by AD8302. As impedance detection and sensing circuit gives compatible measurement results with ideal transfer characteristics for the magnitude ratio and phase difference as plotted in Figure 4.5 and Figure 4.6, respectively, the output voltages of AD8302 can be fed to the non inverting integrator circuit with reference voltages which produces two separate control voltages for the variable transformer and 90 degree tunable phase shifter.

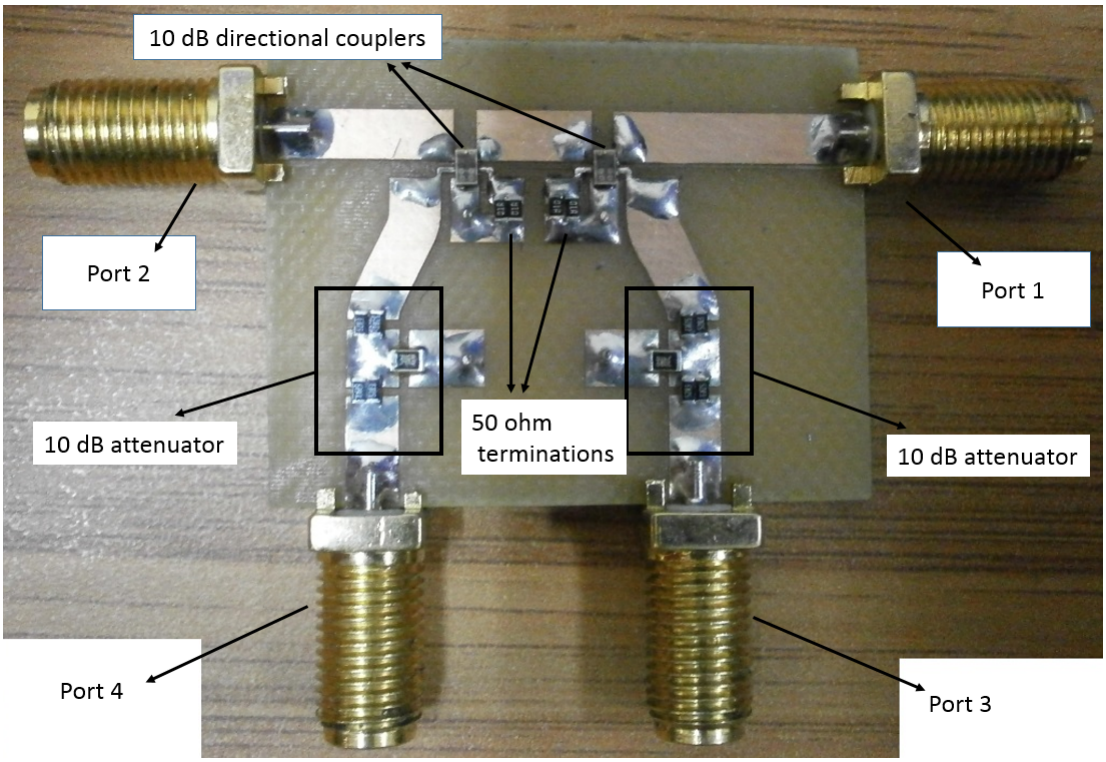

Figure 4.8: Photo of the fabricated impedance sensing circuit

4.3 Implementation of Automatic Impedance Tuning Unit

In this section, the overall automatic impedance tuning unit is implemented based on analog tuning technique by connecting impedance detection-sensing unit and impedance tuner unit with simple impedance control circuit. It is tested for different load impedances to measure the tuning performance of the overall system. VSWR and the percentage of the reflected power values are tabulated and compared for load and tuned impedances at 900 MHz. Besides, VSWR values of load and tuned impedances are also compared in the frequency bandwidth of 880-920 MHz for different load impedances.

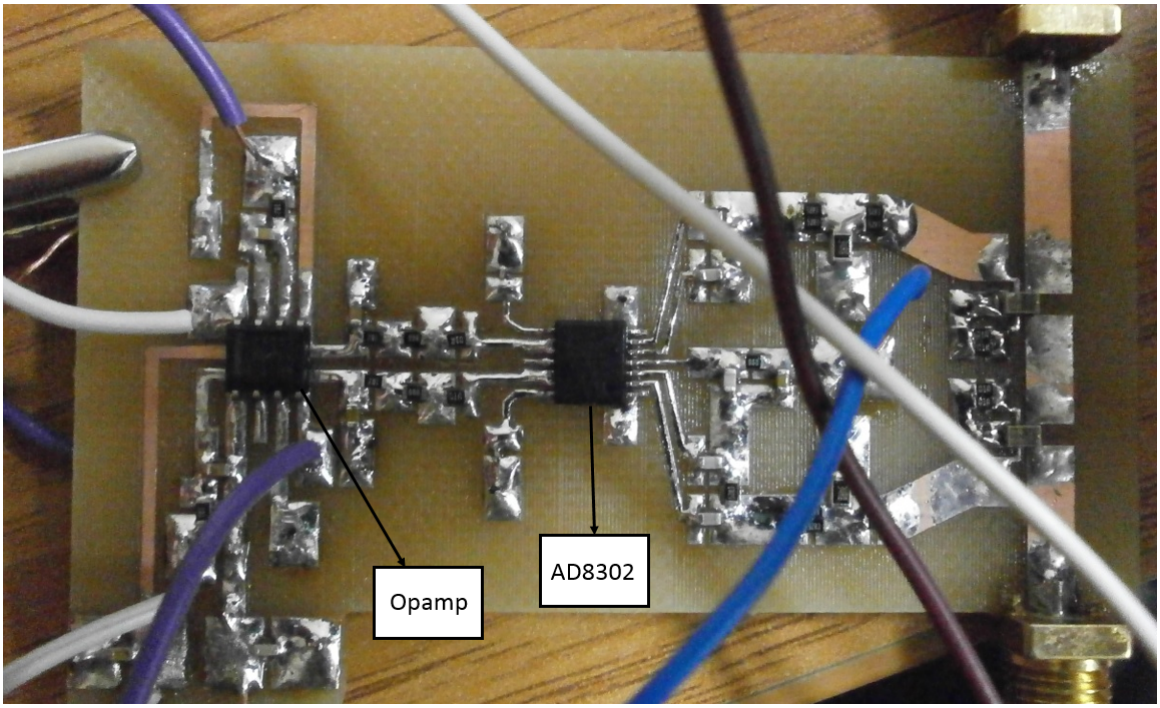

Figure 4.9: Photo of the manufactured impedance detection and sensing circuit

A prototype of the automatic impedance tuning unit is fabricated on a 1.6mm-thick FR-4 board ($\epsilon_r = 4.4$, tanσ = 0.016) by combining the impedance detection and sensing unit, the impedance tuner designed in previous sections, and simple control circuitry. A general block diagram of the automatic impedance tuner is shown in Figure 4.10.

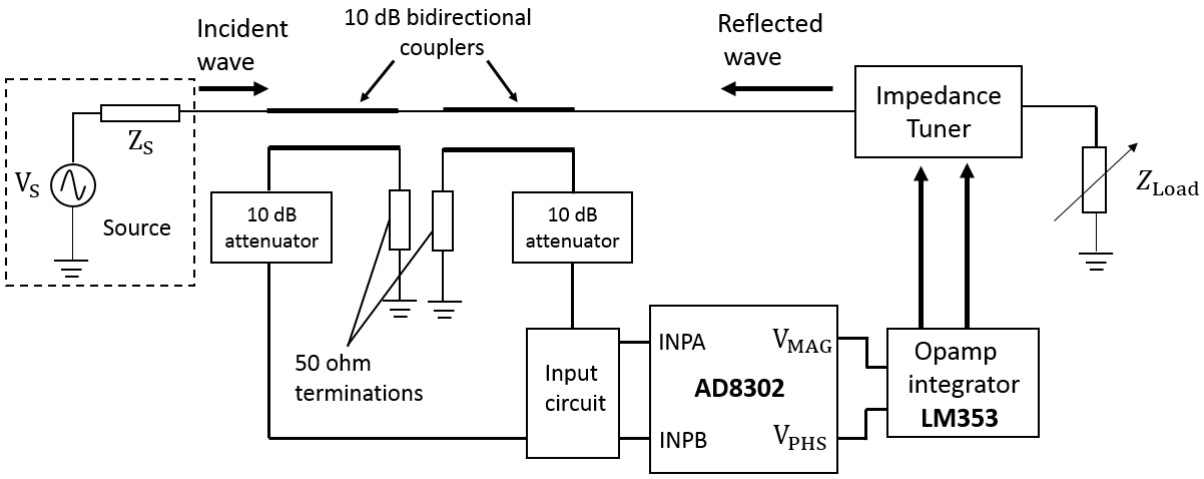

Figure 4.10: General block diagram of automatic impedance tuner circuit

It is composed of 10dB bidirectional couplers from ANAREN (DC0710J5010AHF

model), 10 dB attenuators, AD8302, opamp, tuner and input circuitry inserted between AD8302 and 10 dB attenuators. Non-inverting integrator configuration including chip resistor, capacitor, and opamp (LM353 from Texas Instruments) components offers suitable transfer characteristics between the impedance detection unit and tuner. Identical input impedance and feedback capacitance values given for the non inverting integrator in previous chapter are used with LM353 opamp to produce control voltages for the magnitude and phase. Since the maximum applied voltage to V_{cc+} pin of LM353 opamp is 3.3 V and V_{cc-} is grounded, the control voltages for impedance tuner vary between 0-3.3 V. V_{MAG} output of AD8302 is fed to opamp integrator which produces the control voltages for variable transformer to adjust the magnitude of the reflection coefficient. Besides, V_{PHS} output of AD8302 is connected to the opamp integrator whose output dynamically adjusts the phase of reflection coefficient. Two identical bidirectional couplers should be connected to each other in cascade as depicted in Figure 4.10 to detect the incident and reflected waves properly. As there is no perfect isolation between the coupled and isolated ports of bidirectional couplers in practice, finite directivity introduced by couplers decreases the absolute value of the minimum detectable reflection coefficient ($|\Gamma_{dB}|$), which degrades the magnitude detection capability of the AD8302. Therefore, couplers having good isolation between the coupled and isolated ports must be chosen to reduce the measurement errors. Anritsu MS2025B vector network analyzer (VNA) is utilized to measure the overall system performance in GSM band (880-920 MHz). VNA port 1 exerting -10 dBm power is attached to the bidirectional coupler on the source side whose coupled port is fed to the INPB port of AD8302 through 10 dB attenuator and input circuitry. Attenuator and coupler can reduce the reference power level to -30 dBm for maximum dynamic range usage. AD8302 is utilized as a reflection coefficient sensor which compares the magnitude and phase of the signals coupling from the source side and tuner side. Load impedance variations directly change V_{MAG} and V_{PHS} output voltages depending on the magnitude ratio and phase difference between the reference (INPB) and reflected signal at INPA port. For example, assume that source power is set to -10 dBm and the reflection coefficient magnitude at the input of the impedance tuner is -10 dB as shown in Figure 4.10. Since the reflected power from the impedance tuner (-20 dBm) passes through a 10 dB coupler and a 10 dB attenuator, the power of the signal that is available at INPA port of AD8302 is -40 dBm. As the available power

	$Z_{load}(\Omega)$	$Z_{tuned}(\Omega)$	$VSWR_{load}$	$VSWR_{tuned}$	$V_T(V)$	$V_P(V)$
1	178.82 + j 6.398	67.16 + j 12.64	3.581	1.442	0.055	1.52
2	227.585 - j 147.124	93.044 + j 23.239	6.520	2.019	0.068	1.397
3	241.707 + j 9.565	78.025 + j 21.451	4.842	1.747	0.038	1.4
4	270.076 + j 32.449	82.89 + j 23.077	5.482	1.849	0.041	1.391
5	38.98 - j 119.807	43.459 + j 58.895	9.318	3.314	0.073	1.607
6	51.321 + j 43.015	49.031 - j 44.31	2.284	2.381	0.06	2.876
7	69.120 - j 77.122	66.441 + j 5.994	3.545	1.353	0.08	1.839
8	76.318 + j 70.193	53.672 + j 7.266	3.156	1.169	0.064	1.35
9	78.383 + j 77.868	57.602 + j 9.281	3.464	1.25	0.055	1.354
10	80.091 + j 47.483	45.766 - j 29.36	2.367	1.438	0.08	2.944
11	91.2 - j 79.253	67.461 + j 8.504	3.463	1.395	0.047	1.685
12	43.459 + j 58.895	46.209 + j 2.105	3.314	1.094	0.045	1.352
13	21.632 - j 106.499	89.209 + j 26.596	13.154	2.004	0.072	1.683

Table 4.1: Tuned impedance and VSWR values at 900 MHz with automatic impedance tuner

at INPA is 10 dB lower than the reference power (-30 dBm), AD8302 measures the reflection coefficient magnitude as -10 dB and produces 0.6 V at V_{MAG} output port in ideal case. The overall system is tested for various load impedances (Z_{load}) that are enumerated in Table 4.1. Tuned VSWR ($VSWR_{tuned}$) and impedance (Z_{tuned}) values are given in the same table with variable transformer (V_T) and the 90 degree tunable phase shifter (V_P) control voltages at 900 MHz.

Percentages of the reflected power levels for load and tuned impedances are also given in Table 4.2 at 900 MHz. Adaptive tuning process of implemented automatic impedance tuner is depicted in the Smith Chart for different load impedances in GSM band (880-920 MHz) as shown in Figures 4.11, 4.12, 4.13, 4.14, 4.15, 4.16, 4.17. The automatic tuning unit generally moves the different load impedances to the impedance region close to the center point of the Smith Chart as illustrated in these figures. It can be inferred from these figures that the automatic impedance tuner generally improves the overall system performance in terms of reflected power levels.

VSWR variations of load and tuned impedances available in Table 4.1 are also plotted in the bandwidth of 880-920 MHz as depicted in Figures 4.18, 4.19,4.20, 4.21. It can obviously be seen from these figures that the automatic impedance tuning unit significantly improves the mismatches of the fixed loads. It also reduces the reflected

	$VSWR_{load}$	$VSWR_{tuned}$	$Reflected\ power(load)$	$Reflected\ power(tuned)$
1	3.581	1.442	31.74%	3.28%
2	6.520	2.019	53.88%	11.39%
3	4.842	1.747	43.25%	7.39%
4	5.482	1.849	47.81%	8.88%
5	9.318	3.314	64.99%	28.77%
6	2.284	2.381	15.29%	16.68%
7	3.545	1.353	31.36%	2.25%
8	3.156	1.169	26.91%	0.61%
9	3.464	1.25	30.47%	1.23%
10	2.367	1.438	16.48%	3.23%
11	3.463	1.395	30.46%	2.72%
12	3.314	1.094	28.77%	0.2%
13	13.154	2.004	73.74%	11.17%

Table 4.2: Percentage of the reflected power levels at 900 MHz when the best matching condition is achieved by automatic impedance tuner

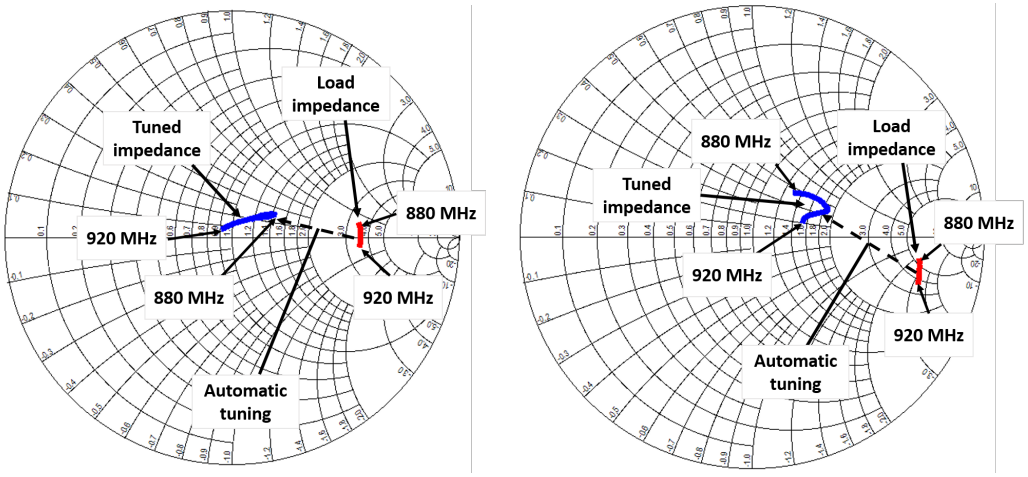

(a) Z_{load} = 178+j6 Ω, Z_{tuned} = 67+j12 Ω (b) Z_{load} = 227-j147 Ω, Z_{tuned} = 93+j23 Ω

Figure 4.11: Load impedance variations on Smith Chart with automatic tuning for the impedances enumerated as (1) and (2) on Table 4.1

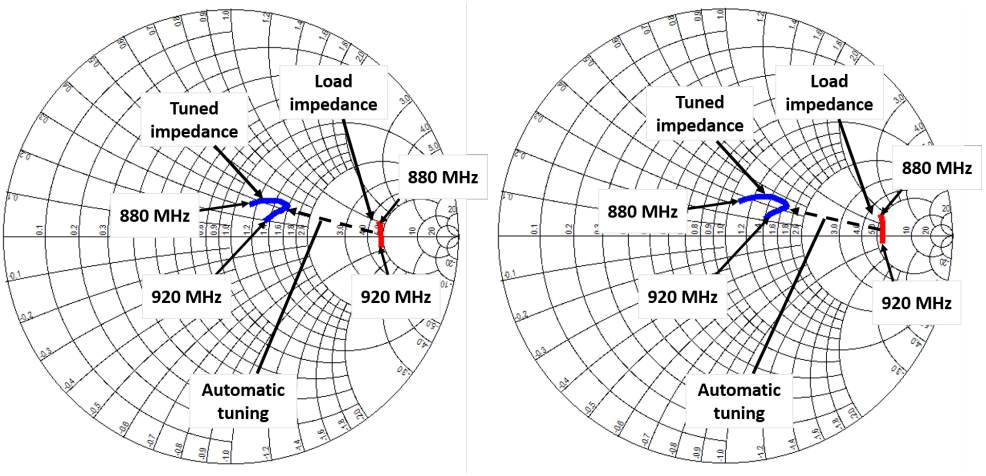

(a) Z_{load} = 241+j9 Ω, Z_{tuned} =78+j21 Ω (b) Z_{load} = 270+j32 Ω, Z_{tuned} = 83+j23 Ω

Figure 4.12: Load impedance variations on Smith Chart with automatic tuning for the impedances enumerated as (3) and (4) on Table 4.1

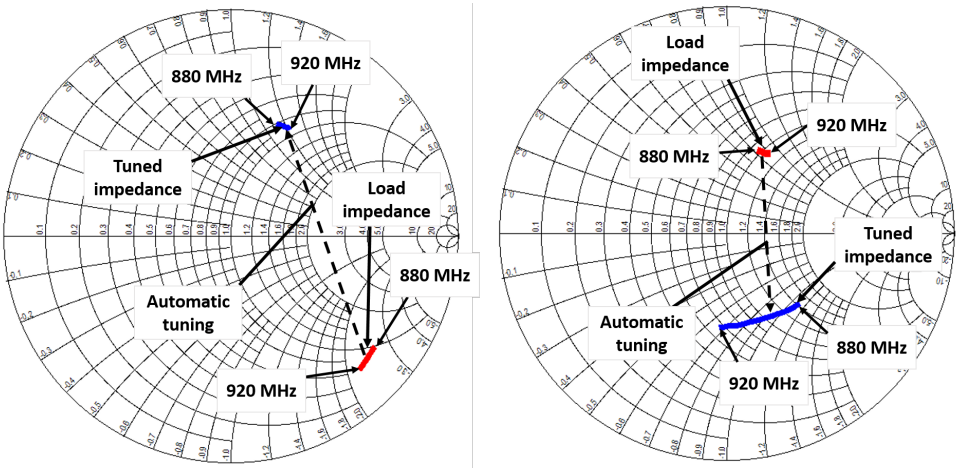

(a) Z_{load} = 39-j120 Ω, Z_{tuned} = 43.4+j59 Ω (b) Z_{load} = 51+j43 Ω, Z_{tuned} = 49-j44 Ω

Figure 4.13: Load impedance variations on Smith Chart with automatic tuning for the impedances enumerated as (5) and (6) on Table 4.1

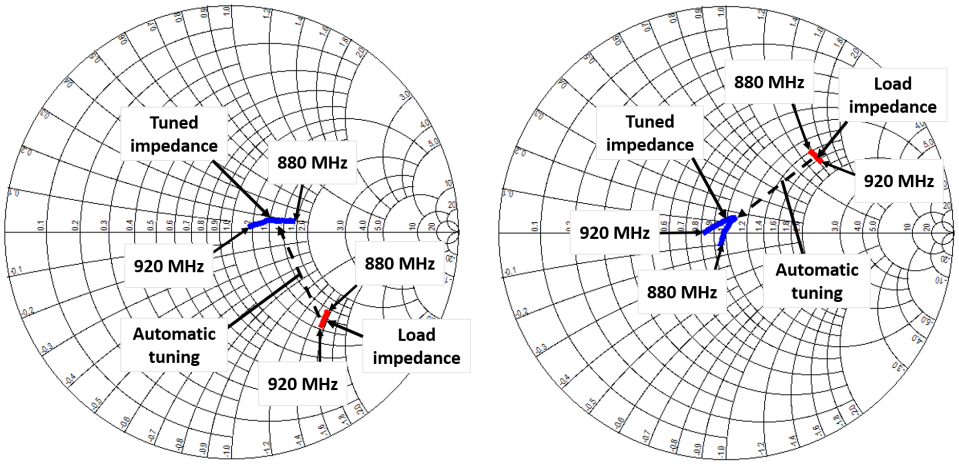

(a) Z_{load} = 69-j77 Ω, Z_{tuned} = 66+j6 Ω (b) Z_{load} = 76+j70 Ω, Z_{tuned} = 53+j7 Ω

Figure 4.14: Load impedance variations on Smith Chart with automatic tuning for the impedances enumerated as (7) and (8) on Table 4.1

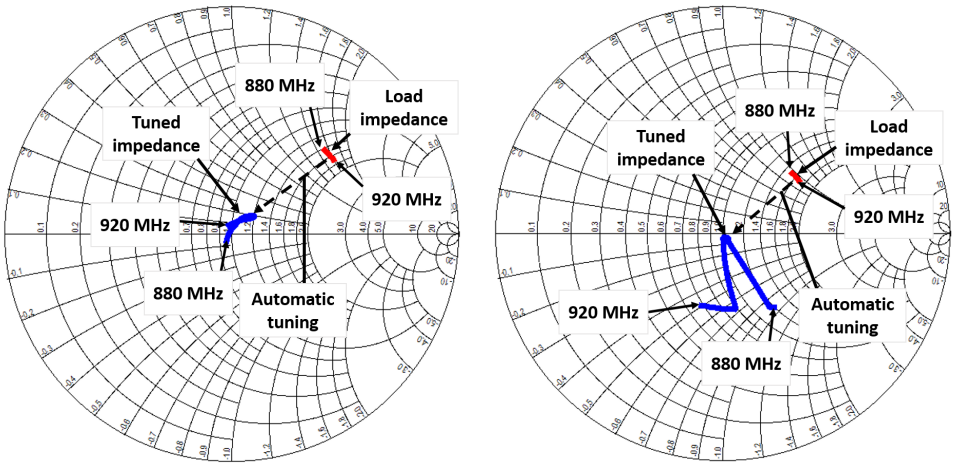

(a) Z_{load} = 78 + j77 Ω, Z_{tuned} = 57+j9 Ω (b) Z_{load} = 80 + j47 Ω, Z_{tuned} = 45-j29 Ω

Figure 4.15: Load impedance variations on Smith Chart with automatic tuning for the impedances enumerated as (9) and (10) on Table 4.1

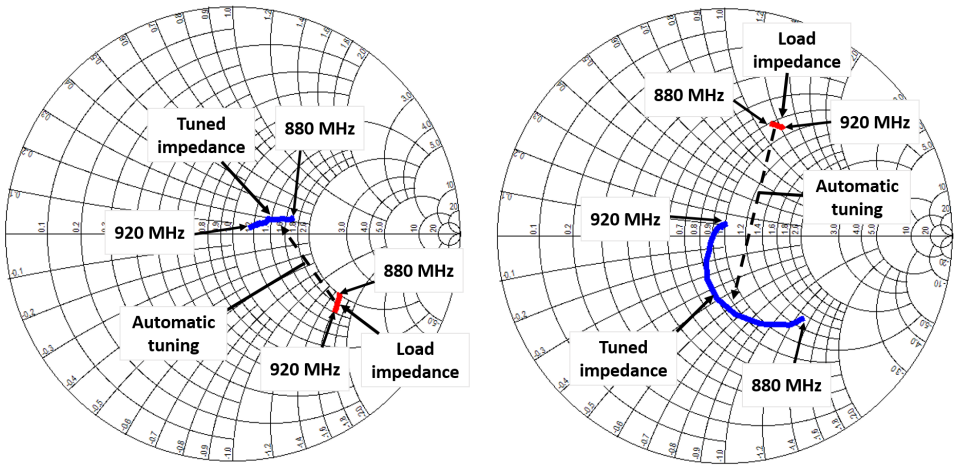

(a) Z_{load} = 91-j80 Ω, Z_{tuned} = 67+j8 Ω (b) Z_{load} = 43+j59 Ω, Z_{tuned} = 46+j2 Ω

Figure 4.16: Load impedance variations on Smith Chart with automatic tuning for the impedances enumerated as (11) and (12) on Table 4.1

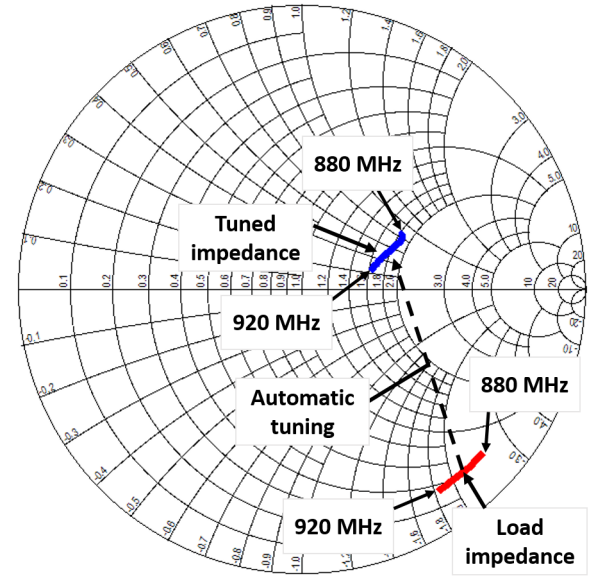

Figure 4.17: Load impedance variation on Smith Chart with automatic tuning for the impedance enumerated as (13) on Table 4.1 (Z_{load} = 21-j106 Ω, Z_{tuned} = 89+j26 Ω)

power from different load impedances.

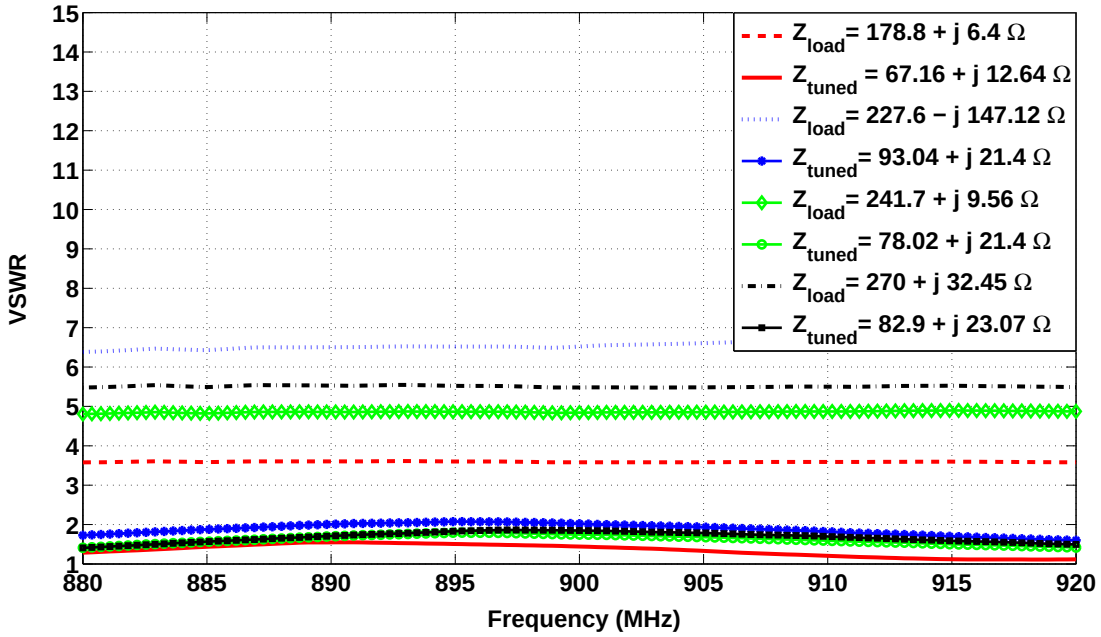

Figure 4.18: VSWR variations with frequency of the load (Z_{load}) and tuned (Z_{tuned}) impedances in the bandwidth of 880-920 MHz

While tunable matching circuit compensates for the impedance variations and reduces the reflections from the antenna by its reconfigurable feature, it introduces different insertion losses for different tuning states. Therefore, the mathematical expression needs to be derived to analyze the performance of tunable systems for different tuning states. Figure 4.22 depicts the circuit block diagram of impedance tuner with a source and a load.

The load and source reflection coefficients are described for the circuit illustrated in Figure 4.22 in (4.4) and (4.5), respectively.

$$\Gamma_L = \frac{Z_L - Z_o}{Z_L + Z_o} \tag{4.4}$$

$$\Gamma_s = \frac{Z_s - Z_o}{Z_s + Z_o} \tag{4.5}$$

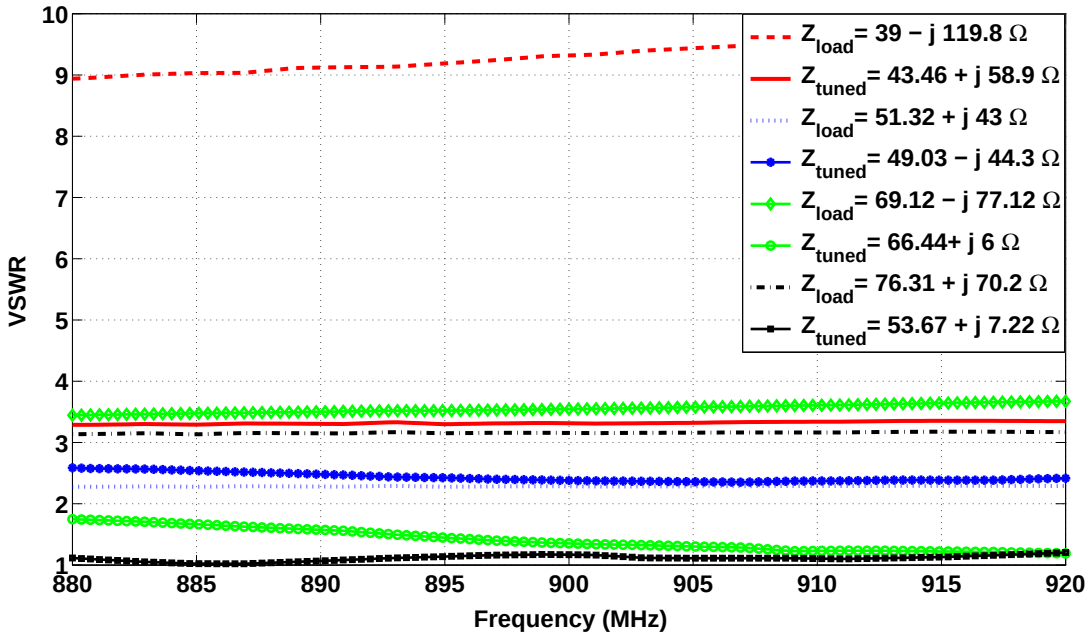

Figure 4.19: VSWR variations with frequency of the load (Z_{load}) and tuned (Z_{tuned}) impedances in the bandwidth of 880-920 MHz

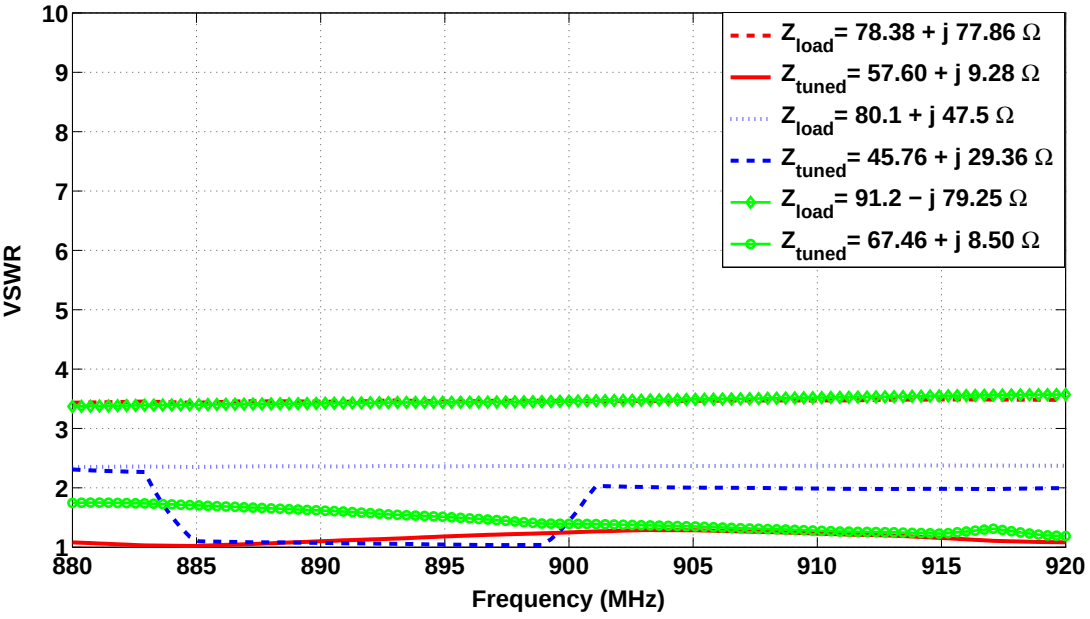

Figure 4.20: VSWR variations with frequency of the load (Z_{load}) and tuned (Z_{tuned}) impedances in the bandwidth of 880-920 MHz

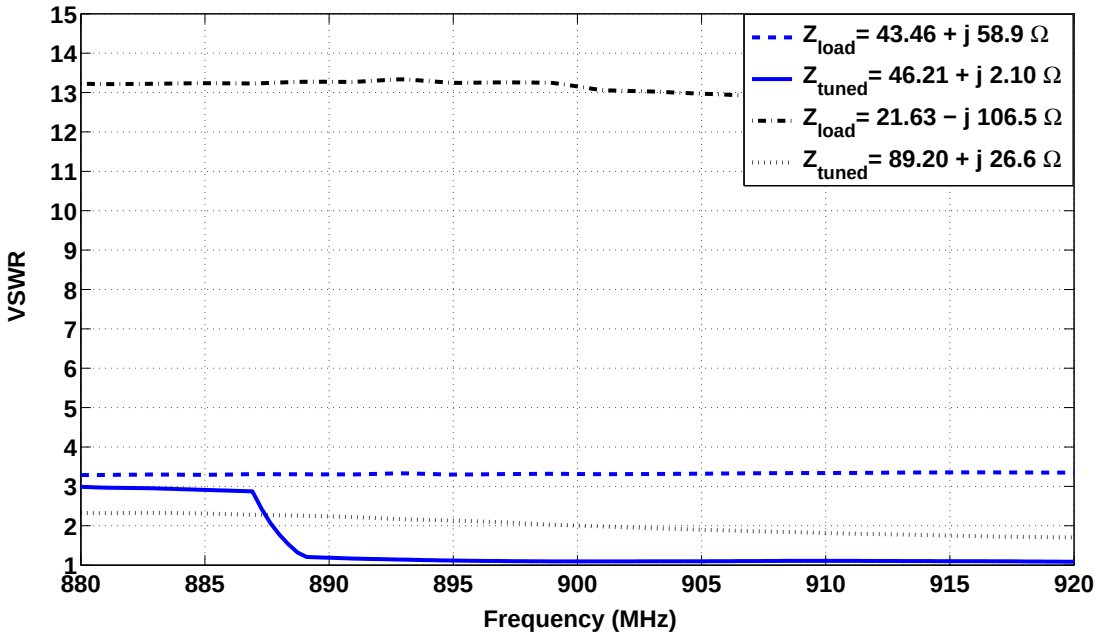

Figure 4.21: VSWR variations with frequency of the load (Z_{load}) and tuned (Z_{tuned}) impedances in the bandwidth of 880-920 MHz

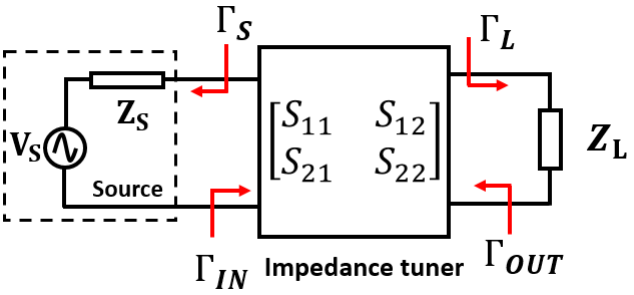

Figure 4.22: The circuit block diagram of impedance tuner when it is fixed between source and load

where Z_o is the characteristic impedance ($Z_o = 50\Omega$) of the network. Transducer gain is an important expression for the characterization of impedance tuner networks. It can be defined as the ratio of power delivered to the load to power available from the source. Transducer gain expression is given as shown below [29].

$$G_T = \frac{P_{load}}{P_{available}} = \frac{|S_{21}|^2(1-|\Gamma_L|^2)(1-|\Gamma_s|^2)}{|1-S_{22}\Gamma_L|^2|1-\Gamma_s\Gamma_{in}|^2} \tag{4.6}$$

where S_{21}, S_{22} are the S parameters of the circuit illustrated in Figure 4.22. Γ_L and Γ_s are the load and source reflection coefficients, respectively. When the source impedance is perfectly matched to 50Ω ($\Gamma_s = 0$), transducer gain expression for the circuit illustrated in Figure 4.22 ($G_{T,tuner}$) can be simplified as:

$$G_{T,tuner} = \frac{P_{load}}{P_{available}} = \frac{|S_{21}|^2(1-|\Gamma_L|^2)}{|1-S_{22}\Gamma_L|^2} \tag{4.7}$$

When the matched source ($\Gamma_s = 0$) is directly attached to the load as shown in Figure 4.23, the transducer gain of this configuration ($G_{T,without\ tuner}$) can also be expressed in terms of S parameters and load reflection coefficient. Due to the fact that there is no available impedance matching network between the source and the load (i.e $S_{21} = 1$ and $S_{22} = 0$), the transducer gain for this circuit ($G_{T,without\ tuner}$) can be simplified from 4.6 as follows:

$$G_{T,without\ tuner} = \frac{P_{load}}{P_{available}} = 1-|\Gamma_L|^2 \tag{4.8}$$

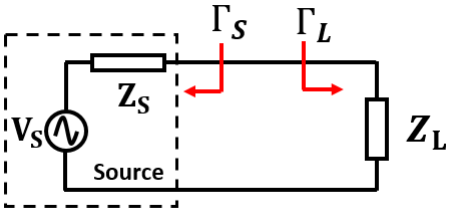

Figure 4.23: The circuit diagram when there is no impedance tuner between the source and the load

It is well documented in literature that relative transducer gain (Δ_{G_T}) is generally utilized to evaluate how much improvement is achieved by tunable matching network

for the best matching state [7], [35], [36] [37]. Relative transducer gain (Δ_{G_T}) can be considered as the transducer gain improvement with the impedance tuner unit over $G_{T,without\,tuner}$. It can be expressed in terms of S parameters of the impedance tuner and the load reflection coefficient (Γ_L) as shown below.

$$\Delta_{G_T} = \frac{G_{T,tuner}}{G_{T,without\,tuner}} = \frac{|S_{21}|^2}{|1 - S_{22}\Gamma_L|^2}$$

in which S_{22} and S_{21} are the scattering parameters of the impedance tuner at tuning state for the load impedance, and Γ_L is the load reflection coefficient. It accounts for both load mismatches and the dissipation loss of the impedance tuner.

The relative transducer gain (Δ_{G_T}) is the key definition to measure how much power improvement (Δ_{G_T} > 0 dB) or loss (Δ_{G_T} <0 dB) is introduced by tunable matching network. Figures 4.24 to 4.26 depict the variation of the relative transducer gain (dB) values of the impedance tuner illustrated in Figure 4.2 with frequency for different load impedances. It can be obviously seen from the relative transducer gain variation for different load impedances that impedance tuner significantly consumes the RF power for different tuning states. Besides, the peak values of the relative transducer gain are moved to the lower frequency region as illustrated in Figures 4.24, 4.25, 4.26. The load impedance and relative transducer gain (dB) values are given in Table 4.3 at three different frequencies. Relative transducer gain measurements show that the loss introduced by this tuner can be very high for some load values which should be considered for RF front end applications. Q values of varactors and fixed inductors primarily affect the insertion loss level introduced by impedance tuner for different tuning states. Besides, S parameter measurements show that S_{22} values of the impedance tuner is not conjugately matched to load impedances for each tuning state. This leads to the reduction of power transfer to the load impedance for different tuning states. Although this tuning unit significantly reduces the reflected power from antenna due to user interaction as tabulated in Table 4.2, it introduces high insertion loss and impedance mismatches at the load side for different tuning states. The main purpose of fixing an impedance tuner between the source and load is to transfer maximum power to the load rather than minimizing reflections from the impedance tuner [37].

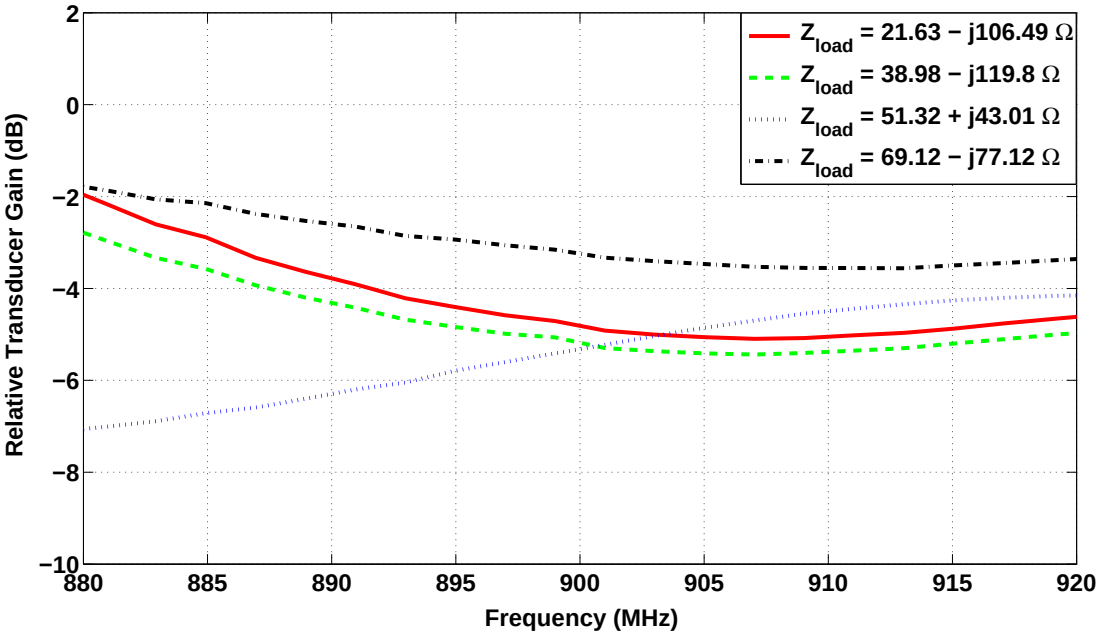

Figure 4.24: Relative transducer gain Δ_{G_T} (dB) variation with frequency for different load impedance values

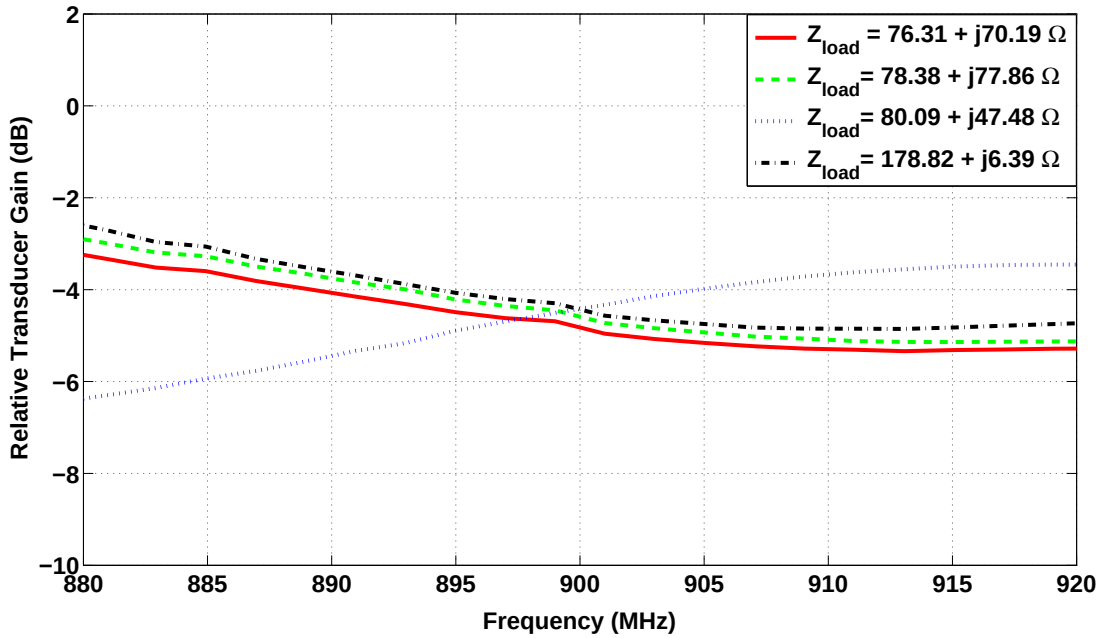

Figure 4.25: Relative transducer gain Δ_{G_T} (dB) variation with frequency for different load impedance values

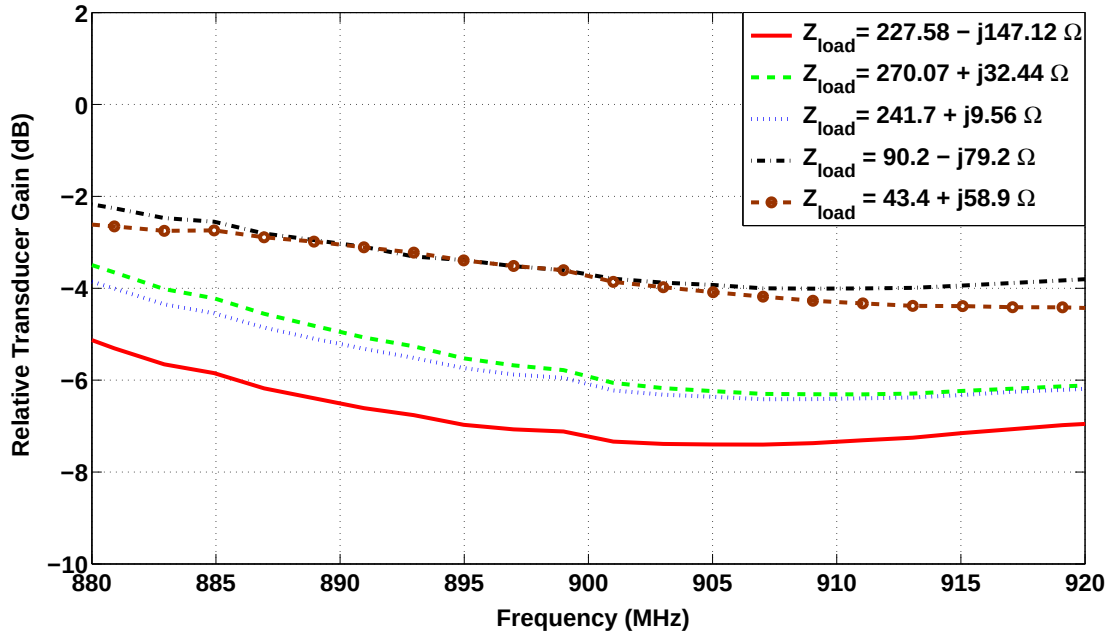

Figure 4.26: Relative transducer gain Δ_{G_T} (dB) variation with frequency for different load impedance values

	880 MHz		900 MHz		920 MHz	
	$Z_{load}\,(\Omega)$	$\Delta_{G_T}\,(dB)$	$Z_{load}\,(\Omega)$	$\Delta_{G_T}\,(dB)$	$Z_{load}\,(\Omega)$	$\Delta_{G_T}\,(dB)$
1	174 + j 27.8	-2.7	178.8 + j 6.39	-4.6	177.2 - j 16.8	-4.75
2	265.5 - j 117.5	-5.3	227.6 -j 147.1	-7.3	187.8 - j 164.9	-6.9
3	230.8 + j 45.9	-4	241.7 + j 9.6	-5.95	239.6 - j 30.7	-6.2
4	247.5 + j 79.5	-3.66	270 + j 32.4	-5.78	272 - j 25.6	-6.13
5	32.1 - j 11.2	-2.96	39 - j 120	-5	46.7 - j 128.3	-4.9
6	49.4 + j 42.1	-7	51.3 + j 43	-5.2	53 + j 43.8	-4.16
7	75.3- j 76.7	-1.87	69.1- j 77.1	-3.15	62.9 - j 77.1	-3.3
8	70.8 + j 68.7	-3.13	76.3 + j 70.2	-4.96	81.6+ j 71.1	-5.3
9	72.2 + j 75.8	-2.9	78.4 + j78	-4.73	84.4+j79.2	-5.13
10	75.9+j47.7	-6.3	80+j47.4	-4.33	83.8 + j 46.7	-3.4
11	99.3 - j 76.5	-2	91.2 - j 79.2	-3.6	82.7 - j 81.2	-3.7
12	41.4+ j 56.8	-2.57	43.4 + j58.9	-3.6	44.9 + j 60.6	-4.44
13	27.4 - j 122.4	-2.15	21.63 - j106.5	-4.71	17.5 - j 92.9	-4.56

Table 4.3: Load impedance and relative transducer gain (Δ_{G_T}) values at three different frequencies

4.4 Overall Assessment of Measured Results

This chapter mainly focuses on the fabrication and measurement of the impedance tuner, impedance detection and sensing subunits and the overall automatic impedance matching circuit. The impedance tuning performance of automatic impedance tuner is tested by connecting fixed load impedances to automatic tuning unit at GSM bands. Besides, the overall efficiency of impedance tuning unit is analysed based on the S parameters of tuner for different tuning states and load reflection coefficient. In view of the impedance tuner measurements for fixed loads, significant VSWR improvement is achieved by using the automatic impedance tuning unit. It is observed from measurements that VSWR value is maintained below 2 for most of the mismatched loads in the frequency band of 880-920 MHz. This means that the overall system performance is generally improved by the impedance tuner in terms of reflected power levels. This impedance tuner performs tuning very well in the frequency band of 880-920 MHz. In addition, as the impedance tuning unit needs bias voltages varying between 0-3.3 V, it is usable for cell phone applications without adding high voltage generating units to the automatic impedance tuning system. The relative transducer gain measurements indicate that the impedance tuning unit can not deliver available power from the source to the load very well due to the insertion loss and load mismatches. The best results in relative transducer gain are observed in the low frequency region of GSM band. Despite the fact that reflected power is remarkably reduced through the impedance tuner, it brings up high insertion loss and mismatches on the load side for different tuning states.

High Q valued semiconductor varactor can be employed to enhance the insertion loss of impedance tuner. Even though MEMS varactors offer improvements in terms of linearity and high Q values, the usage of this varactor causes high voltage generation problems in cell phone. For the purpose of using this impedance tuner in high power applications, antiseries connection of varactors can be employed to avoid turn on and breakdown operation modes. In addition, this connection can reduce modulation effects on capacitance owing to large RF swing across the varactor. Nevertheless, the increase in the number of components degrades the overall performance of this tuner due to parasitic effects and insertion loss.

CHAPTER 5

CONCLUSION AND FUTURE WORK

This thesis investigates the design and simulation of automatic impedance tuning units that dynamically compensate for the input impedance variations of a cell phone in GSM band due to the user interaction between the body and antenna.

In this thesis, a Planar Inverted F Antenna which consists of a tapered patch, a ground plane, feeding point and shorting pins is investigated. It is simulated in free space in the frequency bandwidth of 750-1050 MHz using WIPL-D Pro 3D EM simulation software based on Method of Moments technique. To verify the simulation results, the tapered PIFA is fabricated by using metal sheets and wires. The manufactured antenna is measured for various holding positions to investigate how the user interaction changes its input impedance in GSM bands (880-920 MHz). The measurement results show that the presence of user hand and head primarily increases the reactive part of the antenna input impedance which is in agreement with measurement results of the previous studies.

Impedance tuners and automatic impedance tuning circuits based on the previous studies in the literature are designed and simulated to dynamically compensate for impedance mismatches. Adaptive impedance tuning units are simulated with ADS Envelope simulator at 900 MHz based on semiconductor and ferroelectric varactor models in order to test the dynamic performance of the designed impedance tuners. Two different tuning mechanisms using two step impedance transformation are also analysed and discussed. The impedance coverage regions of designed tuners using two different tuning techniques are plotted on the Smith Chart at 900 MHz to investigate whether the impedance tuners cover the mismatched impedance region due to

various holding positions of the antenna. Although cascade connected T-matching and 180 degree phase shifter tuning unit proposed based on the second tuning technique offers the design of general purpose impedance tuner, it also encloses the detuned impedance region determined by previous measurements of PIFA with user hand and head. Simple impedance detection unit is tested in automatic tuning system with modified version of proposed tuner in the literature and a novel tuner designed by cascade connection of proposed tuner blocks in the literature. The second automatic impedance tuner design consists of variable transformer and 90 degree phase shifter . After the assessment of simulated performances of these two automatic tuner circuits, it is decided to fabricate the latter one. Two impedance tuner circuits providing independent control in magnitude and phase domain of antenna input impedance are tested with automatic impedance tuning unit. These circuits can be compared in different ways such as control voltage level, coverage region, compactness, and insertion loss. Since the first one requires high control voltages beyond the maximum cell phone battery supply voltage, it is not appropriate for cell phone applications. Although this circuit offers tuning capability in a wide coverage region, it may bring up some problems in terms of compactness, and insertion loss. However, the second one is more suitable than this tuner for such applications. Although its coverage area is limited compared to the impedance tuner including T matching circuit and 180 degree phase shifter, it is sufficient for cell phone applications. Besides, it provides tuning capability in the cell phone battery supply range without requiring any extra circuit.

This automatic impedance tuning unit composed of directional couplers, attenuators, AD8302 is also fabricated on FR4 substrate to test the performance of the impedance tuner for various load impedances in GSM band. The impedance tuner measurements for fixed loads demonstrate that significant VSWR improvement is achieved using automatic impedance tuning unit. It is observed from measurements that VSWR value is maintained below 2 for most of the mismatched loads in the frequency band of 880-920 MHz. However, the relative transducer gain measurements show that the loss introduced by this tuner for different tuning states can be very high for some load values which should be considered for RF front end applications in GSM band. As a conclusion, the developed impedance tuner is compact and needs control voltage

levels up to 3.3 V, so that it is a good candidate for cell phone applications.

As a future work, the insertion loss of impedance tuner can be improved by using high Q valued semiconductor varactors. Although MEMS varactors offer high Q factor, high voltage requirement for tuning brings up problems related to high voltage generation in cell phones. In order to use this impedance tuner in high power applications, anti series connection of varactors can be utilized to reduce RF swing across the varactors in the varactor tuning range. Besides, this connection can reduce modulation effects on the capacitance due to large RF swing across the varactor. However, the increase in the number of components lead to an increase in the parasitic effects and insertion loss introduced by tuner, which degrades the performance of this tuner. EVM (error vector magnitude) analysis can be done to investigate how much deterioration is introduced to modulated signal by the impedance tuner for different tuning states.

REFERENCES

[1] J. Papapolymerou, K. Lange, C. Goldsmith, A. Malczewski and J, Kleber, Reconfigurable Double Stub Tuners Using MEMS Switches for Intelligent RF Front Ends, IEEE Trans. On Microwave Theory and Techniques, Vol. 51, No. 1, pp. 271-278, Jan. 2003.

[2] T. Vaha-Heikkila, J. Varis, G.M Rebeiz, "A reconfigurable 6-20 GHz RF MEMS impedance tuner," 2004 IEEE MTT-S, Int. Microwave Symp. Dig., June 2004, pp. 729 - 732.

[3] R.E.Collin: "Foundations For Microwave Engineering,"

[4] R. Quaglia, et.al., "A double stub impedance tuner with SiC diode varactors," Proc. APMC, December 2011, Melbourne

[5] N. Deve, A. B. Kouki, and V. Nerguizian, "A compact size reconfigurable 1–3 GHz impedance tuner suitable for RF MEMS applications," in Proc. 16th Int. Microelectron. Conf. , Dec. 2004, pp. 101–104.

[6] Ming Chen, Chi-Chih Chen and John L. Volakis, "Reconfigurable 800–1500 MHz double stub tuner using MEMS capacitive switches," Antennas and Propagation Society International Symposium (APSURSI), 2013 IEEE, July 2013, pp. 2157-2158.

[7] C. Sánchez-Pérez, J. deMingo, P.L.Carro, and P. García-Dúcar, "Design and applications of a 300–800 MHz tunable matching network," IEEE J. Emerg. Sel. Topic Circuits Syst., vol. 3, no. 4, pp. 531–540, Dec. 2013.

[8] Y.-H. Chun, and J.-S. Hong, " Variable Z_C transmission line and its application to a tunable impedance transformer," IEEE European Microwave Conference, pp. 4, Oct. 2005.

[9] J. Mingo, A. Valdovinos, A. Crespo, D. Navarro, P. García, "An RF Electronically Controlled Impedance Tuning Network Design and Its Application to an Antenna Input Impedance Automatic Matching System", IEEE Trans. Microwave Theory and Tech., vol. 52, no. 2, pp. 489-497, February 2004.

[10] Jia-Shiang Fu, "Adaptive Impedance Matching Circuits Based on Ferroelectric and Semiconductor Varactors," Ph.D. dissertation, Dept. Elect. Eng., University of Michigan., Ann Arbor, 2009.

[11] L. Sankey and Z. Popovic, “Adaptive tuning for handheld transmitters,” IEEE MTT-S Int. Microwave Symp.Digest, paper TU4E-4, pp. 225 - 228, Boston, MA, June 7 - 12, 2009.

[12] K. Ogawa, T. Takahashi, Y. Koyanagi, K. Ito, “Automatic impedance matching of an active helical antenna near a human operator,” 33rd European Microwave Conference Proceedings, Vol.3, pp. 1271-4, 2003.

[13] A. van Bezooijen, M. A. de Jongh, C. Chanlo, L. C. H. Ruijs, F.vanStraten, R. Mahmoudi, and A. H. M. vanRoermund, “A GSM/EDGE/WCDMA adaptive series-LC matching network using RF-MEMS switches,” IEEE J. Solid-State Circuits, vol. 43, no. 10, pp. 2259–2268, Oct. 2008.

[14] E. L. Firrao, A.-J. Annema, and B. Nauta, “An automatic antenna tuning system using only RF signal amplitude,” IEEE Trans. Circuits Syst. II, Exp. Briefs, vol. 55, no. 9, pp. 833–837, Sep. 2008.

[15] A. van Bezooijen, M. de Jongh, C. Chanlo, L. Ruijs, H. J. ten Dolle, P. Lok, F. van Straaten, J. Sneep, R. Mahmoudi, and A. H. M. van Roermund, “RF MEMS based adaptive antenna matching module,” in Proc. IEEE RF IC Symp., 2007, pp. 573–576.

[16] http://www.wipl-d.com/products.php?cont=wipl-d-pro

[17] K. L. Wong, “Planar Antennas for Wireless Communications,” John Wiley and Sons, Hoboken, 2003.

[18] C. K. Byung, D. P. Ju, and D. C. Hyumg, “Tapered type PIFA design for mobile phones at 1800 MHz,” in Proc.IEEEVeh.Technol.Conf., Orlando, FL, USA, 2003, vol. 2, pp. 1012–1014.

[19] A. Sarolic, D. Senic, Z. Zivkovic, and A. Zorica “Influence of human head and hand on PIFA antenna matching properties and SAR,” International Conference on Software, Telecommunications and Computer Networks (SoftCOM), 2011.

[20] K. R. Boyle, Y. Yuan, and L. P. Ligthart, “Analysis of mobile phone antenna impedance variations with user proximity, ”IEEE Trans. Antennas Propagat., vol. 55, pp. 364–372, Feb. 2007.

[21] M. Pelosi, O. Franek, M. B. Knudsen, and G. F. Pedersen, “User’s impact on PIFA antennas in mobile phones,” in IEEE 69th Vehicular Technology Conference Proceedings, VTC Spring 2009, 2009.

[22] I. Ida, J. Takada, T. Toda, and Y. Oishi, “An adaptive impedance matching system and its application to mobile antennas,” in TENCON 2004. 2004 IEEE Region 10 Conference, vol. C, nov. 2004, pp. 543 – 546 Vol. 3.

[23] Andre van Bezooijen, Reza Mahmoudi, Arthur van Roermund, Adaptive RF Front-Ends for Hand-held Applications, Springer, 2011.

[24] http://www.keysight.com/find/eesof-ads2011-help

[25] Koul, K. S. and Bhat, B., Microwave and Millimeter Wave Phase Shifters, Vol II: Semiconductor and Delay Line Phase Shifters, Artech House, 1991.

[26] Pozar, D. M., Microwave Engineering, 2nd Edition, John Wiley and Sons, 1998.

[27] Maloratsky, L. G., Passive RF and Microwave Integrated Circuits, Elsevier, 2003.

[28] A. Keerti, J. Xiang, and A.-V. Pham, "High power linearized RF phase shifter using anti-series diodes," IEEE Microw. Wireless Compon. Lett., vol. 16, no. 4, pp. 200–202, Apr. 2006.

[29] Guillermo Gonzales, Microwave Transistor Amplifiers, Analysis and Design 2nd edition Prentice Hall, Upper Saddle River, NJ, 1984.

[30] http://www.coilcraft.com/

[31] H. M. Nemati, C. Fager, U. Gustavsson, R. Jos, and H. Zirath, "Design of varactor-based tunable matching networks for dynamic load modulation of high power amplifiers," IEEE Trans. Microwave Theory Tech., vol. 57, no. 5, pp. 1110 - 1118, May 2009.

[32] http://www.skyworksinc.com/

[33] http://www.analog.com/en/index.html

[34] https://www.anaren.com/

[35] A. S. Morris, Q. Gu, M. Ozkar, and S. P. Natarajan, "High performance tuners for handsets," in IEEEMTT-SInt. MicrowaveSymp. Dig. , 2011, pp. 1–4.

[36] Q. Gu and A. S. Morris, III, "A new method for matching network adaptive control," IEEE Trans. Microw. Theory Tech., vol.61, no.1, pp. 587–595, Jan. 2013.

[37] Gu, Qizheng. RF Tunable Devices and Subsystems: Methods of Modeling, Analysis, and Applications. Springer, 2015.

APPENDIX A

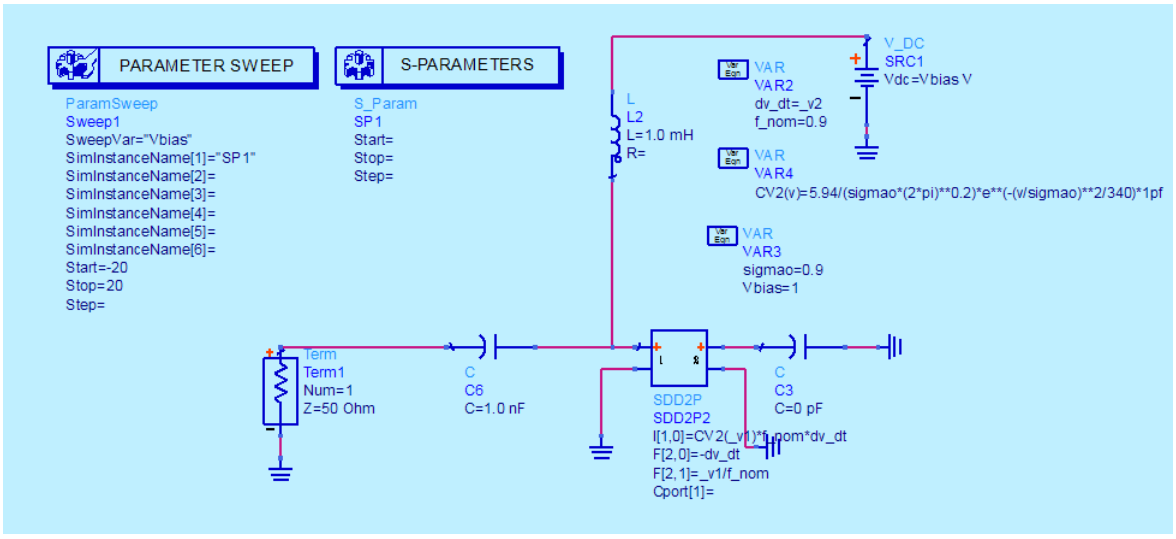

Figure A.1: Representation of BST varactor model in ADS schematic

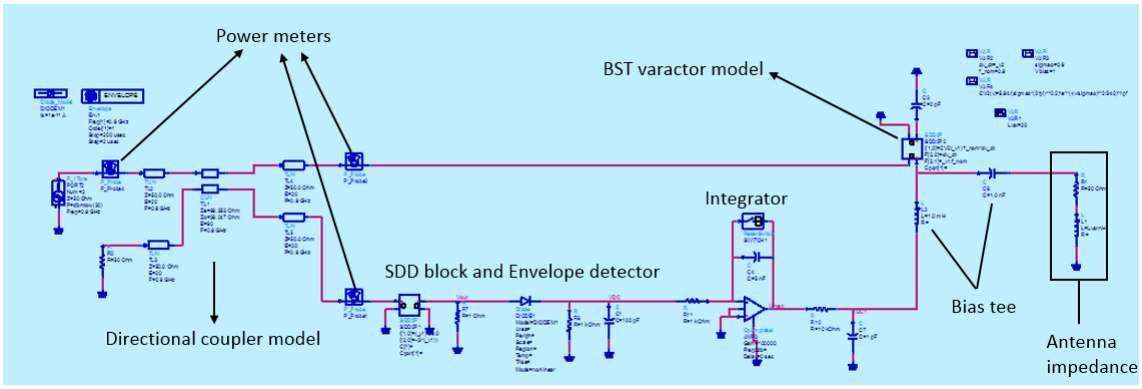

Figure A.2: Circuit schematic of overall impedance tuning system in ADS

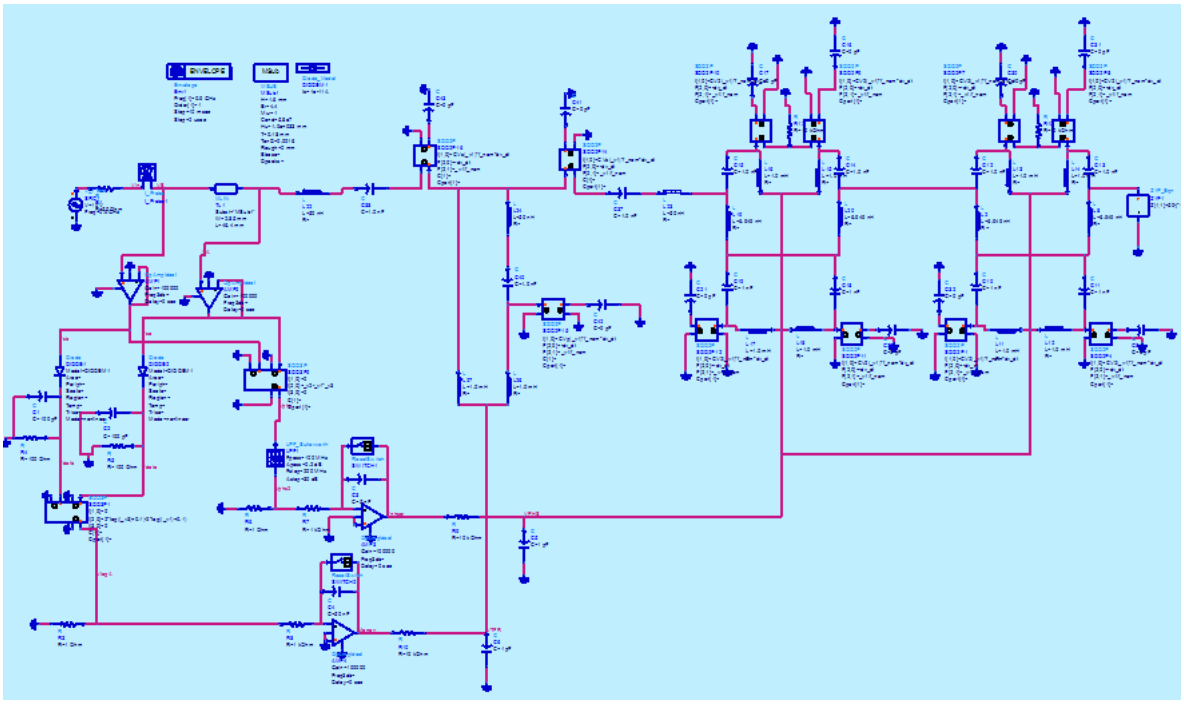

Figure A.3: The automatic impedance matching system with T-matching circuit and 180 degree phase shifter

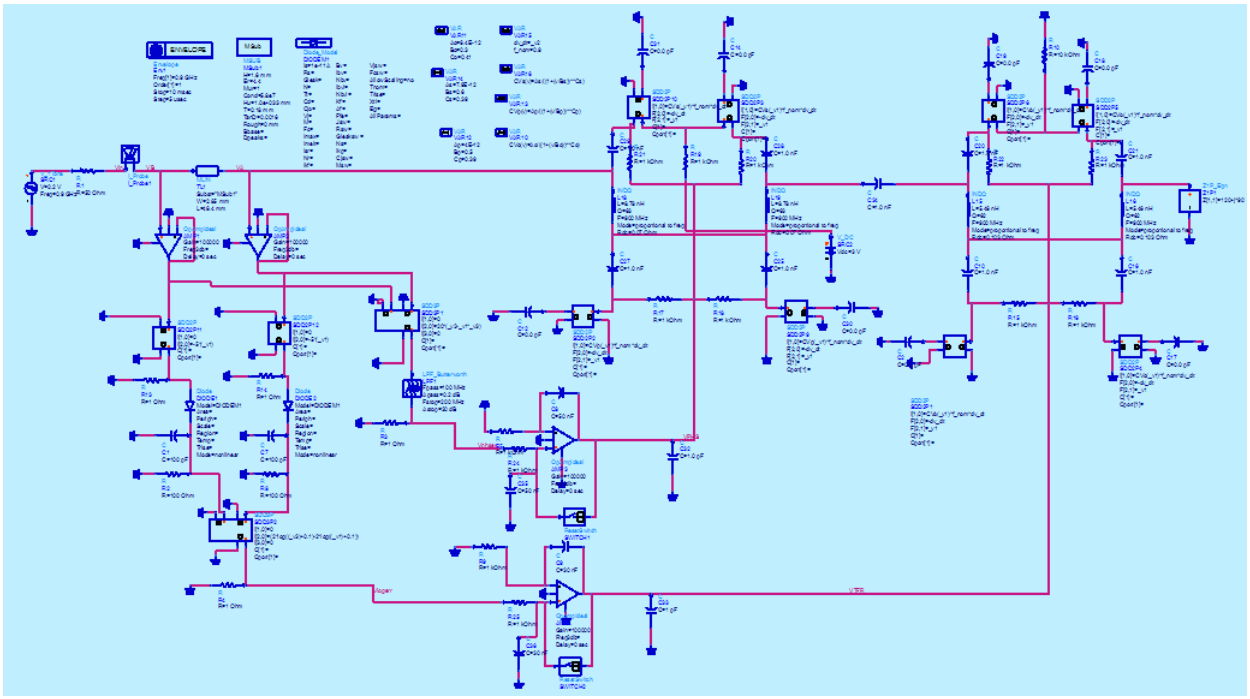

Figure A.4: The automatic impedance matching system with variable transformer and 90 degree phase shifter

CURRICULUM VITAE

PERSONAL INFORMATION

Surname, Name: Öztürk, Mehmet Ali
Nationality: Turkish (TC)
Date and Place of Birth: 05.03.1988, MANİSA
Marital Status: Single
Phone: 0 312 210 13 00
Fax: 0 312 0000000

EDUCATION

Degree	Institution	Year of Graduation
M.S.	METU Electrical and Electronics Engineering	2015
B.S.	Hacettepe University Electrical and Electronics Engineering	2011
High School	Manisa Anadolu Öğretmen Lisesi	2006

PROFESSIONAL EXPERIENCE

Year	Place	Enrollment
2 year	Anketek Electronics	Engineer